Implementation of a DVB-T2 Passive Coherent Locator Demonstrator

Presented by:
Micheal Thatohatsi Malape

Prepared for:
Assoc. Prof. D.W. O'Hagan
and
Dr. W.P.F Schonken

A dissertation submitted to the Department of Electrical Engineering, University of Cape Town, in partial fulfilment of the requirements for the degree of Masters of Science in Engineering specialising in Radar and Electronic Defence

.

October 8, 2019

Declaration

I know the meaning of plagiarism and declare that all the work in the document, save for that which is properly acknowledged, is my own. This thesis/dissertation has been submitted to the Turnitin module (or equivalent similarity and originality checking software) and I confirm that my supervisor has seen my report and any concerns revealed by such have been resolved with my supervisor.

Micheal Thatohatsi Malape

Signed by candidate

Signature

2019/10/20

Date

Abstract

Passive Coherent Locator (PCL) radar's have seen extensive research in the past decade. PCL radars utilize illuminators of opportunity (IOO) as transmitters to perform target detection. Particular interests in FM (analogue) and DVB-T/T2, DAB (digital) radio frequency signals has seen significant focus as possible illuminators for radar processing. The University of Cape Town (UCT) , in particular, has extensive history on passive radar research including the implementation of a full narrowband FM PCL radar demonstrator.

This dissertation details the design and implementation of a DVB-T2 Passive Coherent Locator radar demonstrator isolating a single DVB-T2 channel. This includes the design, construction, testing and evaluation of the full PCL radar system.

System planning was implemented detailing the possible IOOs available in the Cape Town area. This was followed by signal propagation simulations to determine the effects the environment would have on the transmitted wave utilising Advanced Refractive Effects Prediction System (AREPS) model.

A front-end design was simulated and implemented utilizing commercial-of-the-shelf (COTS) hardware including the National Instruments Ettus N210 software defined Radio (SDR) based on the system planning results.

A processing chain for DVB-T2 based PCL radar was then investigated to determine the most optimal processing chain structure, with the mismatched filtering technique being proposed as an ideal choice for DVB-T2 PCL radar. The proposed processing chain was implemented and tested on both the Ettus N210 front-end as well as a commercial system.

The full radar demonstrator was then tested by observing the air traffic surrounding the Cape Town International airport resulting in successful detections of aircraft in the surveyed environment.

For Lindelwa and Abbey.

Acknowledgements

I would like to thank my supervisor's Daniel O'Hagan, Francois Schonken and the RRSG group. For introducing the topic of PCL radar to me and all the assistance and guidance along the way.

I would like to thank my friends and colleagues of "team PCL" Phil Philane, Motlatsi Setsubi, and Xavier Frantz. For their assistance, knowledge shared and laughter.

Secondly, to Darryn Jordaan and Johan "Skippy" Burger. For all your input, guidance and discussions shared on all things radar.

To Zwivhuya Ramudzuli who coincidentally moved with me to Cape Town and did the radar masters. Thanks for the friendship and proof reading this dissertation.

To the two TAs of the Radar Masters, Po-kai "Randy" Cheng and Stephen Paine. For all their assistance on the courses. Also like to thank Stephen for all his assistance on PCL radar theory and knowledge.

To all the friends I met along the way on this journey. Many thanks to you all. This includes Lebo Mbhele, Shane, Keegan Naidoo, Riyaad Jacobs, Jarryd Son, Asif Parker and those not mentioned but still appreciated. Thank you.

I would like to thank Peralex Electronics. For the exposure to PCL radar, additional funding and assistance with hardware for this dissertation such as the N21O and ComRad DVB-T. I'd specifically like to thank Francois Louw, Alex Bessios, Jean Swart, Jean Wessels, Craig Tong and Adriaan Zeeman.

I would like to thank Molahlegi Molope at Armscor for planting the idea in my head of specializing in radar for my masters. I'd also like to thank Ledger for the postgraduate funding.

Lastly, to my mother and father. Lindelwa and Abbey Malape. For first tolerating my dreams to do my Masters and supporting me with all my endeavours. I couldn't wish for better parents.

Contents

Declaration i

Abstract ii

Acknowledgements iv

Contents v

List of Figures viii

List of Tables xii

List of Symbols xiii

Nomenclature xv

1 Introduction 1

1.1 Background . . . 2

1.2 Problem Statement . . . 3

1.2.1 Motivation for PCL . . . 3

1.2.2 Scope and Limitations . . . 4

1.2.3 System Requirements . . . 4

1.2.4 Plan of Development . . . 4

1.2.5 Publication Related To The Research Done . . . 5

2 Literature Survey 6

2.1 Passive Coherent Locator Radar . . . 6

2.1.1 History of Passive Coherent Locator Radar . . . 9

2.1.2 Passive Coherent Locator Radar in the Modern World . . . 10

2.2 OFDM Signals . . . 15

2.2.1 Auto-Ambiguity function of the DVB-T2 Signal . . . 18

2.2.2 Cross Ambiguity Function of the DVB-T2 Signal . . . 19

2.3 Radar Signal Processing of OFDM Signals . . . 20

2.3.1 Reference Signal Processing . . . 20
2.3.2 Direct Path Interference & Clutter Cancellation . . . 21
2.4 Summary . . . 21

3 DVB-T2 Front-end Receiver Design 22
3.1 System Planning . . . 22
3.1.1 Transmitter Coverage . . . 22
3.1.2 Propagation Modelling . . . 27
3.1.3 Summary . . . 32
3.2 RF Front-end Design . . . 33
3.2.1 System Requirements . . . 34
3.2.2 Antenna . . . 34
3.2.3 Receiver Design . . . 37
3.2.4 Heterodyne and ADC . . . 41
3.3 Summary . . . 45

4 DVB-T2 Processing Chain 46
4.1 Mismatch Filtering . . . 46
4.1.1 Surveillance Branch . . . 51
4.1.2 Reference Branch . . . 56
4.1.3 Range and Doppler Processing . . . 62
4.1.4 Target Detection . . . 64
4.2 Summary . . . 65

5 Results 66
5.1 System Geometry and Configuration . . . 66
5.1.1 System Geometry . . . 66
5.1.2 System Configuration . . . 67
5.2 Target Detection . . . 69
5.2.1 Multi Band PCL Demonstrator . . . 71
5.3 Summary . . . 77

6 Discussion and Conclusion 78
6.1 Front-end Design . . . 78
6.1.1 Future Work . . . 79
6.2 Processing Chain . . . 80
6.2.1 Future Work . . . 80

References 82

A Labview 88

A.1 Setting Up Labview 88

List of Figures

2.1 bi-static Radar Geometry 7

2.2 PCL bi-static Radar Geometry 8

2.3 PCL Radar System Architecture 9

2.4 FDM Signal with Guard Intervals 16

2.5 DVB-T2 OFDM Frame Structure without cyclic prefix [36, 37] 16

2.6 Ambiguity Function of the DVB-T Single Frame Signal 18

2.7 CAF of a DVB-T2 Signal 19

3.1 DVB-T2 Transmitters Cape Town 24

3.2 Potential IOO baselines 25

3.3 Spectrum of the DVB-T2 UHF Band Broadcast Measured from UCT . . 26

3.4 Channel Power of the DVB-T2 signal at 706 MHz Broadcast Measured from UCT 27

3.5 Elevation Pattern of Broadcast antenna 28

3.6 Refraction 29

3.7 Knife-edge diffraction 30

3.8 8 bay DVB-T/T2 Elevation Antenna Pattern 31

3.9 Transmitter power density-density plot in dBw/m^2 of the 8-bay DVB-T/T2 antenna with transmitter power set to 50 kW 31

3.10 Constantiaberg Transmitter Propagation loss AREPS plot 32

3.11 Northern Flight path from or to the Cape Town International Airport . . 33

3.12 Grid reflector with four bow-tie phased array feed 35

3.13 Grid reflector with four bow-tie phased array antenna pattern 36

3.14 Antenna S-parameters with and without 75Ω to 50Ω matching pad . . . 37

3.15 Antenna S-parameters with and without 75Ω to 50Ω matching pad . . . 37

3.16 Proposed Front-end Receiver for Reference Channel 40

3.17 Proposed Front-end Receiver for Surveillance Channel 40

3.18 Proposed Front-end Receiver 41

3.19 SBX Daughter Block Diagram[50] 42

3.20 Ettus USRP N210s with MIMO synchronisation cable. 43

3.21 Labview Receiver Program Flow 43

3.22 Reference Signal Recorded with N210 board using Labview. 45

4.1 DVB-T2 processing chain. 47

4.2 DVB-T2 Frame Structure consisting of Superframes, Frames and OFDM Symbols[36][37] 48

4.3 P1 Symbol Structure[37] 49

4.4 P1 Symbol Detection Block Diagram[37] 50

4.5 CAF map of DVB-T2 system with a simulated target at 400 Hz bistatic Doppler and 100 km bistatic range with no direct signal cancellation or demod-remod processing 54

4.6 CAF map of DVB-T2 system with a simulated target at 400 Hz bistatic Doppler and 100 km bistatic range with direct signal cancellation or demod-remod processing. 55

4.7 DVB-T2 Frame Structure with Scattered and Continual Pilots 59

4.8 Spectrum of reference DVB-T2 signal before and after Demod-Remod . . 62

4.9 CAF of remodulated reference signal with normalised pilots 62

4.10 ARD Map of DVB-T2 signal for a CPI equal to the frame length. The maximum bistatic range is approximately 52 km with a range bin of 32.7898 metres. The maximum bistatic Doppler is approximately +/-425 Hz with a Doppler bin of 4.23155 Hz. This corresponds to an ARD map of 1201 range bins X 201 Doppler bins. 64

5.1 PCL Radar System Geometry with Antenna Configuration 67

5.2 CFAR output with two targets detected around the Cape Town International Airport. First target at a bistatic Range of 36.6 km and a bistatic Doppler of -97 Hz. The second target was detected at 36.1km bistatic range and at +94 Hz bistatic Doppler. The results presented here are from real data collected in the field with UCTs prototype radar system and the Peralex ComRad receiver. 70

5.3 ASD-B Data of Air Namibia Flight NMB703 taking off from the airport from the south. The green dots correspond to the transmitted target GPS information at a certain instant in time. The white triangle illustrates the bistatic triangle with the black arrow the direction of the target. 71

5.4 Combined PCL Radar System Geometries with Antenna Configurations . 72

5.5 FM Processing Chain 74

5.6 CFAR output with five targets detected around the Cape Town International Airport. Three targets can seen approaching the system from the positive Doppler. The other two targets are moving away from the system on the negative Doppler side. The results presented here are from real data collected in the field with the Peralex ComRad FM receiver 74

5.7 ARD comparison of the two detections from the FM and DVB-T2 based systems. The FM target at 135.2 km bistatic range and 15 Hz bistatic Doppler corresponds to the target at 36.1 km bistatic and 94 Hz bistatic Doppler. The second FM target at 136.5 km bistatic range and -40 Hz bistatic Doppler corresponds to the target at 36.6 km bistatic range and -97 Hz bistatic Doppler. 76

A.1 Example of NI-USRP Configurator Utility 89

A.2 Example of NI-USRP Configurator Utility with Connected Devices . . . 90

A.3 Example of Updating Firmware and FPGA with NI-USRP Configurator 91

A.4 Example of Labview USRP User Interface 92

A.5 Example of Labview USRP User Interface Sampling at 2.4GHz. 92

List of Tables

2.1 Commercial Passive Radar Systems 15

3.1 Frequency Bands of Digital Televion 23

3.2 Transmitter Specifications 24

3.3 Received and expected signal strength 27

3.4 Antenna Specifications 35

3.5 Sumnmary of N210 SDR and SBX Daughterboard Specifications 38

3.6 Summary of Amplifier Specifications[52] 39

4.1 Scattered pilot pattern to be used for each allowed combination of FFT size and guard interval in SISO mode[36, 37] 58

4.2 Boosting for the continual pilots 59

4.3 Parameters Used In The Cape Town Region, South Africa 60

5.1 DVB-T2 System parameters 69

5.2 FM System parameters 73

List of Symbols

c	—	Speed of light in a vacuum (3×10^8) [m/s]
β	—	Bistatic Angle [deg]
R_T	—	Distance to Target from Transmitter [m]
R_R	—	Distance to Target from Receiver [m]
ΔR_{res}	—	Range Resolution[m]
f_D	—	Bistatic Doppler [Hz]
SNR	—	Signal to noise ratio before [dB]
λ	—	Operating wavelength of radar [m]
f_c	—	Operating frequency of radar [Hz]
F	—	Noise figure [dB]
B	—	Bandwidth [Hz]
χ	—	Ambiguity Function
r	—	Reference signal in time domain
τ	—	Delay in time [s]
s	—	Surveillance signal in time
P_r	—	Receive power [dBm]
P_t	—	Radar transmit power [dBm]
G_r	—	Gain of receive antenna [dBi]
R	—	Propagation Distance [m]
P_{ch}	—	Channel Power [dBm]
F	—	Propagation Factor
$\|E_0\|$	—	Electric Field under Free-Space
$\|E\|$	—	Magnitude Electric Field
L_{fs}	—	Free Space Path Loss
L	—	Propagation Loss
$S11$	—	Scattering Parameters referring to Reflection Coefficient

$P1$	—	Preamble 1 Symbol of a DVB-T2 signal
$P2$	—	Preamble 2 Symbol of a DVBT-T2 signal
S_s	—	Surveillance Signal in samples
S_{echo}	—	Echo Signal in Samples. This is the skin echo return from a target
$S_{interference}$	—	DPI interference in Surveillance Signal in Samples from Clutter
$\hat{S}_s$	—	Cancellation Output of DPI Cancellation
$\hat{S}_{inteference}$	—	Estimated Interference in Surveillance Signal in Samples
A	—	A Matrix is a Copy of the Reference Signal Made Up of Delayed Doppler Shifted Versions of the Reference Signal
$\hat{x}$	—	Filter Weights Used to Compute the Estimated Interference in Surveillance
b	—	Set equivalent to S_s during Cancellation Process
ΔR_{bin}	—	Range ARD Bin Resolution[m]
ΔF_{D-bin}	—	Doppler ARD bin Resolution[Hz]
T_{CPI}	—	CPI Length in Time [sec]
T_x	—	Transmitter
R_x	—	Receiver
T_u	—	OFDM Symbol Length [sec]
T_g	—	Guard Interval Length
P_d	—	Probability of Detection
P_{fa}	—	Probability of False Alarm

Nomenclature

5G—Fifth Generation.

ADC—Analog to Digital Converter.

ADS-B—Automatic Dependent Surveillance—Broadcast.

AF—Ambiguity Function.

AoA—Angle of Arrival.

ARD—Amplitude Range Doppler.

AREPS—Advanced Refractive Effects Prediction System.

ASO—Analogue Switch Over.

ATC—Air Traffic Control.

ATM—Air Traffic Management.

BBC—British Broadcasting Corporation.

BPSK—Binary Phase Shift Key.

CAF—Cross Ambiguity Function.

CFAR—Constant False Alarm Filter.

CGLS—Conjugate Gradient Least Squares.

COTS—Commercial Off the Shelf.

CPI—Coherent Processing Interval.

CUT—Cell Under Test.

CW—Continuous Wave.

DAC—Digital to Analog Converter.

DAB—Digital Audio Broadcast.

DBS—Direct Broadcast by Satellite.

DPI—Direct Path Interference.

DPS—Direct Path Signal.

DRM—Digital Radio Mondiale.

DTED—Digital Terrain Elevation Data.

DVB-T—Digital Video Broadcast - Terrestrial.

DVB-T2—Digital Video Broadcast - Terrestrial 2.

DVB-T/T2—Digital Video Broadcast - Terrestrial and/or Digital Video Broadcast - Terrestrial 2.

ECA—Extensive Cancellation Algorithm.

ECA-B—Batches Extensive Cancellation Algorithm.

ECA-CD—Extensive Cancellation Algorithm-Carrier and Doppler.

ERP—Effective Radiated Power.

FDM—Frequency Division Multi-plexing.

FFT—Fast Fourier Transform.

FM—Frequency Modulated.

FPGA—Field Programmable Gate Array.

FX—Fourier Transform - Cross Correlation.

GIF—Guard Interval Fraction.

GLONASS—Global Navigation Satellite System.

GOCA—Greater of Cell Averaging.

GPSDO—Global Positioning System Disciplined Oscillator.

GPU—Graphics Processing Unit.

GSM—Global System for Mobile.

ICASA—Independent Communications Association South Africa.

IFFT—Inverse Fast Fourier Transform.

IOO—Illuminator of Opportunity.

ISI—Inter-Signal Interference.

ITU—International Telecommunications Authority.

LOS—Line Of Site.

LPDA—Log-Periodic Antenna.

LTE—Long Term Evolution.

MIMO—Multiple Input Mutiple Output.

OFDM—Orthogonal Frequency Division Multi-plexing.

PC—Personal Computer.

PCL—Passive Coherent Location.

PLP—Physical Layer Pipes.

PP—Pilot Pattern.

PSD—Power Spectral Density.

PSLR—Peak Side Lobe Reduction.

QAM—Quadrature Amplitude Modulation.

QPSK—Quadrature Phase Shift Key.

RBW—Resolution Bandwidth.

RCS—Radar Cross Section.

RF—Radio Frequency.

SDR—Software Defined Radio.

SFN—Single Frequency Network.

SISO—Single Input Single Output.

SNR—Signal to Noise Ratio.

UCT—University of Cape Town.

UHF—Ultra High Frequency.

UTMS—Universal Mobile Telecommunications System.

VHF—Very High Frequency.

WW2—World War 2.

Chapter 1

Introduction

Passive Coherent Locator (PCL) radar or as also commonly known as Passive Radar (PR), Passive Bistatic Radar(PBR), and Commensal Radar(CR) are radar systems that do does not have nor use a dedicated radar transmitter. PCL radars use pre-existing communication based transmitters such as Frequenct Modulated (FM), analogue television, Digital Audio Broadcast (DAB), Digital Video Broadcast (DVB-T), WiFi, Global System for Mobile (GSM) etc. or in other instances other radars as Illuminators of Opportunity (IOO) to perform target detections using target skin returns. Research and development of PCL radars has seen a significant increase in the last couple of years from both academia and from commercial industry [1]. This is partly due to spectrum demand from emerging technologies, such as in the telecommunication industry, increasing in the last couple of decades. The most recent drive for greater spectrum allocation has been communications and broadcasting that need greater bandwidths for increased data rates demand from consumers as technology improves. As advancements in communications keep being made such as, 5G communications, more and more spectrum will be needed particularly in the bands under 6 GHz. These advancements imply that other users of spectrum have to find innovative ways to either share spectrum or try and find other means of maintaining operations at the expense of declining spectrum availability in a high spectrum demand environment. PCL radar is one such solution as it attempts to solve some of the issues arising from increased Radio Frequency (RF) spectrum demand.

PCL radar systems come with significant benefits and there are also some disadvantages to the technology. Some of the challenges that PCL systems have are lack of control of the IOOs means you dependent on a third party and are therefore not in control of content, which is an issue in FM based passive radars. Secondly, in the situation where the transmitter is not transmitting anything for any particular reason such as the transmitter having to undergo maintenance for example, an alternative would have to be found or the radar system would be would effectively be non-operational. Another challenge for

PCL radar is the system geometry. This due to the PCL radar essentially being a bistatic radar where the receiver and transmitter are separated by a significant distance (in the order several km or ±100 km in FM based PCL) and thus the receiver location has to be chosen with care. The system performance of PCL is highly dependent on the system geometry[1]. Other challenges include Direct Path Interference (DPI) in the surveillance channel of a PCL system, in the case of Continuous Wave (CW) bistatic radar which is true of PCL radar[2]. Waveform suitability is another challenge in PCL systems as some waveform characteristics are not ideal for radar applications [3].

For this dissertation it is proposed that a DVB-T2 PCL Radar demonstrator which includes both the RF front-end and full processing chain be developed for deployment and operation at the University of Cape Town for ongoing research in the field of PCL. The front-end should be designed to maximise the dynamic range of the Analogue to Digital Converter (ADC) to sample a channel of interest. An investigation and implementation of a processing chain architecture for DVB-T2 based PCL radar should be completed.

The preceding sections detailed the background to the project, requirements of the project in the form of a project statement and aim. Lastly, the chapter ends with a detailed development plan that outlines the rest of the dissertation.

1.1 Background

University of Cape Town (UCT) has done significant research in PCL radar in the past decade [4, 5, 6, 7, 8]. However, most of the work has focused on FM based PCL radar which culminated in a narrowband PCL demonstrator[9] being implemented including a real-time processing chain. With the development of digital television and the release of new digital television standards DVB-T and then DVB-T2 respectively, the world began a process of digital migration. Each region in the world and their specific member countries would have a deadline to switch over from analogue television transmission to digital. The European and African deadline for digital migration, when analogue television is phased out, was set at 17 June 2015 by the International Telecommunication Union in Geneva 2006[10]. In that time, some western countries had already migrated to DVB-T and thus in the late 2000s research into DVB-T based PCL systems commenced with notable results. During that time an update to the DVB-T standard was updated and DVB-T2 was released in the early 2010s. Some of the initial countries that adopted DVB-T early on chose to remain with DVB-T and not upgrade to the T2 standard. Some countries which were still utilising analogue transmission began migrating digital television transmission including South Africa. South Africa's choice for digital transmission standard was the newer DVB-T2 standard rather than the older DVB-T variant. DVB-T2 allows carriers more flexiblity, robustness and efficiency than the DVB-T standard. With DVB-T2 being

significantly different to DVB-T, the signal processing techniques for the older DVB-T would not work on DVB-T2. This meant that research into DVB-T2 based PCL radar was required.

1.2 Problem Statement

PCL radar has the ability to detect targets utilising the target skin returns from RF signals transmitted from IOOs rather than having a dedicated transmitter as is typical with most radar systems. This makes PCL systems ideal for Air Traffic Management (ATM) in a time when spectrum allocation for radar systems is slowly reducing due to competition from ever-growing communications environment. From a defence and civilian perspective PCL systems has the added benefit of giving the radar community access to the Very High Frequency (VHF) and Ultra High Frequency (UHF) fields which allows for detection of low observable targets and counter-stealth as well as long range surveillance capabilities.

1.2.1 Motivation for PCL

The demand and development of wireless communications has led to greater demands for spectrum allocation especially in the desirable bands that some radar systems operate in. There has already been some discussion from the communications perspective of reducing the role of some of the radar systems to secondary users rather than primary users. The main difference between secondary users and primary users is the fact that preference on band utilization is given mainly to the primary users and that secondary users are allowed to use the band as long as they do not interfere with the functions of the primary user [11]. However these solution has inherent problems associated with it such as the performance effects of the different technologies due to interference from either technology.

PCL radar has been noted as a possible solution as spectrum demand grows from multiple industries. This due to the fact that PCL radar is dependent on pre-existing transmitters and doesn't require spectrum allocation. Secondly, PCL radar can operate in the VHF and UHF bands implying that the interference from new technologies in the S band won't have as much an effect as on current primary active radar. However, as passive radar is still an emerging technology in the immediate future, PCL systems can be seen as a system to augment currently existing Air Traffic Control (ATC) radar systems.

Research into PCL systems can assist in ensuring that as the technology matures it can become more reliable and an effective replacement for ATC radar. This is especially crucial for developing countries where traditional air surveillance coverage is either poor

or non-existent and the cost of obtaining a primary air surveillance radar are too high.

1.2.2 Scope and Limitations

The scope of this project was to design and implement a full DVB-T2 based PCL radar demonstrator. The aim was also to investigate and implement a processing chain for DVB-T2 passive radar. A low cost PCL radar demonstrator was designed, implemented and deployed at UCT monitoring the air traffic at the Cape Town International Airport.

One of the limitations of the project was the procurement of the requisite hardware for the front-end receiver due to limited budget and availability of funds. This could also affect the development time as some of the hardware would have to be procured from overseas based manufacturers and equipment can take a certain amount of time to arrive.

1.2.3 System Requirements

This dissertation focused on designing and implementing a DVB-T2 PCL radar that operates in the UHF frequency band. The radar should encompass both the front-end signal conditioning and digitization as well as the back-end radar signal processing. The following criteria needed to be met:

- 2 Channel UHF Front-end Receiver
- Fully Coherent Receiver Sampling Single DVB-T2 UHF Channel
- High Dynamic Range
- CPI $\geq$ To the DVB-T2 Frame Length (250 ms)
- Coverage of the Cape Town International Airport Airspace

1.2.4 Plan of Development

Chapter 2 examines the literature study performed on PCL radar for the work executed in this dissertation. A detailed look at PCL radar research from various bodies is described in depth to give a general view of where PCL is today. It is followed by a review of current DVB-T/T2 PCL systems. The overall structure of an Orthogonal Frequency Division Multiplexing (OFDM) signal is then examined and described leading into the structure of DVB-T/T2 the OFDM signal. Finally, different types of processing techiques for DVB-T/T2 based PCL was covered in great detail.

Chapter 3 focuses on the system planning and the RF front-end design of the PCL system. System planning is done by analysing the available transmitters in the region of

interest. This is followed by propagation modelling using Advanced Refractive Effects Prediction System (AREPS) at the specified UHF frequencies of the available transmitters. The receiver front-end design was then implemented based on the results of the system planning and propagation modelling. The RF design process of the front-end up to and including the ADC is initially described. This is then followed by how a 2 channel PCL radar system was implemented as well as synchronised in order to implement coherent processing of the received data.

Chapter 4 looked at the PCL processing chain and described the proposed system design. This section began by describing the DPI cancellation process of the data. This was then followed up by a discussion of the demod-remod process and the particular form of demod-remod processing that was implemented for this dissertation. Lastly, the range and Doppler processing was described leading up to the target detection and extraction. The final processing chain pipeline for DVB-T2 was then be described and demonstrated.

Chapter 5 details the results obtained from full system deployment testing both the front-end as well as the processing chain, giving a full PCL radar system. The trials were able to show that the system was able to consistently detect a target in the area of interest. The processing chain was shown to work for both the demonstrator implemented as well as a commercial system supplied by an industry partner.

Chapter 6 contains a discussion on the results found in chapter 5 and conclusions reached in the work completed in this project. Recommendations and future work on improving the system are also given at the end of the chapter.

1.2.5 Publication Related To The Research Done

The research implemented in the process of the completion of this dissertation led and contributed to the following publications:

S. Paine, F. Schonken, Micheal Malape et al., "Multi Band FM and DVB-T2 Passive Radar Demonstrator," *2018 19th International Radar Symposium (IRS)*, Bonn, 2018, pp. 1-10.[12]

The work in the publication related to this dissertation is Section 4 DVB-T2 Based PCL and Section 5 the DVB-T2 PCL results.

Chapter 2

Literature Survey

In this section the aim was to assess and critique some of the work done in open literature on PCL radar. The section begins by introducing PCL radar. The history and operation of PCL radar is covered. This looks at the detailed history and early research and experiments of PCL in the 1900s. They then looked at the work done on PCL radar systems since the turn of the century, looking at notable contributions made to PCL radars today from academia, industrial research institutions and commercial industry. The chapter then discusses the OFDM signal to assess why it's a viable radar signal. The chapter then ends by critiquing the various signal processing techniques of OFDM based PCL radar systems.

2.1 Passive Coherent Locator Radar

There are 3 primary types of radar configurations. These are the monostatic, bistatic or multi-static radar. Monostatic radar is a radar where the transmitter and receiver are co-located. Bistatic radar is described as a radar system that utilises antennas that are separated by a significant distance to be used for either transmission or reception[13]. The bistatic system geometry can be seen in Figure 2.1. The transmitter (T_x) is separated by a distance L, the baseline, to the receiver (R_x). The target is located at a third location and is a distance separated by R_T to the transmitter and a distance R_R to the receiver. The triangle formed by the lines R_T, R_T and L form an angle opposite the L line known as the bistatic angle β.

A multi-static radar configuration is a radar system that consists of multiple separately spaced mono-static, bistatic or both radar systems with a shared surveillance coverage. A bistatic radar is considered to be monostatic or pseudo-monostatic if the angle β is close to 0. In this case the system follows the rules of a monostatic radar. PCL radar is a form of bistatic radar which utilises a IOO as the transmitter. A PCL system can be considered

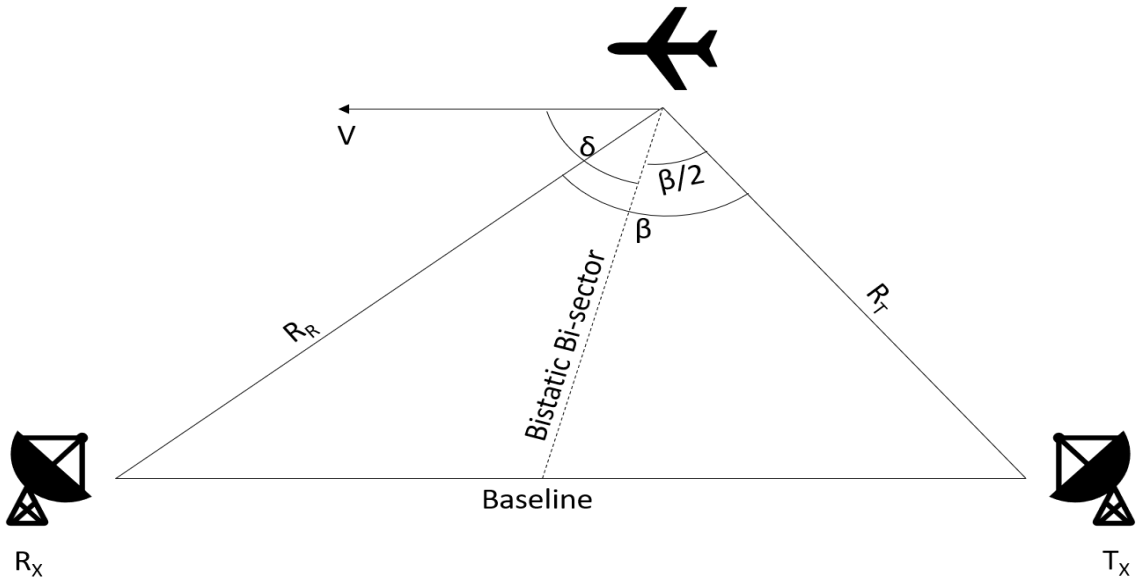

Figure 2.1: bi-static Radar Geometry

multi-static if the system has multiple baseline pairs either by having a single transmitters-multiple receivers, single receiver-multiple transmitters, or multiple receivers-multiple transmitters. The range of the bi-static radar is determined by summing the distances R_T and R_R and is known as the bi-static range. The range resolution, or the ability of the radar to separate two or more targets in range, for a bistatic radar is a function of the bandwidth and the bistatic angle described by Equation 2.1.

$$\Delta R_{\text{res}} = \frac{c}{Bcos(\beta/2)} \tag{2.1}$$

The Doppler frequency for a bistatic radar is a function of the wavelength (carrier frequency), the bistatic angle, and the angle of the velocity component of a target relative to the bistatic bisector of the bistatic radar known as δ. The bistatic bisector is the line from the centre point between the transmitter and receiver to the target. The bistatic Doppler frequency can be described as

$$f_{\text{D}} = \frac{2V}{\lambda} cos\delta cos(\frac{\beta}{2}) \tag{2.2}$$

PCL radar as a form of bi-static radar differs slightly to traditional bistatic radar as there is a third antenna system that must be taken into consideration. The receiver system of a traditional bi-static system can be split up into two parts. These are known as the reference receiver channel and the surveillance receiver channel in the PCL context. The System pair of the IOO transmitter and the surveillance channel receiver form the bi-static triangle described in Figure 2.1 above for a typical bi-static radar. The full system

description of the PCL bistatic system is given in Figure 2.2 below

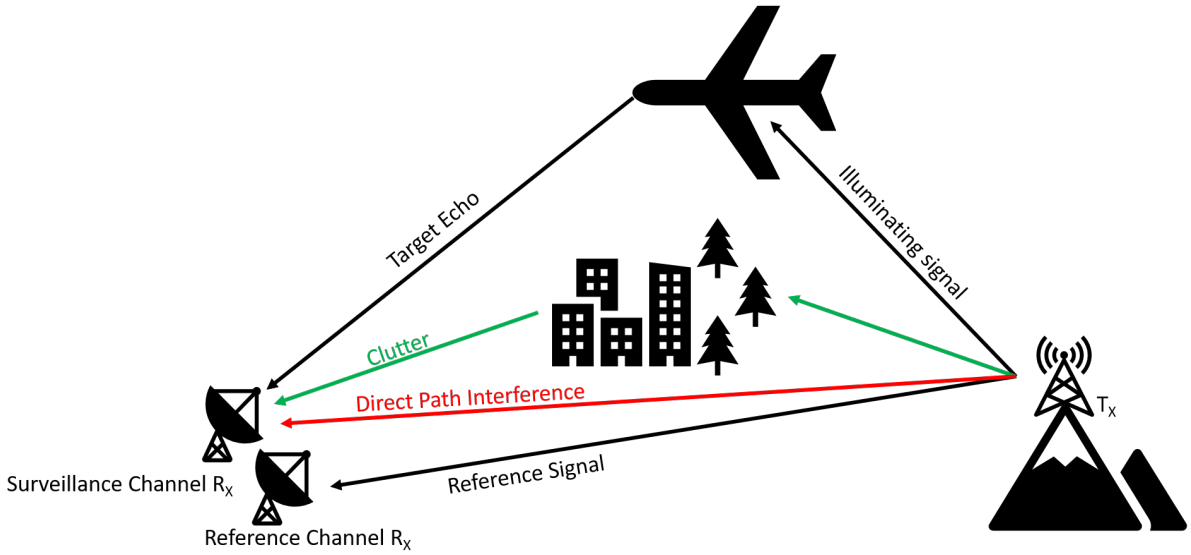

Figure 2.2: PCL bi-static Radar Geometry

Both the standard monostatic radar configuration, radar which uses a single antenna for both transmission and reception, and the traditional bistatic radar configuration utilise a copy of the signal they transmit to do a matched filter correlation between the return echo and transmit signal copy to determine the range of the target. However, as a PCL radar is not in control of the transmitted signal to do matched filter processing with the return target skin echo, it utilises the reference channel to receive the direct signal copy from the transmitter. The reference channel antenna main lobe typically faces the IOO transmitter. The reference channel and the surveillance channel are typically co-located but however, separated references have been investigated [14]. A separated reference would need to be time synchronised, i.e. using a Global Positioning Satellite Disciplined Oscillator (GPSDO) clock synchronisation, in order to do coherent processing. The surveillance channel is used to receive the target skin echos based on the transmitted signal. However due to the complex nature of the PCL radar geometry the surveillance signal also receives two unwanted signal components. These are the Direct Path Signal (DPS) which is the signal received directly from the transmitter as well as multipath component in the form of ground clutter. These two components have to be removed from the received signal as they could mask the weaker target skin echo. A typical PCL radar architecture used is given in 2.3 below

The architecture composes of the RF front-end. This includes the antenna, signal conditioning stage and ADC. The digitised data is then passed through the cancellation stage to cancel the out DPS signal in a process called direct path interference cancellation,

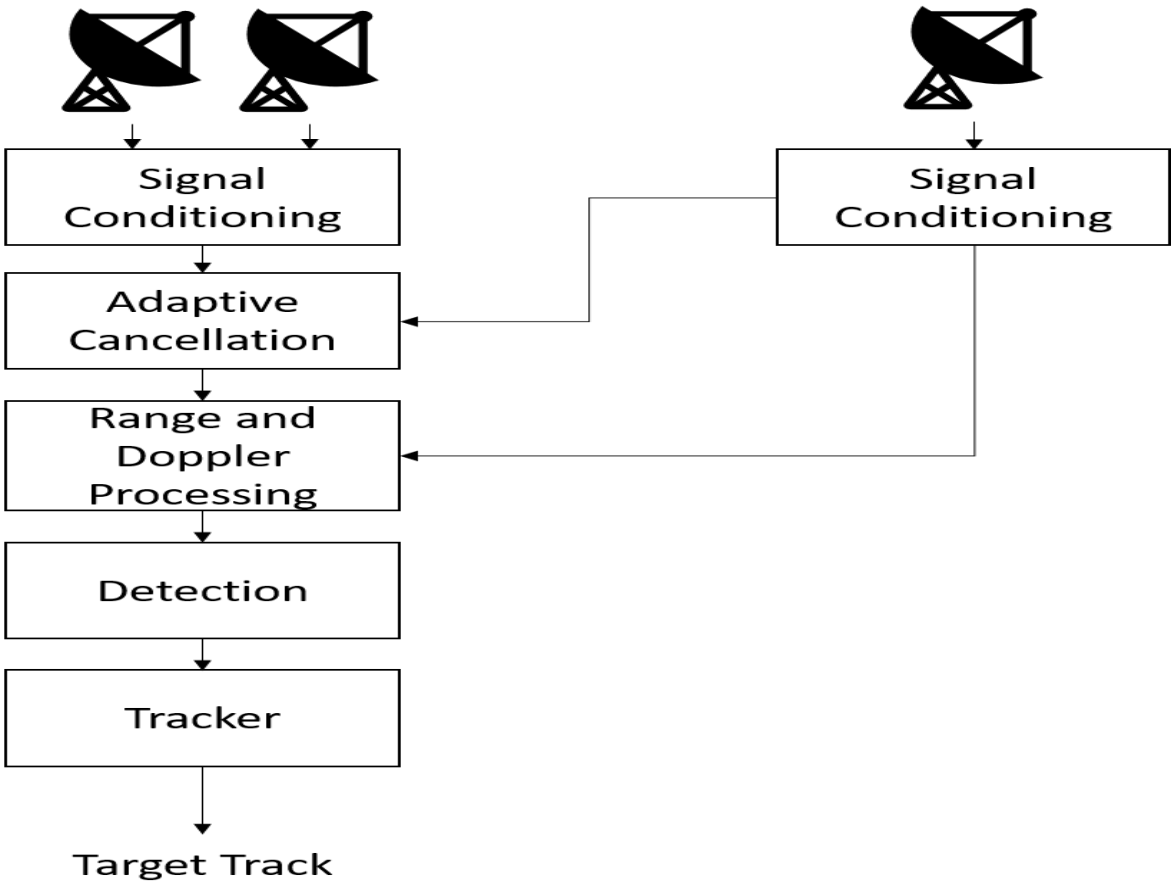

Figure 2.3: PCL Radar System Architecture

or DPI cancellation. This suppresses the multi-path clutter as well as the DPS in the surveillance channel. The "clean" surveillance is then cross correlated and Fast Fourier Transformed (FFT) with the reference signal in order to calculate the 3 dimensional cross ambiguity function, or CAF. The matrix is then passed through a detection stage which is typically a Constant False Alarm Rate (CFAR) filter to more accurately determine a target detection from a false positive. Lastly, if necessary the data can be passed onto a tracking module.

2.1.1 History of Passive Coherent Locator Radar

PCL radar has a rich history, beginning in the 1930s with the birth of radar. Most early radar systems were bistatic radars as the radar duplexer had not been built yet. In the period pre-,post- and during World War 2, or WW2, many nations such as the England, France, Germany, Japan, Canada, and the United States[15] were investigating the use of radar to gain an advantage over their adversaries. In 1935, work done by Watson-Watt on using radio signals to locate aircraft at far distances commenced after being asked to comment on reports of utilising radio waves to disable electrical ignition systems of aircraft engines or incapacitate aircraft crew due to the progress in high-power radio

transmitters at the time. He discovered that this was impossible at the time, but during this experiment alongside Arnold F. Wilkins they discovered that radio waves could be used to detect aircraft. The experiment used short-wave transmitter from the British Broadcasting Corportation ,or BBC, to illuminate a Handley Page Heyford plane. This led to development of the Chain Home radar system in 1938 [16], though this radar would be an active radar the experiment using the BBC transmitter as an IOO was one of the first recorded PCL radar experiments.

Over in Germany during the same period, a PCL system known as Kleine Heidelberg using the signals transmitted from the Chain Home Radar that were deployed on the coast of England as IOO was developed. As the system did not transmit any signal the allies were unaware of its presence.[15]

After the invention of the duplexer however most radar research would focus on monostatic radar and active bistatic radar, with radar technology being implemented in other non-defence commercial aspects such as ATC and weather radar. Interest in Passive radar would surface again with research conducted at University College London by Griffiths and Long as detailed by [17] . Their interest would focus on using analogue television as IOO. It was found however that the ADC at the time did not offer significant dynamic range due to the limited effective number of bits of the maximum 8 bit ADCs available in the 1980s.

In the 1990s research into PCL radar would continue with Griffiths et al continuing work on television based IOO however this time considering Direct Broadcast by Satellite Television (DBS TV) as possible IOO. Further work on analogue based PCL was done by [18]. Further research in PCL radar began with Sahr and Lindt looking at using FM transmitters as possible IOOs to monitor atmospheric effects[19] and Koch and Westphal looking at using global positioning system (GPS) and Global Navigation Satellite System (GLONASS) satellite transmitters[20]. Work on commercial system began at IBM, though later transferred to Lockhead Martin, with the silent sentry project. The research took 15 years and in the late 90s a system was demonstrated that used FM and television signals[21].

2.1.2 Passive Coherent Locator Radar in the Modern World

Since the turn of the century research into PCL systems increased as advancements in electronic capabilities drastically improved from the 1900s. This increase has coincided with an increase in transmitter waveform diversity in the communications area. Digital variations of FM and TV based waveforms have been introduced such as DAB, DRM, and DVB to name a few. These could potentially be utilised as possible IOOs. The next section is broken up into the continued work from early 2000s in analogue based PCL

radar such as FM and analogue TV moving into the digital based systems which utilise DVB etc. The use of analogue and digital here is merely based on the signal modulation of the transmitted waveform.

Analogue PCL Radar Systems

Interest in FM based PCL carried on with notable contributions from Griffiths and Baker[1], where they analysed the performance predictions of PCL radar looking at FM radio as well as analysing digital based GSM and DAB. In the paper they noted that the PCL radar performance is dependent on the transmitter, receiver and target location. The system is also limited by the bistatic radar Radar Cross Section (RCS), receiver noise figure and lastly the interference of the direct signal and multi-static effects. The metrics for performance prediction was based on a desirable SNR based on the radar range equation and making certain certain assumptions on the system and target. From they determined the theoretical detection ranges of PCL systems. In part two of the work they analysed the waveform characteristics of the signal taking particular note on the "self-ambiguity" of the signal to ascertain the limits of the range and Doppler resolutions of the particular wave type. Secondly they analysed the bistatic ambiguity to note the effects that transmitter and receiver locations have on the system performance. Lastly, the radar range equation for a bistatic radar with the PCL system in mind was revisited as well.

Griffiths and Baker furthered their work in waveform ambiguity by doing a comparison of analogue waveforms to their digital waveforms[3]. They noted that the analogue modulated systems in particular depended significantly on the instantaneous bandwidth program content. The ambiguity was noted to be quite poor in situations such as pauses in speech. Digital modulated systems however are much more consistent in ambiguity regardless of program content.

Howland[22] implemented a experimental radar system where they were able to demonstrate detections of aircrafts at ranges beyond 150 km in real time by optimizing the cross-correlation process of the PCL signal processing stage. Here they used a Coherent Processing Interval (CPI) of 1 second and found that the FFT stage of range and Doppler processing was a significant bottleneck of real-time operation due to the excessive processing load for long input signals. They thus proposed a modified version of the detection stage where they decimate the signal thus allowing them to discard Doppler data where the target is known not to have been before doing the FFT calculations thus speeding up the process.

Work from University of Rome "La Sapienza"[23] analysed the performance of a multi-frequency FM based PCL radar relative to a single frequency FM radar. They analysed

the benefits of a PCL system that has frequency diversity by utilising more than a single FM channel at an instance to increase the performance capabilities of FM PCL system. Six different channels were recorded and the output of each channel was incoherently added with one or more channels in order to mitigate the performance effects of the instantaneous bandwidth of an FM signal.

Colone et al[24] proposed a novel approach to DPI cancellation by proposing multi-stage processing method. The approach, the batches Extensive Cancellation Algorithm (ECA-B), applies cancellation on a set of consecutive smaller signal portions over the CPI. The algorithm was an iterative process that cancels the strongest disturbance in range and Doppler during every iteration. This allowed the cancellation of strong DPI signals from the surveillance channel which masks target echoes.

"La Sapienza" continued their work on Multi-frequency FM PCL radar and extended it to investigating a method to integrate the multi-channel signals in order to increase the Signal to Noise Ratio (SNR) and ensure system robustness with regards to instantaneous bandwidth fluctuations of the FM system. The second part of the work led to a another paper evaluating the angle of arrival, AoA, estimation for each FM channel in the multi-channel radar to enhance the performance.[25]

Research done by the University of Cape Town in FM based PCL radar began with Lange on the performance prediction and planning tool for networked PCL radar systems. Lange utilised AREPS propagation modelling software to based the prediction and planning tool[8]. The performance prediction tool analysed the effects that the environment has on the propagating electromagnetic wave in the form of SNR and signal-to-noise-plus-interference ratio coverage maps. These coverage maps could be related to the probability of detection, probability of false alarms, as well as the required dynamic range of the receiver. Heunis in 2010 then analysed the design and performance of open-source tools to detect targets using FM systems. He used the USRP-1 software defined radio, or SDR, platform with a TV tuner board as the receiver front end. Heunis also analysed the performance of different DPI cancellation algorithms[7].

Tong, continued the work on FM based passive radar at UCT and implemented a PCL radar signal processing chain directed at off-the-shelf computing hardware. He was able to show real time performance on a single high-end graphics card can be achieved on a system that has a single reference and two surveillance channels. He also illustrated that the chain implemented could do processing on 100% duty cycle of sampled data using only 25% of the resources. He also proposed a novel deployment of a separated reference and surveillance channel removing the need to have a copy of the reference signal at each receiver node, thus reducing receiver complexity[4].

Coetser then proposed a narrowband FM PCL front-end that enhances the dynamic range of the PCL system by using a sharp narrowband crystal filter as a channel select filter thus suppressing the out-of-band interference components to between 130 and 150 dBs[6]. He and Tong [9] then proposed a minimal architecture for real time PCL system utilising FM transmitters as an IOO. The system comprised of Commercial of the Shelf (COTS) RF components and Ettus N210 SDR as the digitiser. The processing chain was then implemented on an NVIDIA Jetson TK1 board to take advantage of the CUDA capable graphics processing unit, or GPU, to do real time processing. The full system cost $5260 at the time (2015) with the SDR accounting for 40% of the cost.

Digital PCL Radar System

As the world started migrating from analogue based wireless communication to digital, investigation into utilising these newer digital modulated transmissions and multiple access schemes for PCL radar picked up in the mid-to late 2000s. Of particular interest was transmissions that use the OFDM multiple access scheme as it became the more universally adopted. It is used in almost all our wireless communications today such as digital audio DAB, digital Radio DRM, digital television DVB-T/H/S, wireless LAN, LTE mobile communications 4G and many more. Covering a broad range frequencies that include VHF, UHF, as well as L, S and C band[26]. The OFDM signal structure and why it is ideal for PCL is covered in section 2.2.

In 2010 Christensen[27] presented work on mitigating the effects of range walk during processing of the radar data within the system integration time. Long integration times are ideal in PCL as the longer the integration time the finer the Doppler resolution, however the issue of range walk is prominent in DVB-T systems due to their wider bandwidths leading to finer range resolution. He proposed a solution utilising non-coherent integration and the Doppler information to limit the range walk effects.

Experimental results for OFDM WiFi-based PCL radar was presented by Falcone. Coupled with his work done on Peak Side Lobe Reduction (PSLR). In[28] Falcone et al was able to demonstrate a system that could be used for local area surveillance applications by detecting car and a person running behind it inside a parking lot.

Berizzi illustrated how the USRP SDR from Ettus could be used to realise PCL radar. DVB-T and Universal Mobile Telecommunications System (UTMS) signals was utilized to implement a multi band passive radar. Two multi band architectures was initially proposed, the first approach consisted of simultaneous usage of both bands of interest using separate channels. One channel for DVB-T another for UMTS. The second approach could only utilise a single band by utilising the SDR's ability to be reconfigurable to tune to a different frequency band[29].

Petri and Capria in collaboration with the University of Pisa proposed a method of improving the range resolution of a DVB-T based PCL system by utilising more than one DVB-T channel based on work by Conti[30]. They exploited three DVB-T channels and improved the range resolution by effectively increasing the bandwidth of system by an order of each of the number of channels recorded. This experiment provided the first step that proved passive radar imaging and target classification was be possible.

Kuschel from Fraunhofer FHR presented a multi-frequency system for medium range air surveillance. He utilised FM, DAB, and DVB-T as IOOs in the proposed system. The system benefit from the detection ranges of a FM PCL, the range resolution of the DVB-T system and the increased elevation coverage in the short to medium ranges of the DAB based IOO. Fusing this results lead to a high performance hybrid PCL[31].

In 2013 Airbus/Cassidian then went further and showed a near production stage multi-frequency mobile FM, DAB, and DVB-T based passive radar that could be used in air, ground and naval applications. The system was proposed to have 200 km diameter surveillance detection range with target location accuracy level of 100 m similar to a active air surveillance radar. It was not explicitly clear if the 100 m was standard deviation or variance. Though more work needed to be done on the fusion of data[32].

The number of commercial system PCL also saw in increase in this period. Though limited information exists on commercial PCL systems due to their inherent benefits to military applications, there are some systems known to be available in open literature. Firstly, Cassidians, now Airbus Defense and space, Parade utilises FM, DAB and DVB-T IOOs. The system was found to be able to detect commercial airlines up-to 160km from the receiver site.

The Selex AULOS passive radar system utilises FM and DVB-T IOOs. The radar uses 4 log-periodic antennas (LPDAs) for surveillance and 2 LPDAs for reference channel antennae for a fixed configuration. The deployable configuration utilised uniform circular arrays[33].

THALES and ONERA developed an FM based PCL radar that has a detection capability of about 100 km[34].

Lastly, in South Africa Peralex Electronics developed the ComRad3 DVB-T and FM based passive radar system. The FM based radar is currently planned for deployment in the Square Kilometer Array (SKA) core site in the Northern Cape province. These nodes allow the SKA-SA to reliably monitor and track targets in the airspace around the core site while avoiding potential damage to the SKA receivers that may have arisen from a traditional radar system[12].

A summary of all the known available commercial systems was summarised in the table below.

Table 2.1: Commercial Passive Radar Systems

Commercial PCL Radar Systems		
System	Manufacturer	Capability
HA-100	Thales	FM
Parade	Airbus	FM, DAB, DVB-T
AULOS	Selex	FM, DVB-T
PR-PET	ERA	FM
ComRad	Peralex	FM, DVB-T2

2.2 OFDM Signals

In this section the OFDM signal structure is detailed. The difference between DVB-T versus DVB-T2 are then discussed. The auto-ambiguity and cross ambiguity detailing the suitability of the signal for PCL usage is detailed.

OFDM stands for orthogonal frequency division multiplexing. OFDM signals contain a number of closely spaced modulated carriers that do not suffer from Inter-Signal Interference (ISI). These number of carriers (sub-carriers) are divided over the given available spectrum. The sub-carriers in that band are then spaced orthogonally from each other. This means that the peak of each sub-carrier is positioned at the null of each of the adjacent sub-carriers as shown in Figure 2.4. This sub-carrier spacing thus means that more data can be transmitted over a limited bandwidth by removing the need of a guard interval between each sub-carrier as is necessary in standard Frequency Division Multiplexing (FDM) access schemes[35].

An inverse FFT is performed on the modulated N sub-carriers (N_c) thus creating an OFDM symbol in the time domain. An OFDM transmitted frame is made up of a number of symbols (N_S). To avoid inter-symbol interference between adjacent symbols as well as to ensure that multiple reflected delayed versions of the transmitted frame do not cause interference at the receiver, a copy of a portion of a symbol is added at the beginning of every OFDM symbol. This is known as the cyclic prefix.

Each wireless communication technology that utilises OFDM such as LTE, WiFi etc. has their own unique OFDM frame structure, such as different symbol lengths that make up a frame; number of scattered pilots, continual pilots; length of cyclic prefix etc. The focus here was the DVB-T2 OFDM frame structure which is shown below in Figure 2.5. The consists of P1, P2 and data symbols. The first part of the structure are the P1

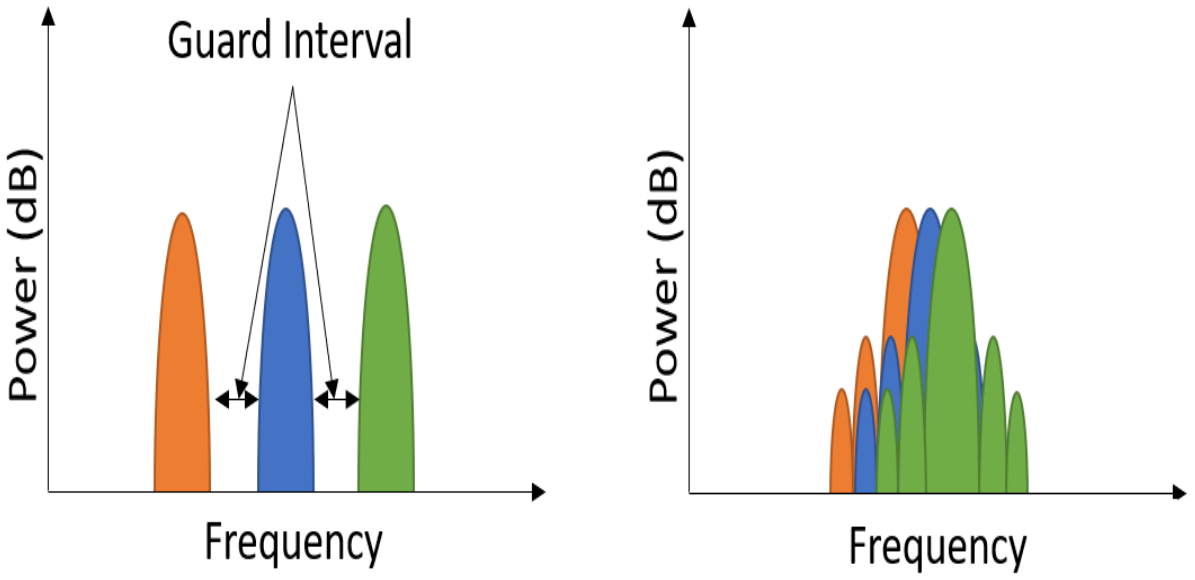

Figure 2.4: FDM Signal with Guard Intervals

symbols. This is used to synchronise the received DVB-T2 frame in time and frequency. The length of the P1 symbol is 2k OFDM symbol.

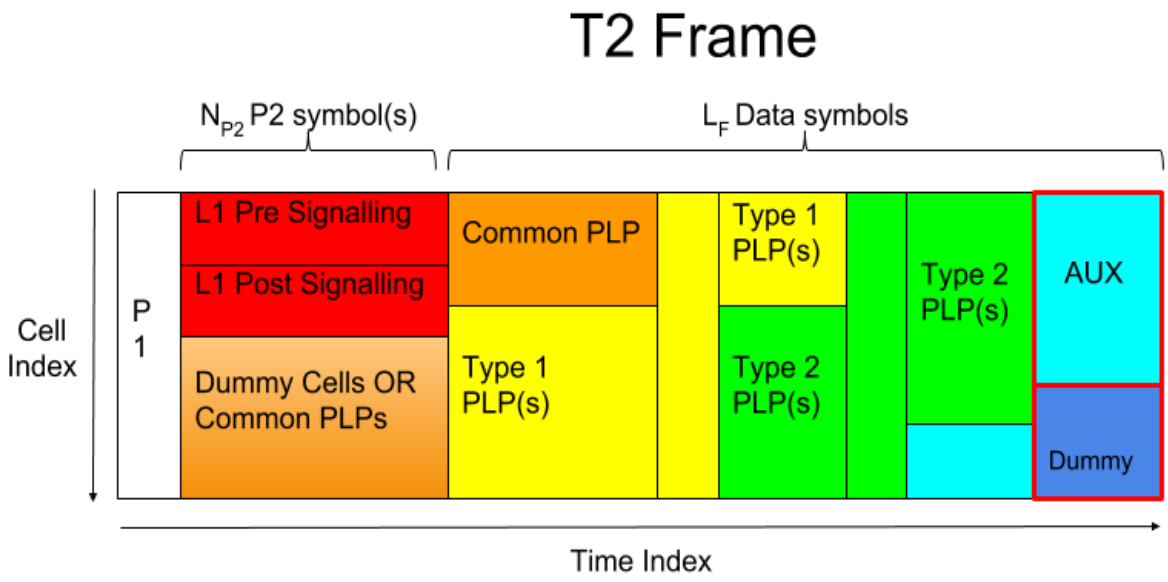

Figure 2.5: DVB-T2 OFDM Frame Structure without cyclic prefix [36, 37]

Following on from the P1 symbol is the P2 symbol. The length of the P2 symbol is dependent on the FFT size of the OFDM signal. This information can be found post detection and extraction of the P1 symbol. The P2 symbol structure is similar to a standard OFDM structure in that they contain information section and a cyclic prefix which is just a copy of the portion of the information section, similarly the data symbol as well. The two symbols, P2 and data, also contain pilot tones which are spread across the two symbols in frequency carriers and symbol indices. These pilots are used by the receiver for channel estimation, and finer time and frequency synchronisation. The P2 symbols

contain the L1-pre and L1-post signalling relevant layer 1. The P2 symbol contains along with L1 signalling layer a significant amount of pilot tones. The pilot tones found in the P2 symbol are considerably more than those found in the data symbols. Lastly, the data symbols contain the Physical Layer Pipes (PLP) and pilots.

DVB-T2 differs to DVB-T, its predecessor, in that it introduces a higher level of flexibility in its transmission. This allows for higher data rates than DVB-T as well as provides usage capabilities in a broad range of transmission environments. This complicates radar signal processing for DVB signals as the steps used for DVB-T cannot be used on the DVB-T2.

The DVB-T2 signal contains multiple OFDM symbols. These symbols arranged in a particular order form the DVB-T2 frames. A grouped number of frames together then form a super frame. The OFDM frame in the time domain can thus be expressed as[36]

$$s(t) = e^{j2\pi f_c t} \sum_{M=0}^{\infty} \{p_1(t - m, T_p) + \frac{5}{\sqrt{27xK_{\text{total}}}} \sum_{i=0}^{L_F} \sum_{k=0}^{K_{\max}-1} c_{\text{m,l}}(k) e^{j2\pi \frac{k}{T_u}(t - T_g - lxT_s - mT_F)}\} \tag{2.3}$$

where

k = Carrier number.

l = OFDM symbol number within the frame (starting from 0 at the first P2 symbol).

m = Frame number.

K_{total} = Number of transmitted carriers.

L_F = Number of symbols per frame.

T_s = Symbol duration for all symbols except the P1.

T_u = Active Guard duration.

T_g = Guard interval duration.

f_c = Carrier Frequency of the transmitted signal.

$c_{\text{m,l}}(k)$ = The modulated symbol for a carrier k of of the OFDM symbol l in T2 frame m.

l = OFDM symbol number within the frame (starting from 0 at the first P2 symbol).

m = Frame number

2.2.1 Auto-Ambiguity function of the DVB-T2 Signal

The auto Ambiguity Function (AF) is a two dimensional output of the matched filter that represents the range and velocity, in the form of Doppler frequency, resolution of a signal. For a signal r(t) the AF is expressed as[38]

$$\chi(\tau, f_D) = \int_{-\infty}^{\infty} r(t) * r^*(t-\tau) e^{j2\pi f_D t} dt \tag{2.4}$$

ambiguity function is used by radar engineers to determine the suitability of a signal for radar applications. The ambiguity function of a DVB-T2 frame is illustrated in Figure 2.6. At zero Doppler and range the ideal radar thumbtack response can be seen, however multiple undesirable peaks can be noted as well. These peaks are due to the continual and scattered pilots. The continual pilots can be seen as ridges across the range profile at fixed Doppler frequencies while scattered pilots can be seen scattered around the range-Doppler map as peaks that seem diagonal but are determined by the cyclic nature of their positioning within the DVB-T2 frame.

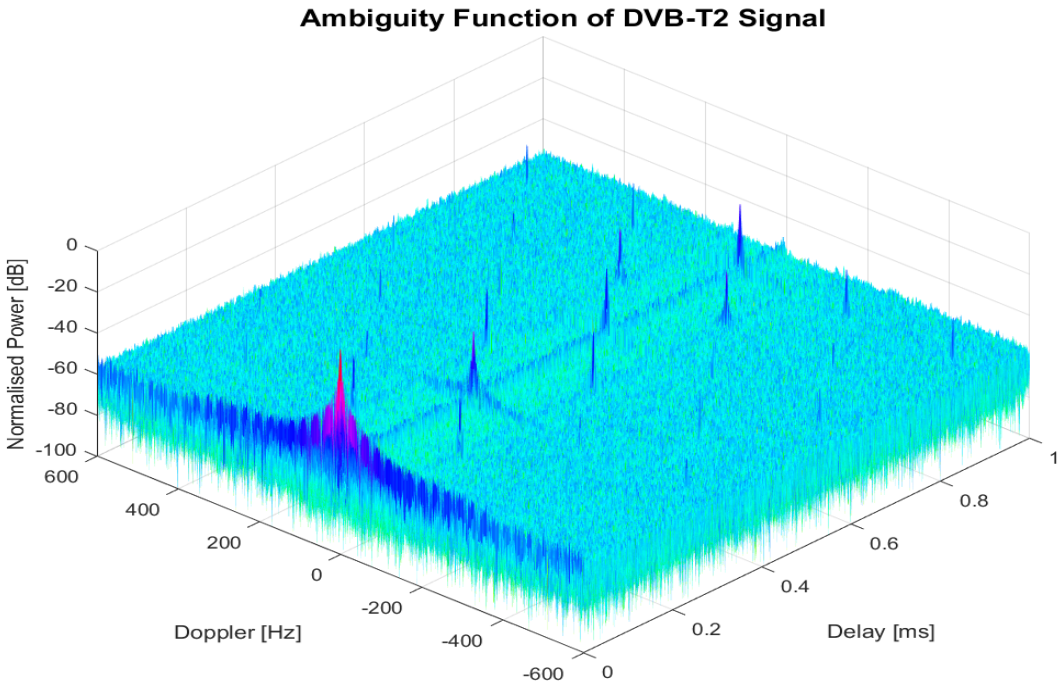

Figure 2.6: Ambiguity Function of the DVB-T Single Frame Signal

Guard intervals within a frame are simply a repetition of the end of each DVB-T2 symbol and therefore add to the periodic nature of the signal. These also result in ambiguous peaks in the AF. These, however only occur at 3.6 ms which corresponds to a range of 1000 km and thus are not considered to be an issue. The AF delay for Figure 2.6 is 1 ms which corresponds to a range of 300 km.

2.2.2 Cross Ambiguity Function of the DVB-T2 Signal

The Cross Ambiguity Function (CAF) of a signal is merely the cross correlation of the signal with another time delayed, frequency shifted, amplitude altered form of the signal. In the PCL sense, this is the cross correlation of the reference signal with the received surveillance signal. If the reference signal is described as r(t) and the surveillance signal s(t) then the cross AF is described as [38]

$$\chi(\tau, f_d) = \int_{-\infty}^{\infty} r(t) * s^*(t-\tau) e^{j2\pi f_D t} dt \tag{2.5}$$

The CAF is typically computed by taking a length of data defined by the CPI of the sampled reference and surveillance data. The CPI length determines the Doppler resolution as well as the processing gain of a practical PCL system. The CAF of a DVB-T2 signals recorded in Cape Town is shown in Figure 2.7.

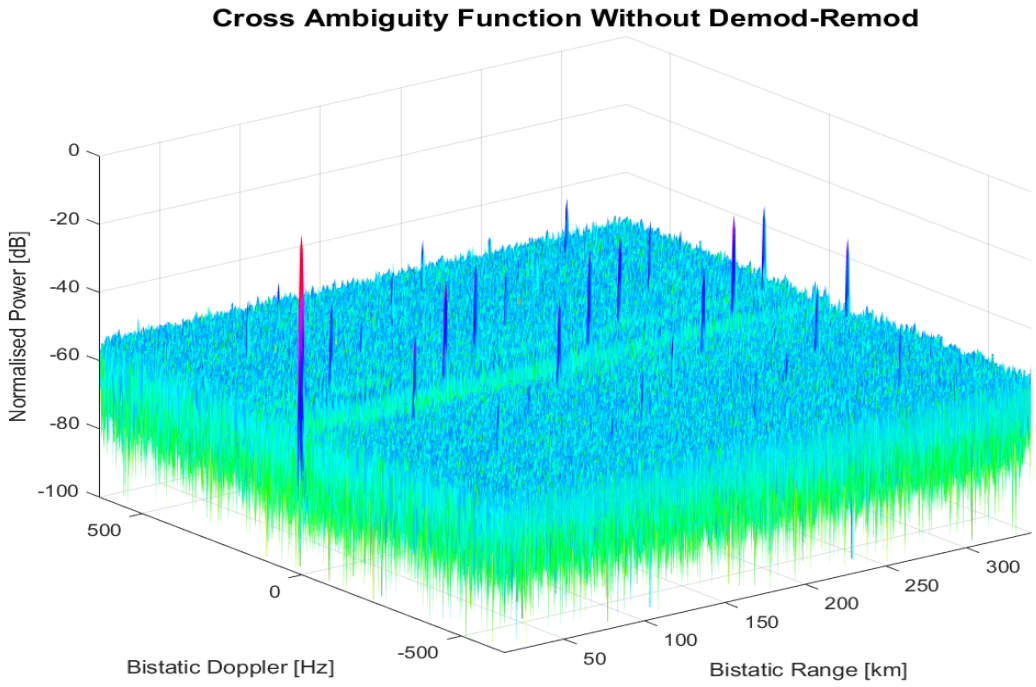

Figure 2.7: CAF of a DVB-T2 Signal

The direct path signal peak can be seen at zero range and Doppler. Ambiguities in the CAF can be seen as has been noted in the 2.6. The nature of the peaks and the direct cause are discussed in detail in Section 4.1.2.

2.3 Radar Signal Processing of OFDM Signals

In this section the proposed OFDM based radar signal processing techniques was be critiqued. The section began with the ambiguous peak removal from the OFDM signal due to pilots and guard intervals. The techniques as well as methods of detection used were covered. Lastly, the DPI cancellation methods proposed for OFDM PCL radar systems would be covered.

2.3.1 Reference Signal Processing

Gao[39] proposed a method to improve the CAF peaks by manipulating the guard interval and pilots in the reference channel. He achieved this by blanking the guard interval of the signal caused by the cyclic prefix. He then FFT'd the output of OFDM signal with zero'd guards and did two processes in parallel. In the first stage the Pilots are blanked to reduce the inter-symbol peaks, though the intra-symbol peaks are still visible to the pilots being boosted above the data symbol power. In the second stage the pilots are equalised to the data power level. This reduces the intra-symbol peaks, though the inter-symbol peaks are still visible. The CAF is calculated for both outputs of the pilot manipulation and combined to reduce the alternate residual peaks from the two stages.

In 2009 by Bongioanni[40] proposed a new method of analysing the CAF of an OFDM DVB-T signal. This method was based on the usage of a linear filter to remove unwanted peaks caused the in cross-correlation OFDM signals due to the knowledge of the expected value of the DVB-T AF. The tests were shown to provide better and/or similar performance to other earlier mechanism proposed with reduction in computational load and system complexity relative to Goa's method as the process only required a single stage of processing before the CAF is calculated rather than the multiple stages of Goa's. It should be noted however that Bongioanni only applied the technique on simulated data at the time.

In 2011, Conti proposed a method of pre-processing a DVB-T multi-channel PCL system. Three adjacent channels were received by a wideband receiver and a single DVB-T channel was then extracted and pre-processed[28]. The pre-processing filter to reduce the ambiguous peaks is based on the estimation of the Power Spectral Density (PSD) of the DVB-T signal and of the PSD of a simulated DVB-T signal composed of random components. The pre-processed channels are then recombined again to form a multichannel DVB-T signal. Through this method they were able to demonstrate side peak reduction of approximately 30 dBs in multi-channel DVB-T signals.

Palmer in 2013 then proposed a method similar to that of Gao but on an 8K mode

DVB-T signal applied to real data[41]. However, unlike Goa there was not a three stage manipulation of the guards and pilot. The proposed method of Palmer is the Demod-Remod process where the reference is demodulated, getting all the information of the OFDM frame. Then remodulating the signal with altered guards and pilots to create a mismatched signal to the original reference and calculating the CAF with the new mismatched reference rather than a matched reference signal. This process eliminates the peaks in the CAF during the cross-correlation of the reference with the surveillance channel. Using this process he was able to demonstrate 29dB reduction in residual peaks relative to previously mentioned mismatched methods as well as greater than 36dB in reduction relative to match filter process.

O'Hagan and Setsubi[42] applied a similar approach as Palmer, however this was applied to DVB-T2 signals as opposed to DVB-T signals. The method proposed by Setsubi was the method used in ambiguous peak manipulation in this dissertation. The full process is discussed in section 4.

2.3.2 Direct Path Interference & Clutter Cancellation

To mitigate the effects of the direct signal leaking into the surveillance channel masking the weaker target skin echoes. A number of techniques have been proposed to mitigate this effects. The main approach proposed is the adaptive filter method. Palmer[2] summarises the different adaptive filter algorithms applied to real DVB-T data. He found the Wiener filter methods performed best in terms of computational cost to interference reduction performance.

Tong[4] compared the ECA algorithm to the conjugate gradient least squared algorithm and found that the Conjugate Gradient Least Squares (CGLS) was better suited for real time processing.

2.4 Summary

In this section the history of PCL radar from the first earliest recorded trials to the first known commercial system was covered. Next, the recent research into PCL system was covered in focusing specifically at the different types of wireless communication technologies that have been used as IOOs for PCL radar. The OFDM signal structure and ambiguity functions for radar usage was covered next. Lastly, the processing of OFDM signals was analysed and different techniques illustrated.

Chapter 3

DVB-T2 Front-end Receiver Design

In this chapter the detailed design of the front-end of the PCL system was discussed. The section begins by detailing the system planning. This covers the transmitter information available in Cape Town such as transmitter power, carrier frequency available, and the location of the transmitter. This is to determine system performance based on the transmitter information and to aid in the receiver design. Propagation modelling is then done on Advanced Refractive Effects Prediction System (AREPS) factoring in the terrain of the region of operation. AREPS software package allows for an accurate modelling of the EM waves propagating in a particular region based on the environmental information provided by the user.

The design of the RF front-end is then covered based on the system planning analysis. This detailed the whole receiver chain from the antenna down to the ADC of choice. A two channel PCL system, one reference and one surveillance, was proposed.

3.1 System Planning

Before any PCL system can be designed or deployed, information on the available transmitter required. The PCL radar's performance is highly dependent on the system geometry. As such a study needed to be done that factors in the available IOOs in the region, the terrain of the environment, and propagation effects. The propagation effects of the transmitted signal could include multipath, diffraction, refraction, and atmospheric absorption.

3.1.1 Transmitter Coverage

Spectrum regulation and licensing is facilitated by the Independent Communications Authority of South Africa (ICASA) in South Africa. They ensure that the frequency

plans and signal power levels are consistent with the international standards set by the International Telecommunications Authority(ITU)[43]. South Africa falls under region one of the ITU-R radio regions along with Western Europe and the African continent. The ITU had set a deadline of 17 June 2015 for migration from analogue television to digital for all countries other than a select few within the UHF band (470 - 862 MHz) in a conference in 2006. ICASA then released a Government Gazette detailing the plans for spectrum within the VHF (87.5 - 23 8MHz) and UHF bands in 2013, the "Draft Terrestrial Broadcasting Frequency Plan 2013" document. The frequency bands allocated for digital television are thus summarised in Table 3.1.

Table 3.1: Frequency Bands of Digital Televion

Frequency Bands (MHz)	Band Number	Number of Channels	Channel Width
VHF(174-214)	III	5	8 MHz
UHF(470 - 854)	IV&V	47	8 MHz

The VHF band of the for DVB-T2 would only go live after the analogue switch over (ASO). Although the stipulated date was June 2015, South Africa missed it's deadline and thus at the time of writing, the VHF transmission wasn't live and analogue signals remain live in majority of the country. However, transmission of DVB-T2 signals are live in the major cities of the country in the UHF band. In the Cape Town area specifically there were three bands selected for transmission pre-ASO. This project was specifically focusing on the UHF band as that's the predominant band for DVB-T2 transmissions. The choice of transmitter as an IOO would thus be based on these criteria for optimum performance of the PCL system:

- Transmitter line of sight(LOS) to receiver site
- Location of Transmitter
- Effective Radiated Power
- Geometry with respects to the receiver and target flight paths

The receiver location would be the University of Cape Town's Menzies building. Figure 3.1 illustrates the transmitters in the Cape Town region (yellow markers), receiver site(UCT red marker) and the surveillance area Cape Town International Airport (aircraft). The area of interest from UCT is illustrated with the red arrows covering the north and south flight paths.

The there were possibly two transmitters that could be used as IOOs based on the terrain and transmitter location. These are the Constantiaberg transmitter and the Tygerberg

Figure 3.1: DVB-T2 Transmitters Cape Town

transmitter. These have direct line of site with the receiver site as well as the region of surveillance. The baselines of both transmitters to the receiver site are shown in Figure 3.2.

The Constantiaberg baseline is 12.6 km and the Tygerberg baseline is 15.6 km and is shown as the red lines from the receiver site to each individual transmitter. Due to DVB-T2 transmissions being on a Single Frequency Network (SFN), all DVB-T2 signals transmit at the same frequency. In analogue systems this would provide a problem as the echo signals of the transmitted signal would add up constructively and destructively at the receiver causing interference that would render the signal unusable. DVB-T2 systems have guard intervals and forward error correction techniques that mitigate the effects of the interference. The specifications of each transmitter in the UHF band are summarised in Table 3.2.

Table 3.2: Transmitter Specifications

Transmitter	Carrier Frequency (MHz)	Band Number	ERP (kW)	Polarization
Constantiaberg	562	32	50	Horizontal
	610	38	50	Horizontal
	706	50	50	Horizontal
Tygerberg	562	32	50	Vertical
	610	38	50	Vertical
	706	50	50	Vertical

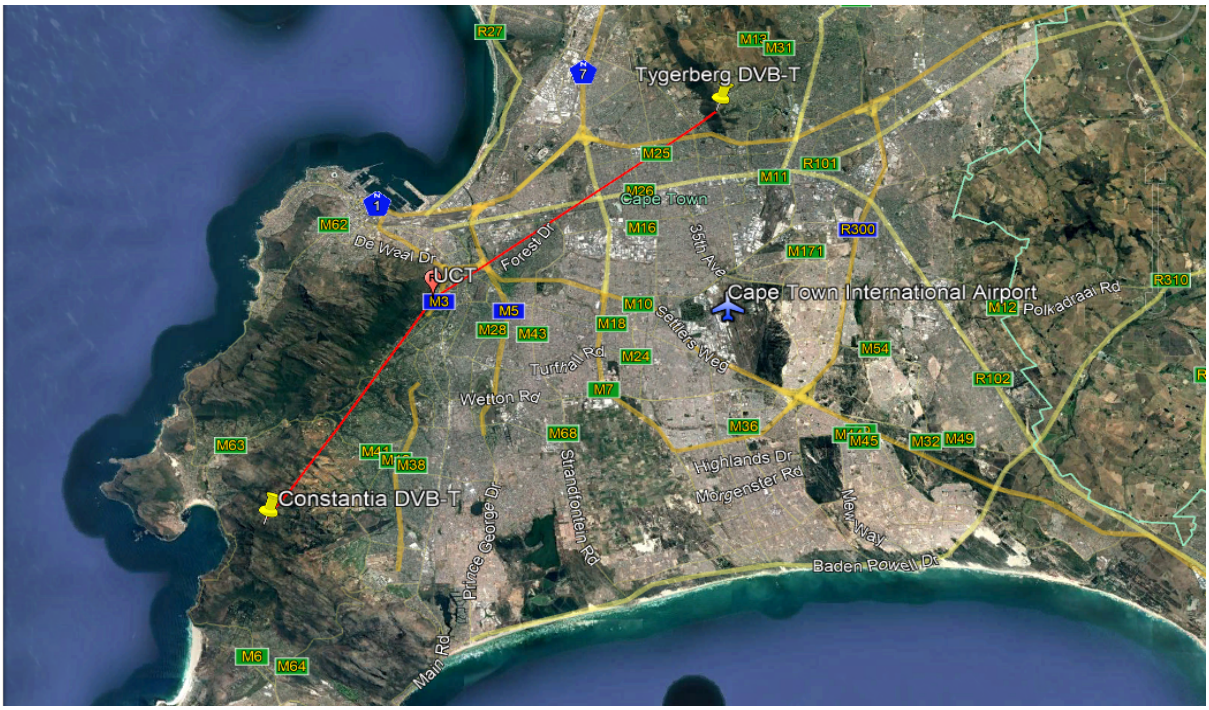

Figure 3.2: Potential IOO baselines

Transmitter Characteristics

It is important to note the expected power to the receive site as this has serious implications to the PCL radar's performance. The stronger the signal the more processing required to suppress the DPS on the surveillance channel the importance of which is covered in Section 4.1.1. The strong signal also has the potential to mask the weaker target echo. The expected received power from both the Constantiaberg and Tygerberg transmitter were calculated using the Friis transmission equation described as[44]

$$P_r(dBm) = G_r(dB) + P_t(dBm) + 10\log(\frac{\lambda^2}{4 * \pi}) - 10\log(4\pi R^2) \tag{3.1}$$

Equation 3.1 calculates the received power based on the transmitter power and the free space path loss over a distance R in meters. The gain of the receiver antenna used was 13.3 dBi. Using the transmitter information given in table 3.2 to determine the transmitted power and carrier frequency, the wavelength was calculated as $\lambda = \frac{c}{f_c}$ where c is the speed of light and f_c is the carrier frequency of the signal. Using the receiver antenna, the transmitted signal was then measured to be compared with the expected power. The antenna was setup at top of the roof of the Menzies building of UCT. The spectrum of the UHF band for both the Tygerberg and Constantiaberg transmitters are shown in Figure 3.3. Two of the three channels were transmitting when the recordings were taken. These were at 610 MHz and 706 MHz. The other digital broadcast in the 500 MHz band was the DVB-H transmission at 530 MHz, which is a mobile digital

video standard. Constantiaberg has less in band transmission of the two spectrums with only out-of-band analogue transmissions at above 764 MHz,whilst Tygerberg had some in-band transmissions from 470 to 680 MHz.

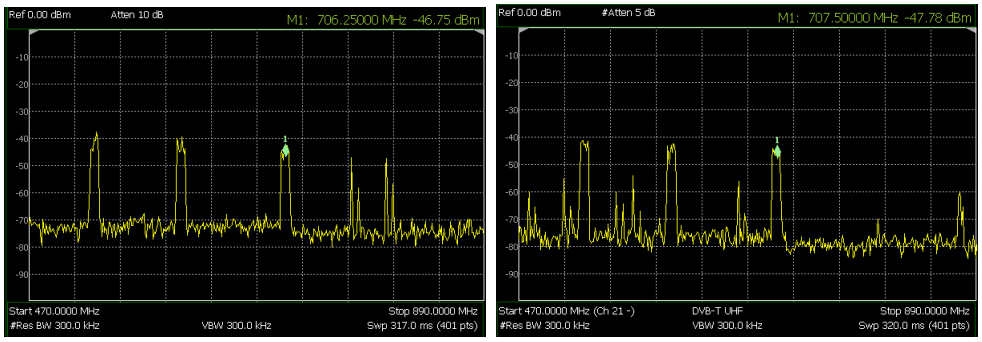

(a) Spectrum of the DVB-T2 from Constantiaberg Transmitter

(b) Spectrum of the DVB-T2 from Tygerberg Transmitter

Figure 3.3: Spectrum of the DVB-T2 UHF Band Broadcast Measured from UCT

The power measured in Figure 3.3 for each transmitter using a spectrum analyser is the integrated power within the Resolution Bandwidth (RBW). Thus the narrower the bandwidth the lower the integrated power measured. For analogue systems this was typically accurate as most spectrum analysers had RBWs that could go up to 2MHz, however digital based transmissions have bandwidths that far exceed the RBWs of most spectrum analysers and the integrated power in a RBW would have to be converted to the channel power where the channel is the bandwidth of the measured signal. This can be done by calculating the channel bandwidth as[45]

$$P_{ch} = (\frac{B}{B_n})(\frac{1}{N}) \sum_{i=n1}^{n2} 10^{\frac{P_i}{10}}$$

where P_{ch} is the channel power, B_s is the signal and/or specified bandwidth, b_n is the resolution bandwidth, N is the number of data points in the summation, P_i is the sample of the power in measurement cell i in dBm units. n1 and n2 are the end-points for the index i within the specified bandwidth, such that $N = (n2 - n1)+1$. An example of the channel power relative to the signal power at 706 MHz for an RBW of 7.5 kHz for Constantiaberg and Tygerberg is given in Figure 3.4 where the bandwidth was the effective bandwidth of a DVB-T/T2 signal of 7.61 MHz. The RBW power level for Constiantiaberg and Tygerberg is -75 and -77 dBm respectively and the corresponding channel power is -34.66 and -36.65 dBm.

Thus the expected power at the receiver based on the transmitted Effective Radiated Power (ERP) for DVB-T transmission and compared with the actual measured channel power from the top of the Menzies building is summarised as

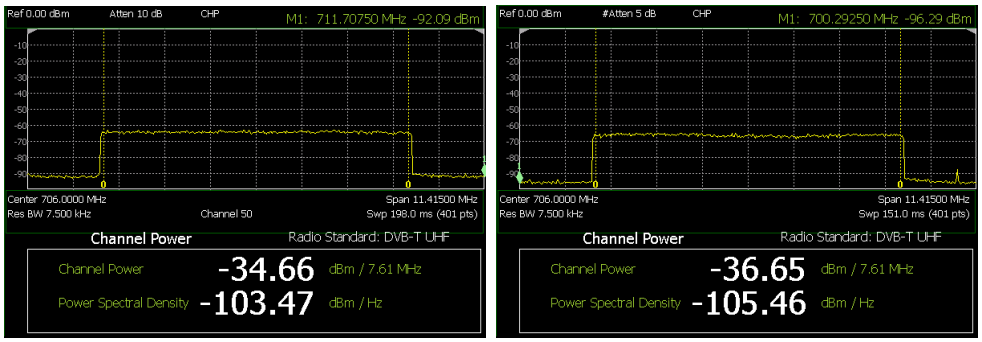

(a) Channel Power of the DVB-T2 signal at 706 MHz from Constantiaberg Transmitter

(b) Channel Power of the DVB-T2 signal at 706 MHz from Tygerberg Transmitter

Figure 3.4: Channel Power of the DVB-T2 signal at 706 MHz Broadcast Measured from UCT

Table 3.3: Received and expected signal strength

Transmitter	Carrier Frequency (MHz)	Expected Result (dBm)	Measured Result (dBm)
Constantiaberg	610	-19.8661	-32.71
	706	-21.1356	-34.66
Tygerberg	610	-21.7212	-33.74
	706	-22.9907-	-36.65

The difference of 12 - 13 dBs in signal power between the expected and measured can be explained by the environmental effects, beam pattern and propagation losses described in the preceding section.

3.1.2 Propagation Modelling

Carrying on from the transmitter selection, propagation modelling was done in the region of operation for the PCL system. Both transmitters were simulated to determine the propagation effects of the direct path signal and determining the range that the receiver can view relative to the area of interest. The propagation wave modelling was done using the Advanced Propagation Model as based on Lange's[8] PCL radar performance predictor. The AREPS software calculates the propagation factor, F, which is defined as the ratio of actual electric field strength created at a point in space to the field strength that would have been created by the same system operating in free space, with the beam of the transmitter directed towards the point[46]. This can be described as

$$F = \frac{|E|}{|E_0|} \tag{3.2}$$

where $|E_0|$ is the magnitude of the electric field under free-space conditions, and $|E|$ is the

magnitude of the field to be investigated at the same point. From the propagation factor the propagation loss can be determined based on environmental effects such as refraction, diffraction, multipath effects, and atmospheric absorption. The total propagation loss would then be determined by subtracting the propagation factor from the free space path loss as given by

$$L = L_{\text{fs}} - 20\log_{10}(F) \tag{3.3}$$

where F is the propagation factor, L_{fs} the free space path loss and L is the real propagation loss. Other factors to consider that effect the PCL radar performance with respects to the broadcast transmitter and propagation effects are the elevation antenna beam pattern and beam tilt of broadcast antennas as described by work from O'Hagan et al[47]. Broadcast transmitter azimuth patterns are usually omnidirectional or have wide enough to provide coverage over a wide area. The elevation pattern however is highly directive with the main lobe tilted downwards to maximise service to the population below. An example of the the scenario is shown in Figure 3.5. The main beam is tilted down and the target is moving at a height above the main lobe and migrating through the side lobes.

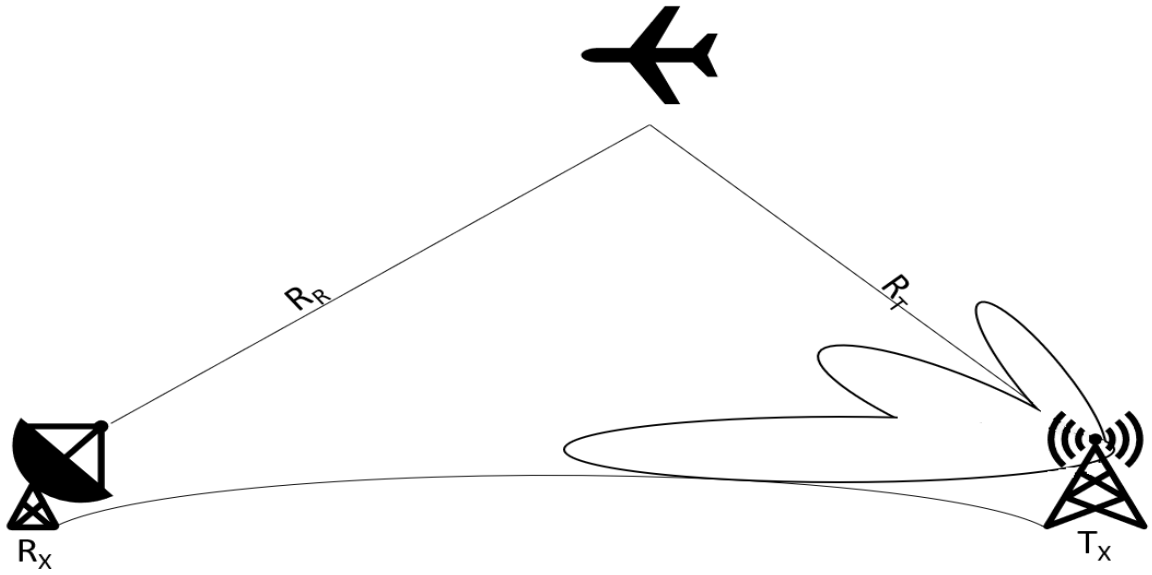

Figure 3.5: Elevation Pattern of Broadcast antenna

At UHF band transmissions are usually line of sight(LOS) to the receiver. This means that the transmitter radio waves travel directly from the transmitting element to the receiving element with minimal or clear propagation path. This typically implies that the coverage is limited to well within 120 km from the transmitter depending on height of the transmitter and the receiver. This is due to the fact that UHF signals cannot travel over the horizon and are blocked by hills[47]. This The RF transmissions typically bend downwards as it traverses along the earth's atmosphere due to the refractive index of the

troposphere and then by the ionosphere. Refraction is the ability of a medium to bend the an electromagnetic wave as it passes through the medium[48]. This phenomena is illustrated in Figure 3.6.

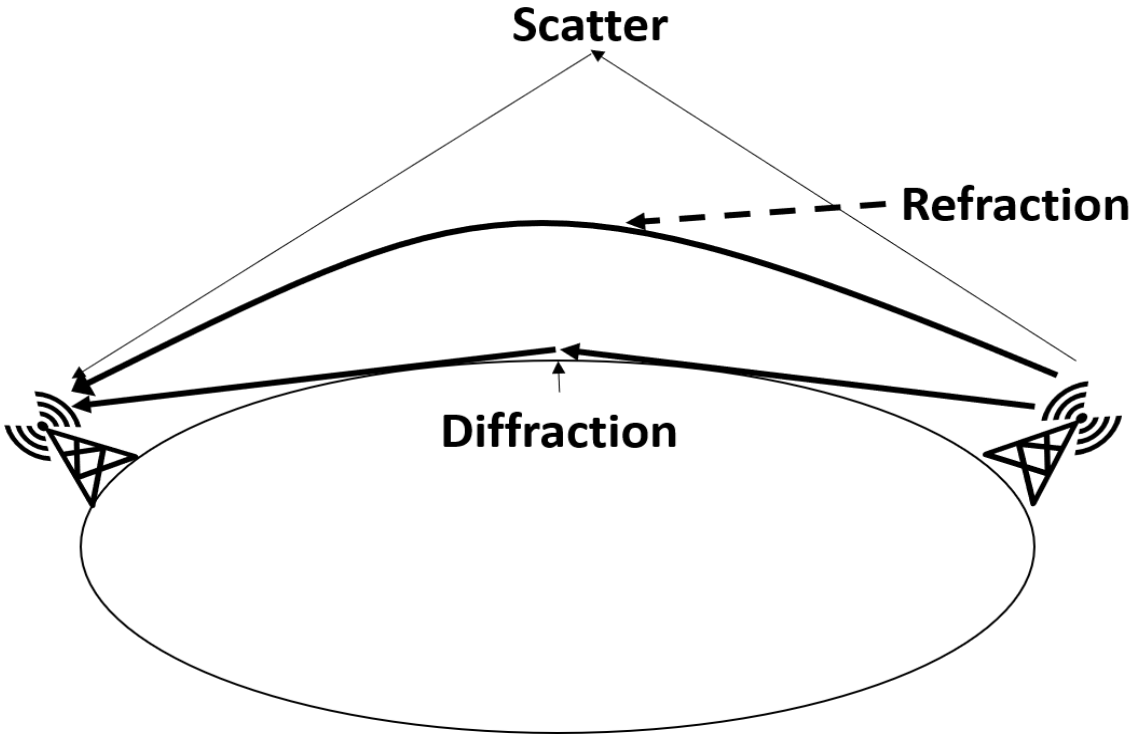

Figure 3.6: Refraction

Due to the terrain environment of the Cape Town area another phenomena of interest is diffraction of the propagating wave due to the numerous mountains that surround the Cape Town area. Diffraction is the process by which the direction of the propagating wave is changed such that it spreads into the geometric shadow region of an opaque or refractive object that lies in the radiation field [48]. The ability of the propagating wave to diffract is dependent on the frequency of the wave. The lower the frequency, the more the wave is diffracted. One form of diffraction is knife edge diffraction, which is the propagation where the wave is bent around sharp edges. The effects of sharp edge diffraction is shown in Figure 3.7.

Cape Town has a Mediterranean climate, ranging from wet winters with strong precipitation and strong winds in winter to warm dry summers. However, atmospheric attenuation is almost negligible at lower frequencies. It is more significant in the microwave bands especially frequencies that exceed 10 GHz. At UHF, where television transmissions typically lie, the two way atmospheric attenuation is less than 0.01 dB/km becoming even less as the altitude increases. Thus, attenuation decreases with increase in elevation angle with attenuation above 10 km generally negligible with not much change either in high precipitation environments. Typically, losses due to rain or water molecules in the atmosphere at frequencies under 1 GHz are generally neglected.

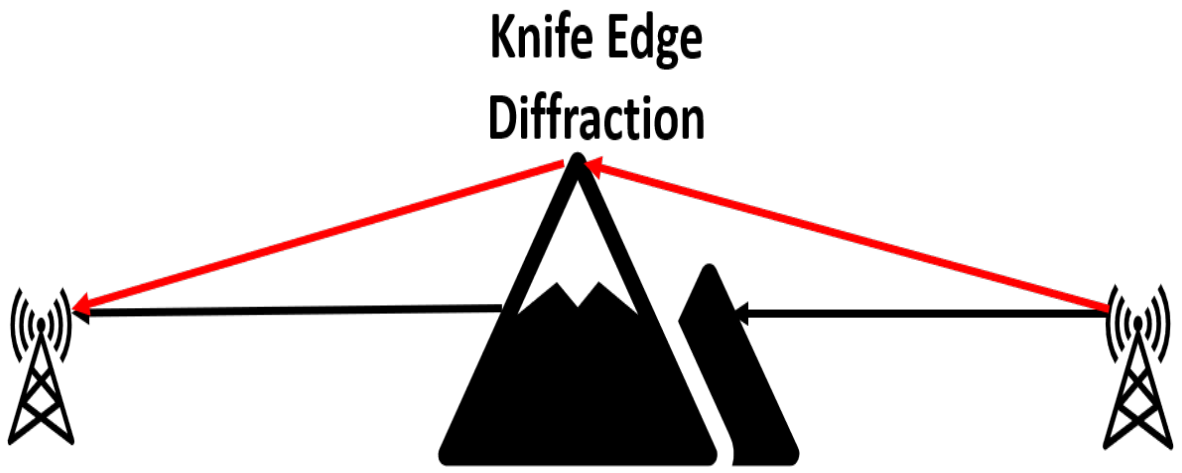

Figure 3.7: Knife-edge diffraction

AREPS Simulations

AREPS uses Digital Terrain Elevation Data(DTED) by default. DTED is a uniform matrix of terain elevation, values, providing basic quantitative data for systems that require terrain elevation, slope and/or gross surface roughness information. The terrain data used in the AREPS simulations is DTED level 1 format and corresponds to 100 m of horizontal resolution. The transmitter information was input into the AREPS data base based on section 3.1.1 parameters. The transmitter antenna pattern was based on the DVB-T/T2 elevation pattern in [47] for an 8 bay antenna was simulated, however for a transmitter power of 50 kW as is used by the two transmitters. The elevation pattern is shown in Figure 3.8.

The field pattern has an half power beamwidth of around -3 dB and the beam tilt of the elevation is approximately -1°. For a aircraft that would be flying at cruising altitude, approximately 10 km, the aircraft would be flying outside of the main lobe beam but would potentially be migrating across multiple sidelobes as seen in Figure 3.9.

AREPS outputs a text file with the propagation loss data with the loss data given in table form for each bearing. The bearing describes the angle in degrees from the transmitter to receiver relative to true north (0°). The table describes height on the Y-axis of the table and the range on the X-axis. Selecting the cell with the corresponding height and range specified for the receiver site the propagation value can be obtained.

The AREPS simulation for the antenna elevation beam pattern for the Constantiaberg transmitter in the direction of the receiver site is shown in Figure 3.10. The transmitter is on the top of the mountain at position 0 km. The receiver site in this instance relative to

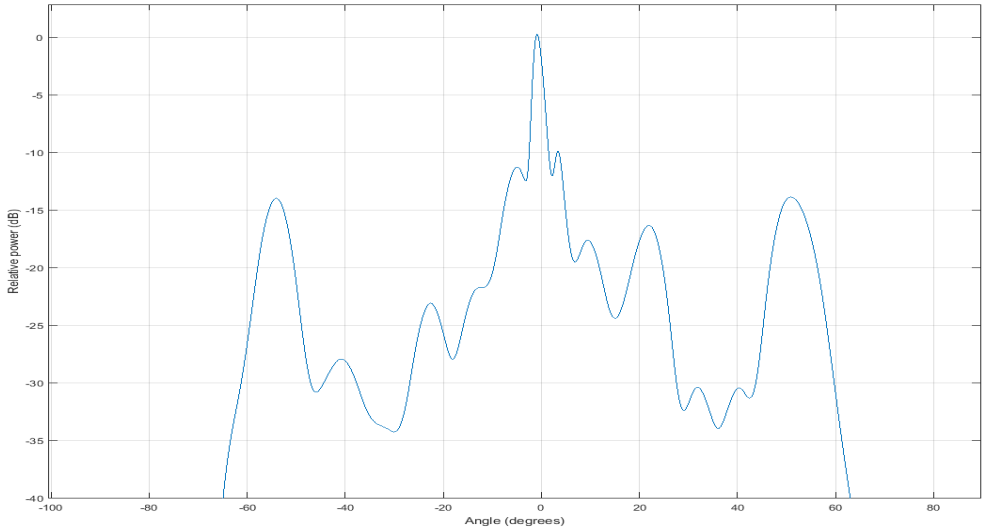

Figure 3.8: 8 bay DVB-T/T2 Elevation Antenna Pattern

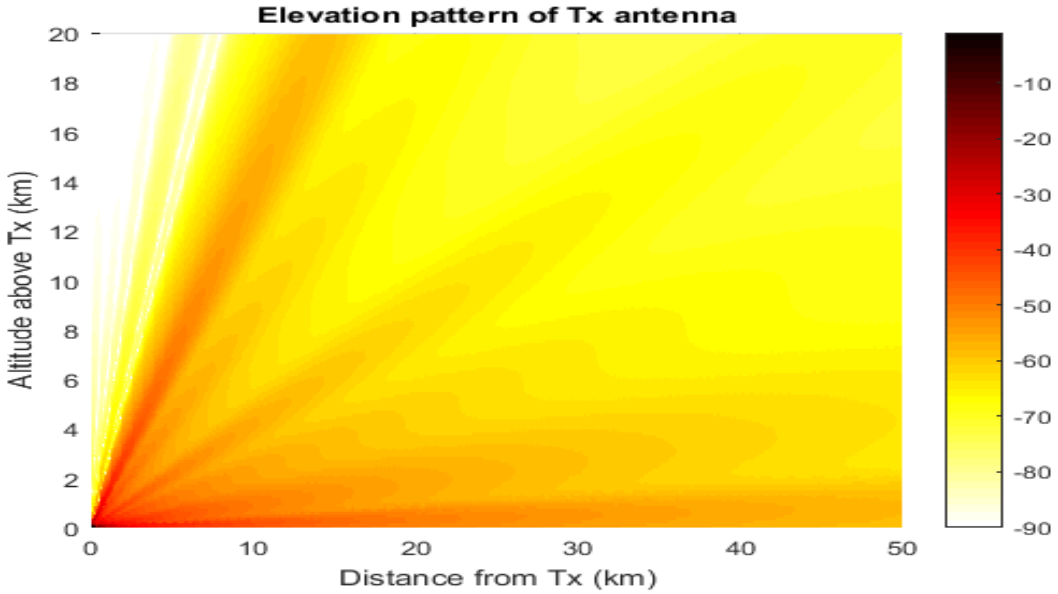

Figure 3.9: Transmitter power density-density plot in dBw/m^2 of the 8-bay DVB-T/T2 antenna with transmitter power set to 50 kW

the Constantiaberg transmitter is 12.6 km away, at an altitude of 140 m. The propagation factor at that distance and height is noted as -6.5 dB and thus the propagation loss amounts to 99.5 dB relative to the free space path loss that was calculated as 93 dB for the same location. The free space propagation loss doesn't take into consideration of the environment, beam pattern, and or configuration of the transmitter-receiver pairs, however from the plot it can be seen that the transmitter has direct line of site with the receiver site and no natural obstacles occur in between and thus a propagation factor of -6.5 dB is to be expected. Similar the simulations were run for the Tygerberg transmitter, using the same transmit powers and antenna beam patterns. The propagation factor for the Tygerberg transmitter was 2 dB and thus the propagation loss was calculated as 93 dB. The difference between the two transmitters is that the Constantiaberg path has a slight mountainous ridges in the path at around 4-8 km from the transmitter due to table mountain on the left of the signal path as seen in Figure 3.2, whereas the Tygerberg path is essentially clear.

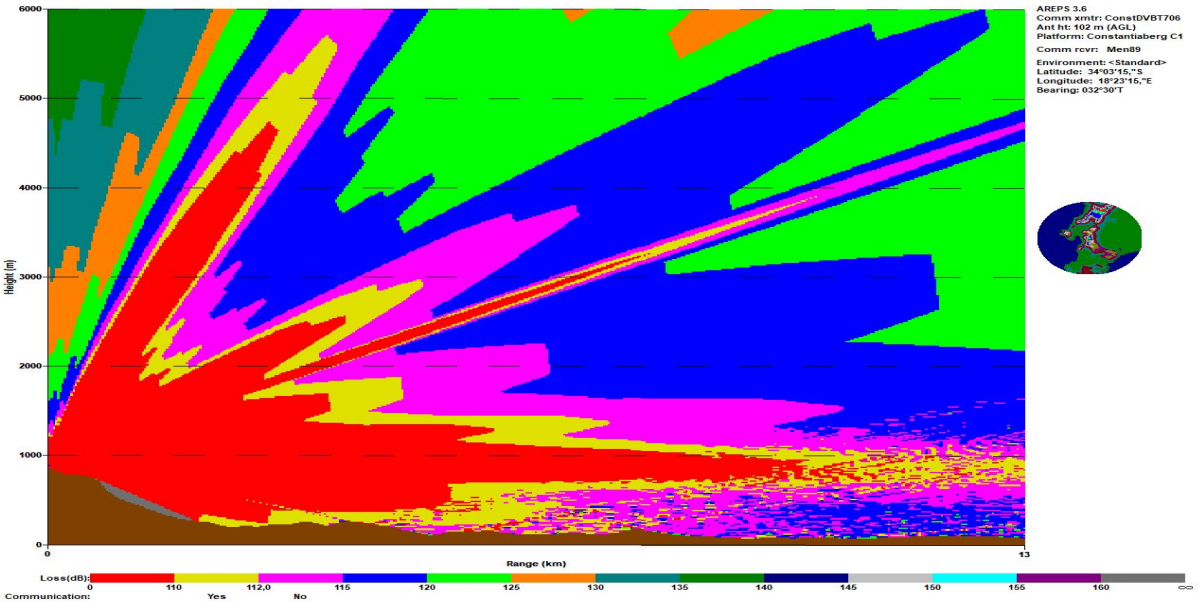

Figure 3.10: Constantiaberg Transmitter Propagation loss AREPS plot

3.1.3 Summary

The propagation effects described can explain the differences in signal power between the expected and the received power from the previous section. The Constantiaberg transmitter was chosen as the IOO. The Tygerberg transmitter had limitations relative to the receive sight such as the flight paths of the aircraft from the north side. The surveillance channel would require more processing power in the DPI cancellation due to the channel possibly staring in the same path as the direct signal and in some instances targets might be flying directly over or close to the Tygerberg transmitter. In this case, the target would be masked by a stronger DPI component. Also in the case where the

targets are flying above the transmitter they could not be illuminated. These examples are illustrated by the truth data taken from automatic dependent surveillance - broadcast, or ADS-B, receiver for three aircraft flying in and out of Cape Town International from the north at different instances in Figure 3.11. The flight paths are shown in red, green and yellow to differentiate between the three flights. All three fly close to the transmitter with the blue flight flying across and almost above the transmitter. Thus, the Constantiaberg transmitter is the better choice of the two and was used for the rest of this dissertation onwards at 706 MHz. The frequency in this instant was arbitrarily chosen.

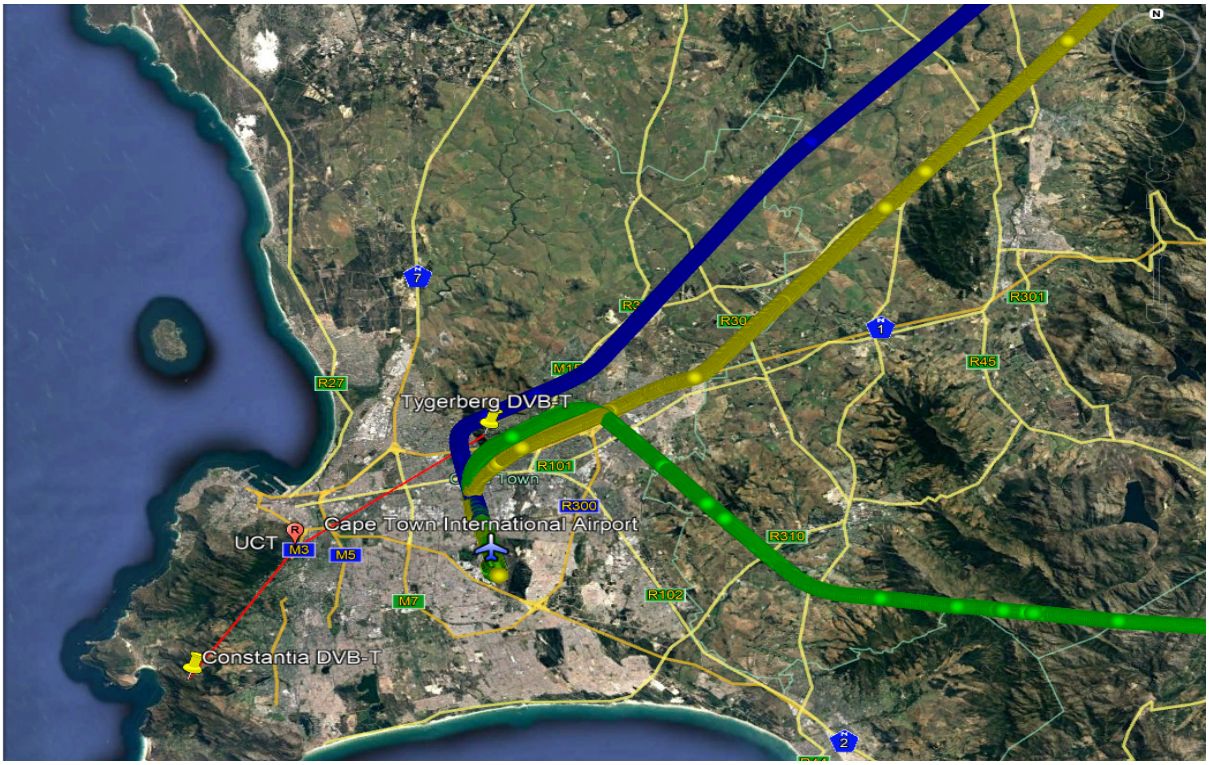

Figure 3.11: Northern Flight path from or to the Cape Town International Airport

3.2 RF Front-end Design

This section covered the design, simulation and implementation of the receiver front-end of the PCL radar. The proposed receiver chain composes of antenna, amplifiers, filters, a heterodyne stage and ADC. The proposed signal conditioning RF receiver stage was designed, however due to financial constraints, signal conditioning components could not be procured and the ADC could only be procured. Thus, to complete the project in the allocated time, design considerations had to be made and the heterodyne and ADC components were prioritised. The section was divided into the antenna and signal conditioning section, heterodyne stage and finally a two channel radar implementation.

3.2.1 System Requirements

As stated in Section 1.2.3, the following requirements need to be met by the Front-end system:

- 2 Channel UHF Front-end Receiver
- Fully Coherent Receiver Sampling Single DVB-T2 UHF Channel
- High Dynamic Range

3.2.2 Antenna

The antenna required for this project would need to be directional and have high gain within the region of interest. This is due to the fact that PCL radar performance is highly dependent on the geometry of the system. This is especially true in the mitigation of DPI on the front-end as the null (part of antenna with least gain) can be directed in the direction of the transmitter thus easing the DPI cancellation requirements of the back-end processing.

The antennas used were commercial television bow-tie grid reflector antennas produced by a local company, Ellies[49]. The antenna used can been seen in Figure 3.12 to have four bow-tie phased array radiators with a grid reflector. The antenna specifications are summarised in table 3.4. The antenna was shown to have decent directivity and good gain over the band of interest. The antenna was also shown to have 27dB of H - V polarization. This is ideal to suppress the DPS of the Tygerberg transmitters since DVB-T2 transmission operate in single frequency networks. The antenna was shown to have a nulls at both 90°and 270°in azimuth direction as seen in 3.13. These can provide signal suppression of approximately 20 - 25 dBs at frequencies between 500 - 700 MHz.

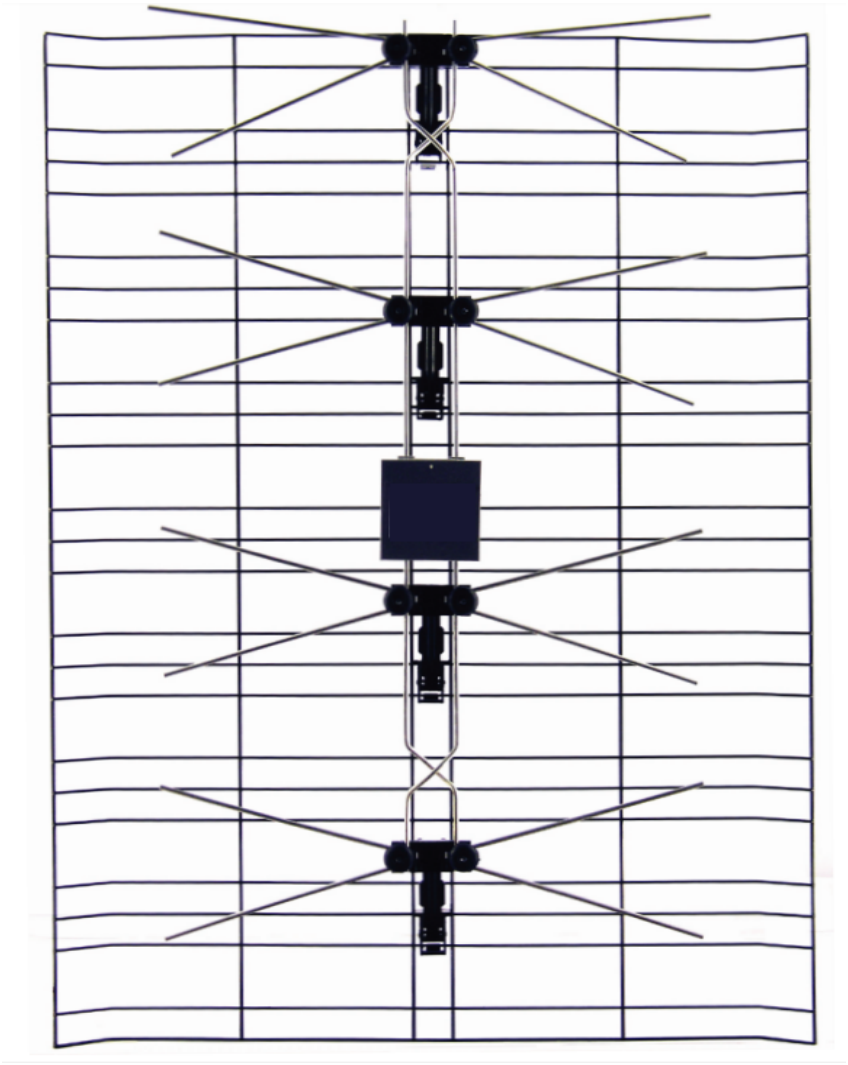

Figure 3.12: Grid reflector with four bow-tie phased array feed

Table 3.4: Antenna Specifications

Specification	**Value**	**Units**
Frequency	470-860	MHz
Gain	9 - 16 (13.3 Nominal)	dBi
Gain	7 - 14(11.3 Nominal)	dBd
Antenna Impedance	75	Ω
Beamwidth	49H & 30V	Degrees
Directivity	18	dB
H - V Polarization Isolation	27	dB

One of the minor problems associated with using the commercial television antennas, however, was that the system impedance for most local television systems was 75 Ω. Whereas most RF components; especially those to be used in this project such as the

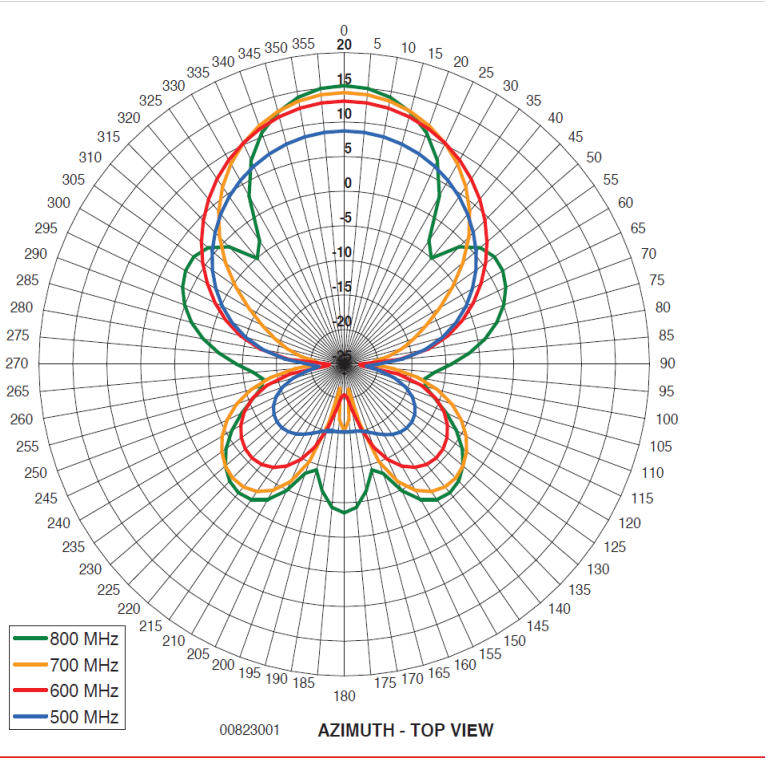

Figure 3.13: Grid reflector with four bow-tie phased array antenna pattern

amplifiers, filters and ADC had impedances of 50 Ω. Thus, to eliminate possible losses due to impedance mismatch, the antenna impedance was matched to 50 Ω using a Mini Circuits impedance matching pad, though this does come at an insertion loss of 5.75 dBs. The antenna S11 parameters were measured using a network analyser to measure the performance of the antenna with a matching pad and without a matching pad. The S-Parameters, or scattering parameters, describe the input-output relationship of RF propagation in n-port systems. For an RF wave incident within an 1 port system for example, some of that signal energy gets reflected back from the port, and some of it would enter into the port. This energy into the port either disappears as heat or would be radiated as electromagnetic energy[48]. This is known as the S11 parameter or the reflection coefficient (Γ). For higher order ports more relationships would have to be considered such as the energy received from one port relative to the energy transmitted from another (radiated). Antennas are typically measured as 1 port systems depending on application and thus the from Figure 3.14 the antenna can be seen to have better reflection coefficient with the matching pad at -30.5 dB rather than without at -13.8 dB at the desired frequency. Though it should be stated that at -13.8 dB the S11 performance of the antenna is still respectable.

The signal channel power measured of both the reference and surveillance channels using the bow-tie antennas can seen to be at -34.66 dBm and -52.26 dBm respectively from the Constantiaberg transmitter. The signal powers would be used to design the RF front-end of the PCL radar system in the subsequent sections.

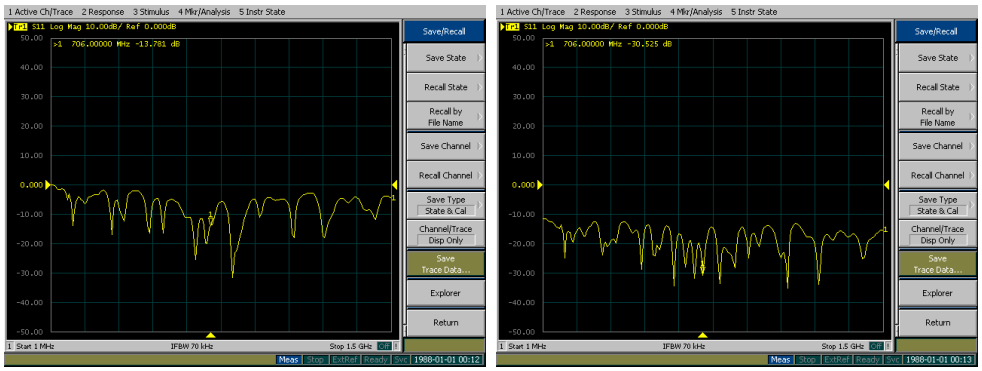

(a) 4 Element Bow-tie antenna with no matching pad

(b) 4 Element Bow-tie antenna with 75Ω to 50 Ω matching pad

Figure 3.14: Antenna S-parameters with and without 75Ω to 50Ω matching pad

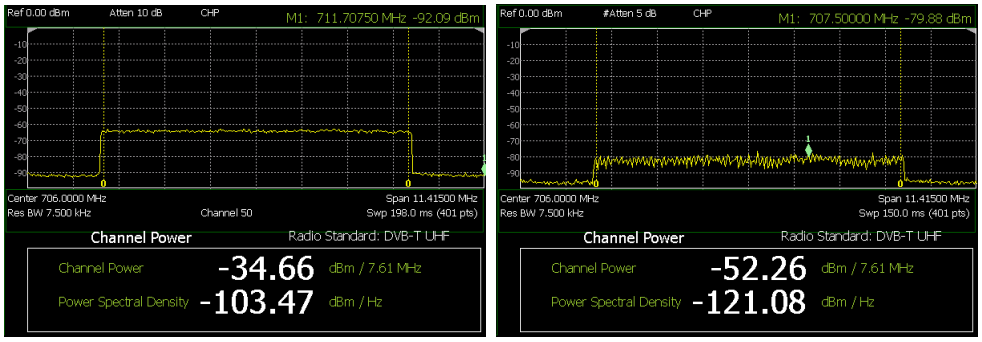

(a) Reference Main Lobe UHF Frequency Band vs Signal Power

(b) Surveillance Main Lobe UHF Frequency Band vs Signal Power

Figure 3.15: Antenna S-parameters with and without 75Ω to 50Ω matching pad

3.2.3 Receiver Design

The N210 SDR from the Ettus Research foundation was used to sample and digitise the received I & Q channels of the surveillance and reference signals. This is due to the fact that a single device was readily available and and due to the limited funding, only a secondary device would need to be purchased. The second benefit of using the N210 board is the ability of to sample two channels coherently, which is a criteria that is crucial in for the processing chain. The SNR has been shown to degrade during processing due to channel incoherency[14]. The Ettus boards would be used with the SBX series transceiver daughterboards. The SBX daughterboard operates in the within the UHF band and thus satisfies one of the requirements of the system. The SBX[50] would be used for the heterodyne stage to mix down the RF signal to baseband and split the I & Q channels before it was passed to the N210 SDR to be sampled and transmitted to a host PC via Ethernet for post processing. The system specifications of the N210 SDR are summarised as

- DC -6GHz(depending on Daughterboard)
- Dual 100MS/s 14-bit ADC

- Dual 400MS/s 16-bit DAC
- Fully Coherent MIMO Capability
- Gigabit Ethernet
- Spartan 3A-DSP 3400 FPGA

The Multiple Input Multiple Output (MIMO) capability allows the two boards to be sampled coherently for both the reference and surveillance channel. This is done by one board acting as a slave and a single ethernet port can be used to transmit sampled data from both boards[51]. The device connected to the ethernet is the master and acted as a switch and would route the data to/from both boards. The master also handles the time synchronisation of the data from both boards and would share it's clock source with the slave so as both devices use the same clock source. The SDR has a max input voltage limit of 2 V_{pp} which corresponds to +10 dBm, thus the signal conditioning and the daughterboard output signal should be less than +10 dBm. The daughterboard specifications are summarised in table 3.5. The maximum input into the daughterboard is -15 dBm. To maximise the dynamic range of the ADC the output signal power from the signal conditioning circuit, including gain and losses, has to lie between -15 dBm and -21.5 dBm (assuming max gain).

Table 3.5: Sumnmary of N210 SDR and SBX Daughterboard Specifications

SBX Daughterboard	
Operating Frequency	400 MHz - 4.4 GHz
Variable Gain	0 - 31.5 dB Gain
Noise Figure	5 dB Noise Figure
MIMO Capability	MIMO Capable
Bandwidth	40 MHz Instantaneous Bandwidth
IIP3	16-22 dBm (Frequency dependent)
Max Input Power	-15 dBm

Proposed Signal Conditioning

The signal conditioning was designed to meet the power requirements of ADC and daughterboard. The signal would need to be amplified and filtered to maximise the SNR and utilise the full dynamic range of the ADC. A signal conditioning chain was designed and implemented for each individual channel. The power received from the antennas for both

the reference and surveillance channel was used to design the signal conditioning chain. To achieve -21.5 dBm to -15 dBm power requirements for the SBX daughterboard, the reference input power as measured with the reference antenna would need to be amplified by 13.66 dB to 19.66 dB. The surveillance channel amplification requirements are calculated to be 31.21 dB - 37.21 dB.

The requirements of the reference chain amplifier are low enough that the gain can be achieved with a single amplifier. The only limiting factor for the amplifier, would be to have a low noise figure as possible. The component with the most effect in terms of noise figure is the first component in the receiver chain, which in this case is the matching pad. This can be seen in Equation 3.4 [44, 48] where F denotes the noise factor of a system, F_x is the noise factor of a particular component and x is the position the component takes in the receiver chain from the antenna. Thus, from this it can be seen that other components' noise factor contributions decrease by a factor of the product of the preceding gains in the chain except for the initial components noise factor. The noise factor is the linear representation of the noise figure. The noise figure can be described as the degradation of the signal to noise ratio from the input of the receiver chain to the output. For this, the amplifier ZX60-P103LN+ from Mini-Circuits was chosen. At the frequency of choice the gain of the amplifier is is 18 dB and a noise figure of 0.4 dB.

$$F = F_1 + \frac{F_2 - 1}{G_1} + \frac{F_3 - 1}{G_1 G_2} + ... + \frac{F_n - 1}{G_1 G_2 ... G_{n-1}} \tag{3.4}$$

For the surveillance channel, a single stage amplifier to meet the requirements could not be found in the region of operation. The maximum gain quoted in the region of interest was 20dB and thus a second amplifier would be needed. For this it was decided that two of the amplifiers chosen for the reference would be utilised thus having a total gain of 36 dB not accounting for losses and a very low noise figure based on the noise figure of the device.

The proposed amplifier to be used for the reference channel and its specifications are summarised in the table below.

Table 3.6: Summary of Amplifier Specifications[52]

Device	Gain (dB)	P_{OUT} at 1 dB Compression (dBm)	Noise Figure (dB)	Output IP3 (dBm)	Operating Frequency (MHz)
ZX60-P103LN+	18	22.7	0.4	40	50 - 3000

The proposed front-ends for both the reference and surveillance can be seen in Figures 3.16 and 3.17 respectively.

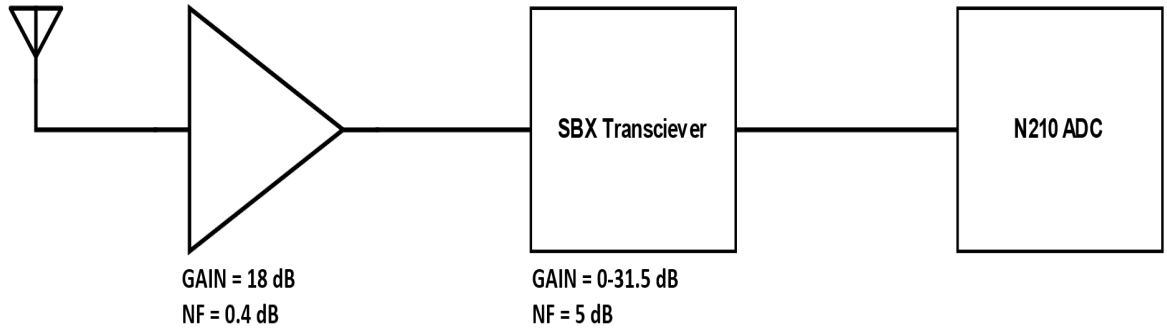

Figure 3.16: Proposed Front-end Receiver for Reference Channel

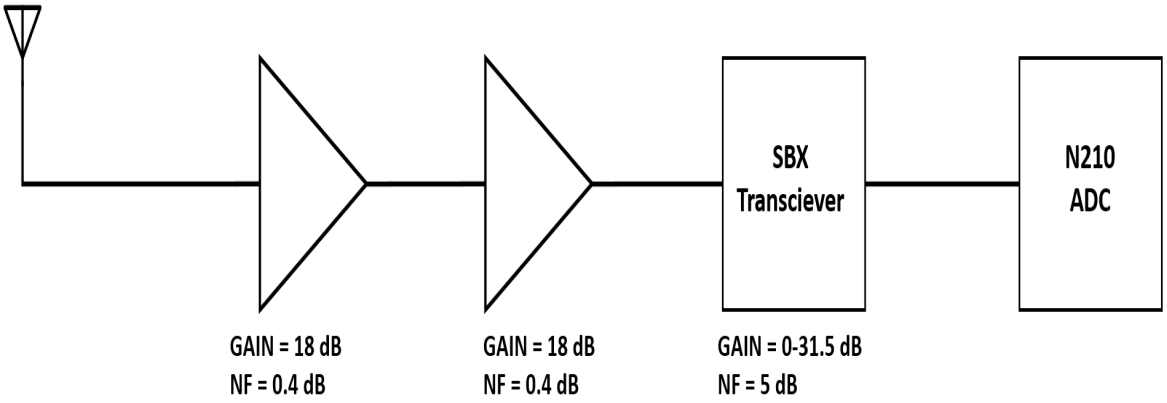

Figure 3.17: Proposed Front-end Receiver for Surveillance Channel

The final input power entering the daughterboard from both the reference and surveillance was thus be -16.66 dBm and -16.26 dBm respectively not accounting for loss in the system meeting the power requirements for both channels of the daughterboard.

To isolate the frequency of interest and suppress out-of-band noise such as adjacent channel interference, a pre-select filter might be added at the front of the receiver chain on both the reference and the surveillance channels. This might come at the cost of insertion loss in the receiver chain however, thus a filter choice and/or design should have low insertion loss at the frequency of operation. Typically pre-select filters have a sharp roll of rate outside the band of interest to be able to suppress any noise outside the band of interest. However, from Figure 3.3 it can be seen that the closest transmissions to the band of interest is approximately 57 MHz away on the one side and 88 MHz away on the other. The closest transmission from the Tygerberg transmitter is approximately 22 MHz, however when the surveillance antenna is facing in the of the area of interest the Tygerberg transmitter is in the null of the antenna beam pattern and the signal is significantly suppressed. Thus, adjacent channel interference is not a major concern at this point.

The other purpose of a pre-select filter is to minimize other large signals in the amplifiers

range that could saturate the amplifier. This was not noted to be an issue in the testing and the results in Section 5. It should also be noted that the design of the filter was not part of the scope of the project. However, due to the lack of pre-select filter, the full dynamic range of the ADC could not be utilized. The design and implementation of a single channel DVB-T2 filter will be left to future work. The final proposed front-end design is shown in Figure 3.18.

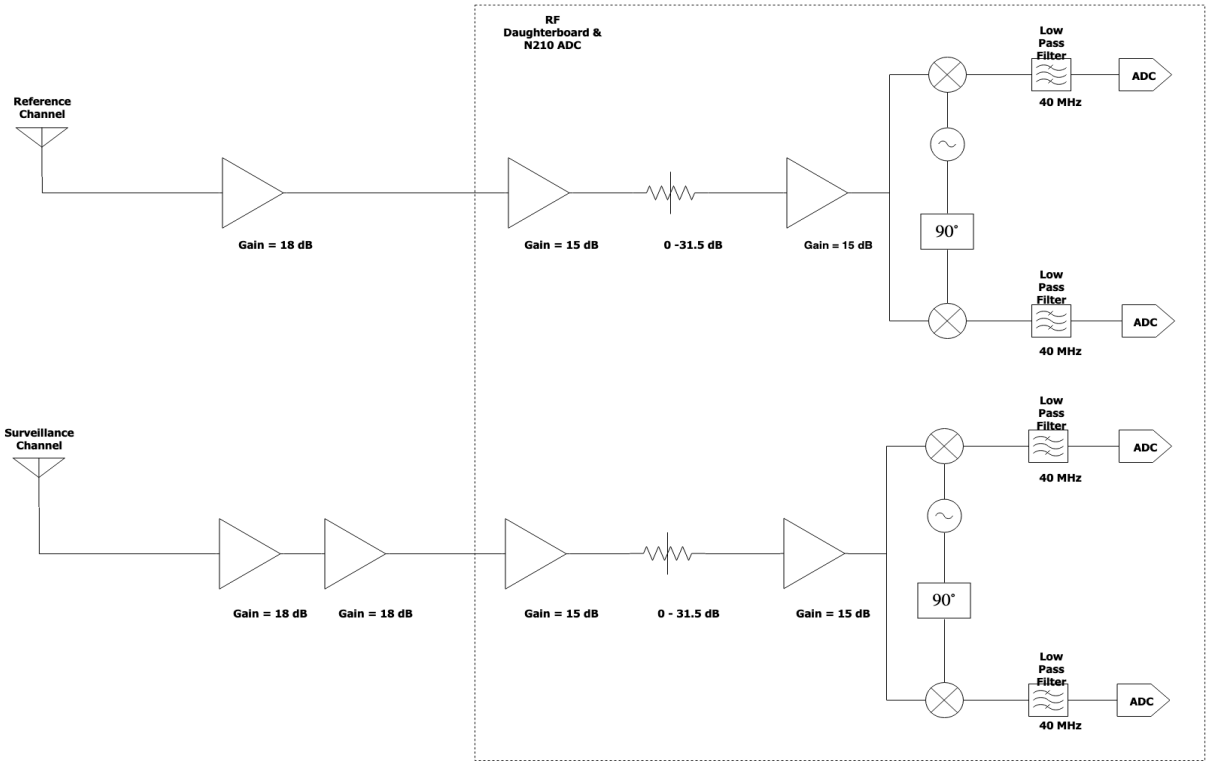

Figure 3.18: Proposed Front-end Receiver

3.2.4 Heterodyne and ADC

As mentioned, due to the lack of resources, the SBX daughterboard and N210 SDR were prioritised for the front-end receiver and a second N210 SDR for the second channel. The SBX daughterboard transciever was used as the RF signal conditioning stage. The block diagram of the SBX from antenna to ADC is shown in Figure 3.19. The SBX has two ports. One of the ports functions purely as a receiver and another port can either be receiver or a transmitter. As with most SDRs, the front-end functionality of the daughterboard can be configured using software. The receiver/transmitter port is controlled using a digital switch. If the transmitter is selected it would use the transmitter dedicated path, which has fixed transmitter based components. If the receiver is chosen then the port connects to the dedicated receiver path which has fixed receiver components.

As PCL radar requires no transmitter the daughterboard were configured to operate as a receivers. Though the two ports are configured to function as receivers, the receiver

path can only service a single port at a time through the use of a second switch. Past the antennas and into the two different ports, each receiver path has a fixed 15 dB gain amplifier. The output of which would feed into the switch that leads to the rest of the path, thus a single board equates to a single channel. Past the second switch, the signal would be fed into a digitally controlled attenuator. The attenuator can attenuate a signal from 0-31.5 dBs in 0.5 dB steps. The output of the attenuator is then fed into another fixed 15 dB gain amplifier. Thus the maximum gain the system can have is approximately 30 dBs. The output of the amplifier is then split into I and Q samples, downconverted to baseband, filtered and fed through to the ADC.

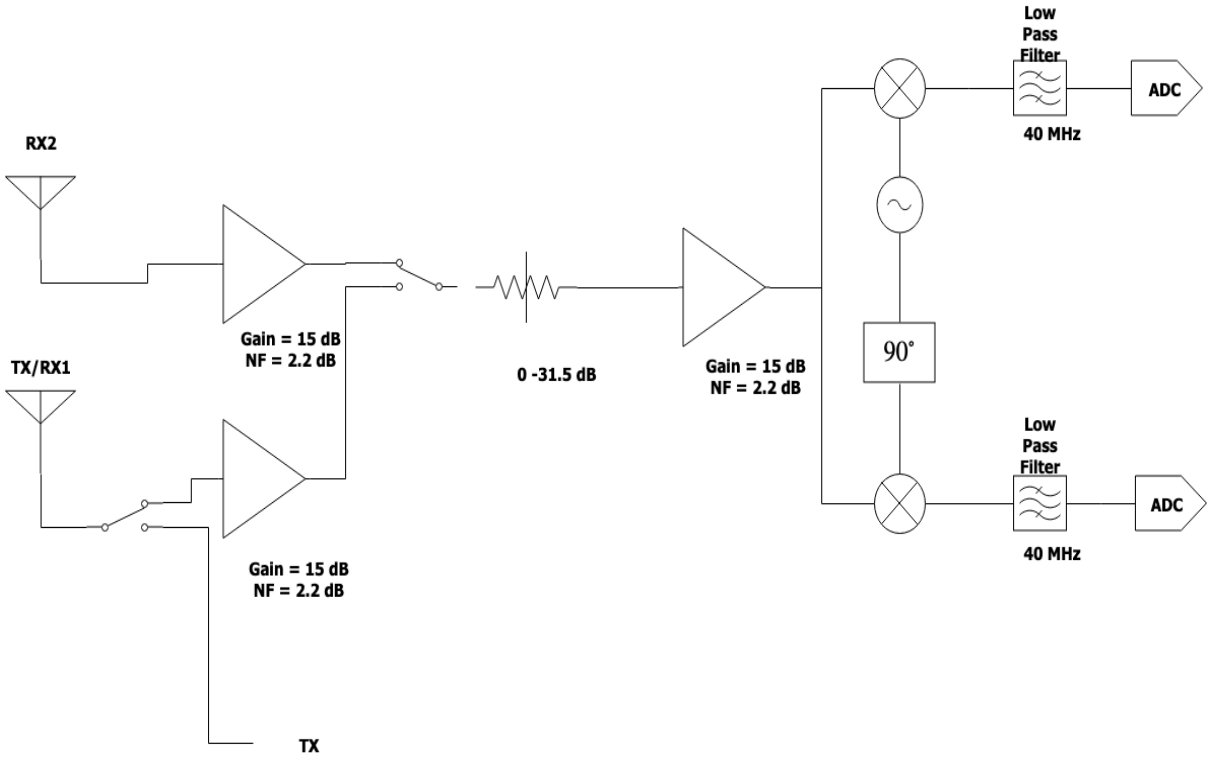

Figure 3.19: SBX Daughter Block Diagram[50]

The digitised I and Q can be transmitted over the N210s Gigabit Ethernet link. The maximum realistic bandwidth that can be transmitted by a single Ettus device is limited by the Ethernet link. For example the theoretical speeds of a Gigabit Ethernet link is 125 MB/s. Assuming that that 16 bit I and Q samples are transmitted or 4 byte samples, the theoretical allowable bandwidth is limited to 31.25 MHz, factoring Nyquist criterion. Practically, however the limit is actually 25 MHz. Since PCL requires two separate receiver chains, reference and surveillance, two Ettus SDRs with SBX daughterboards would be required. For coherent processing the two SDRs would have to be synchronized. A MIMO cable was used to synchronise the two clocks of the separate receivers. However, the data would now be streamed over a single Ethernet connection and thus the maximum bandwidth to be sampled in a MIMO configuration is 12.5 MHz. The MIMO synchronized N210 boards are shown in Figure 3.20 below.

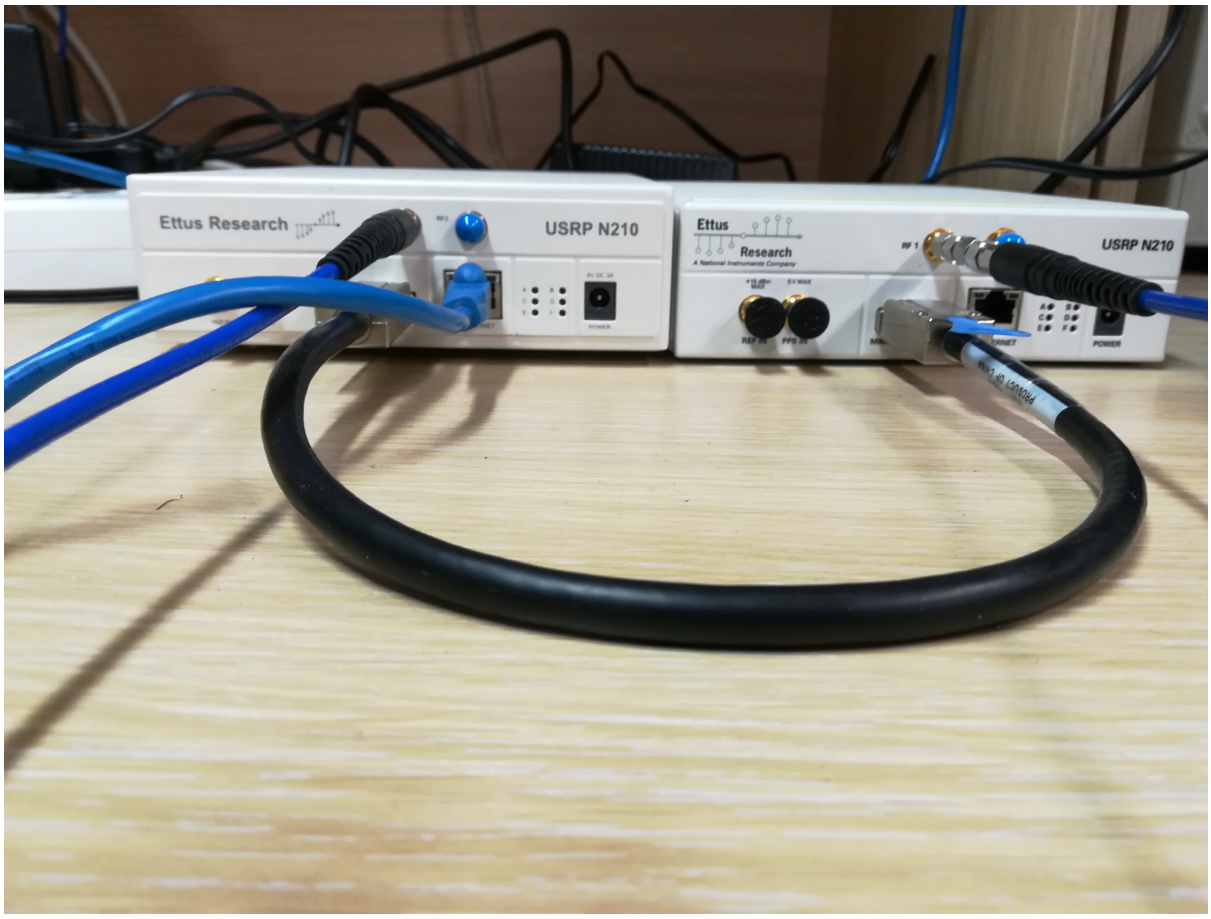

Figure 3.20: Ettus USRP N210s with MIMO synchronisation cable.

The Ettus boards were controlled using the National Instruments Labview Software. Labview is a graphical programming environment. The USRP receiver flow diagram programmed in Labview is described as[53, 54]

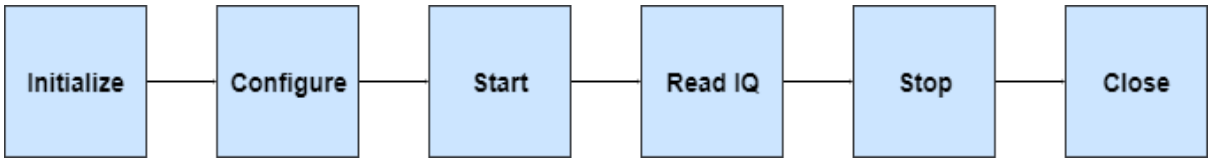

Figure 3.21: Labview Receiver Program Flow

The full description of setting up labview and programming the Ettus board can be found in Appendix A. The receiver flow diagram can be summarised as

- Initialise - sets the device information such as IP address to setup a session handle. This would determine the device used. This is then passed to the configuration action.
- Configure - sets the USRP parameters such as Gain (variable attenuator), Sampling rate, number of samples to fetch in the receiver Ethernet buffer, carrier frequency, and receiver channel (port). Based on the session handle and configure parameters,

the system would hard limit gain, carrier frequency and sample rate based on the device being used. I.e. the SBX has a max gain of 31.5dB if a user enters more than that in the UI the gain is forced to the max value of 31.5dB.

- Start - is a simple control that informs the SDR to commence the recording process.
- Read I and Q - this fetches the IQ samples and displays the time and frequency domain plots of the sampled spectrum.
- Stop - is a simple control that informs the device to stop recording
- Close - The stop instruction would inform the session handle to terminate connection and end process.

The data recorded had to be stored on the host PC for post-processing. The data was stored on the host PC storage unit as a binary file in big-endian byte order. The process of recording the binary files to disk was based on Labview's Producer/Consumer design pattern[55], which is based on the Master/Slave pattern. This is due to the fact that the host PC storage unit write speed rate could not keep up with the sample rate of the device or the device was producing data far quicker than the host could consume causing the system to hang and crash. The producer/consumer process overcomes this by decoupling the processes that produce data to the process that consumes data at different data rates. This process is typically used when a user wants to process data in the order that the data was received through use of data queues. The queues acted as buffers between the data production process and the data storage process allowing the two processes to act simultaneously at different data rates. Thus, the data could be streamed continuously without interruption with the limiting factor only being the storage capacity available. The received signal from the Ettus USRP receiver can be seen in Figure 3.22

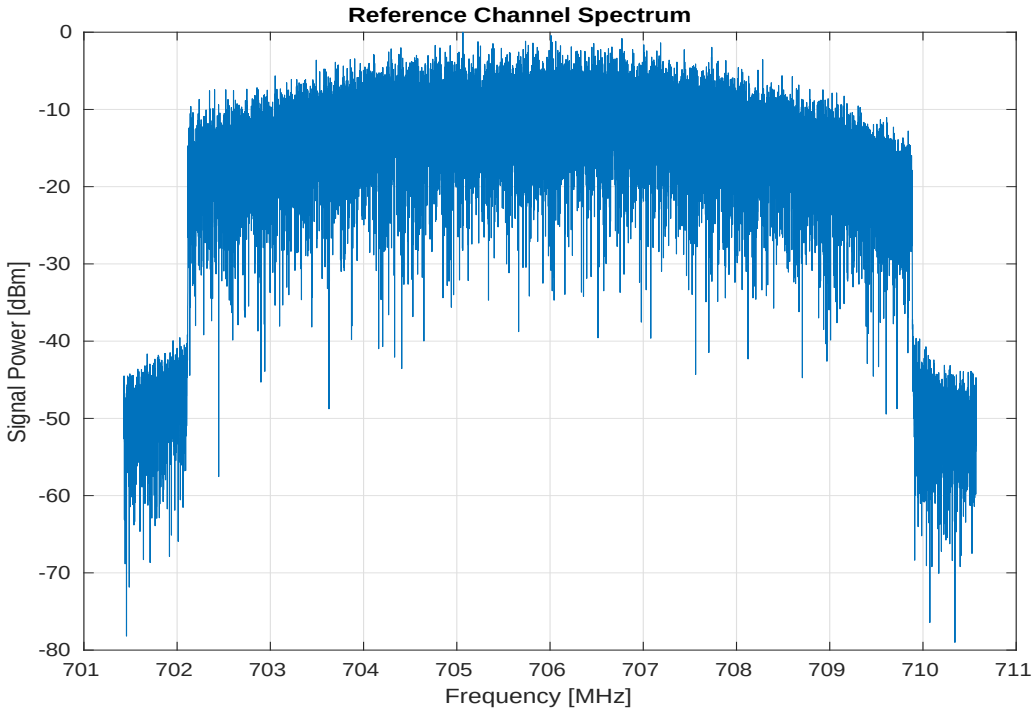

Figure 3.22: Reference Signal Recorded with N210 board using Labview.

3.3 Summary

To summarise, investigation into PCL radar performance prediction was completed. This took into consideration propagation effects, transmitter information, and terrain environment to ascertain a theoretical system performance of a PCL radar. A RF front-end design was then proposed based on the results of the performance prediction, though due to financial constraints a secondary design was successfully implemented to achieve a radar front-end.

Chapter 4

DVB-T2 Processing Chain

In this chapter a processing chain for DVB-T2 was proposed and implemented. The processing chain was tested on both a commercial system and the designed radar front-end in chapter 3. The processing chain proposed takes in raw I and Q data and initially performs DPI cancellation on the surveillance channel to suppress the channel effects, clutter and direct path signal from the surveillance channel. The reference channel is then demodulated to determine the DVB-T2 signal parameters and again remodulated with altered guard and pilot tones to create an ideal de-noised reference signal for mismatch filtering. The outputs of both the DPI cancelled surveillance and the remodulated reference are then mismatch filtered to produce amplitude range and Doppler (ARD) plots.

4.1 Mismatch Filtering

In typical radar systems, pulse compression is done by convolution of the received signal with the matched filtered. Matched filtering describes the process of cross-correlating the received signal with an unchanged copy of the transmitted signal to determine if the transmitted and received signals "match"[38]. However, mismatched filtering is the process of cross-correlating the received signal with a manipulated and/or altered version of the transmitted signal. To apply matched filtering in PCL radar, Doppler shifted versions of the original transmitted signal, in the PCL case the received reference signal, are created and cross-correlated with the received signal surveillance signal. This process is true for most PCL radar processing that applies matched filtering, particularly the analogue based transmission signals such as FM radio and analogue television[26, 41, 4, 22].

Where OFDM based signals differ however is that the reference signal is altered due to the ambiguities caused by certain signal properties, specifically the pilot tones and guard interval[56, 57]. The reference signals pilot tones and guard interval length cause

multiple undesirable peaks in the AF and CAF as seen in Figures 2.6 and 2.7 respectively. These peaks could mask potential targets or could create false target tracks thus in the reference signal the pilot tones and guard interval needs to be either suppressed and/or removed. This is called demod-remod. The reference signal is demodulated on reception to determine the type of DVB-T2 OFDM signal and get the signal parameters of the received signal. This is further described in Section 4.1.2. The signal is then remodulated with the same parameters, without noise and with altered pilots and guard interval. This remodulated signal is then mismatched filtered with the unchanged surveillance in a similar method as described by the matched filtered process.

The mismatched filtering DVB-T2 processing chain block diagram can be seen in Figure 4.1. This is the proposed radar processing chain for this dissertations' DVB-T2 demonstrator.

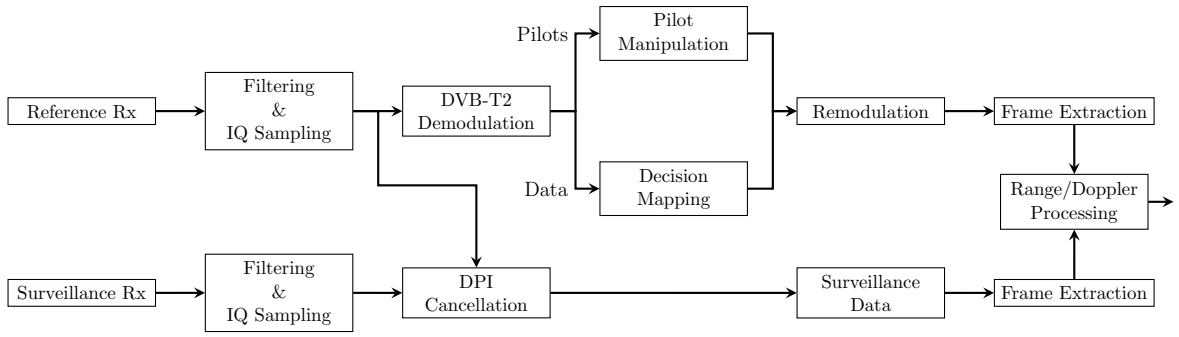

Figure 4.1: DVB-T2 processing chain.

The processing chain is broken up into two parts, the reference and the surveillance branches. On the reference branch, the DVB-T2 demodulation and was done. This was followed by Pilot manipulation, Decision mapping and signal remodulation. Lastly, this was followed by frame extraction. On the surveillance branch DPI cancellation was implemented with an unchanged copy of the reference signal followed by frame extraction. The output of both branches are then used to do the range and Doppler processing. Before all this, however, the receiver needs to synchronise with the transmitter and determine whether the signal received is indeed a DVB-T2 signal and the receiver needs to detect and correct the frequency and timing (symbol) synchronisation the beginning of a DVB-T2 frame. This was done with the detection of the P1 symbol of the DVB-T2 signal. To extract the P1 symbol the receiver needed to receive one full frame of the DVB-T2 signal. This process is done on the reference branch in Figure 4.1.

The transmitter transmits a DVB-T2 superframe, this superframe is the largest entity of a DVB-T2 system. The maximum length of a superframe is 63.75 seconds. The superframe can be broken up into frames of up to 250 milliseconds in length. A superframe can contain at most 255 frames. A summary of the DVB-T2 system can be seen in Figure 4.2

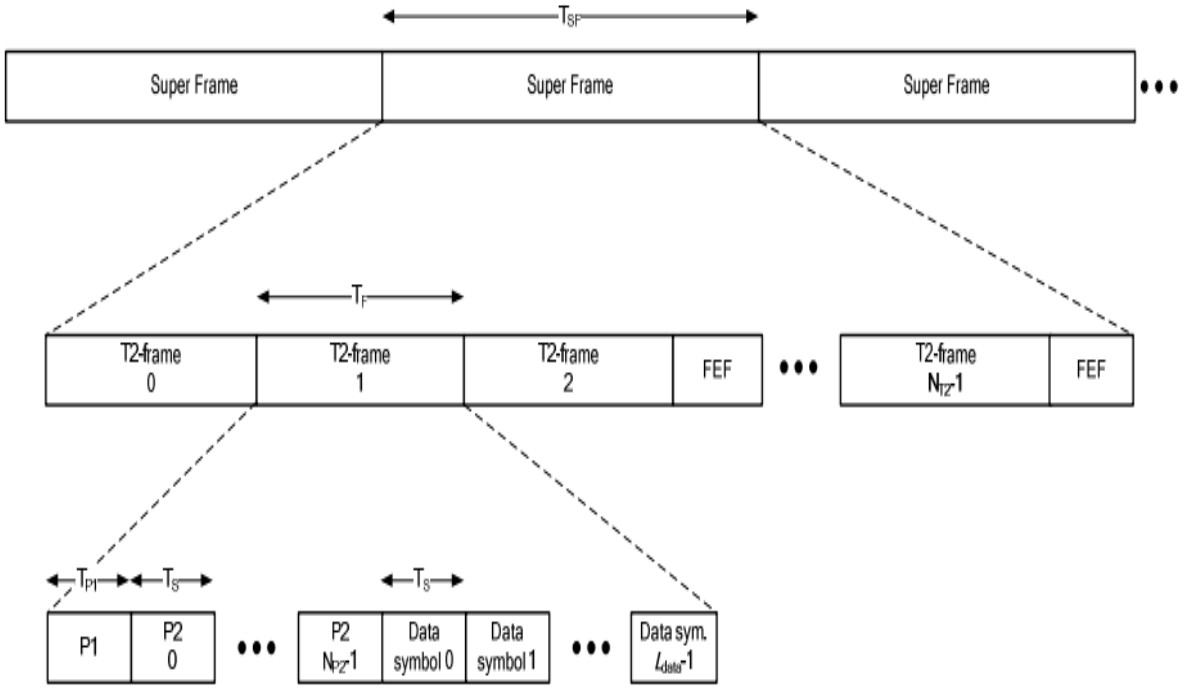

Figure 4.2: DVB-T2 Frame Structure consisting of Superframes, Frames and OFDM Symbols[36][37]

A single frame can be divided into OFDM symbols.The frame consists of 3 types of symbols[36, 37]:

- P1 Symbols
- P2 Symbols
- Data Symbols

Every frame begins with a P1 symbol. The P1 symbol only appears once every frame, thus the spacing between each P1 symbol is 250 milliseconds. The P1 symbols has these specific purposes:

1. Enable the receiver to determine whether it has received a DVB-T2 signal
2. To determine some transmission information that can be used down the demodulation chain. This includes information such as FFT mode of the transmission, the type of P1 symbol it is, some guard interval information and other information needed to decode the rest of the DVB-T2 signal
3. Allow the receiver to synchronise in time and frequency

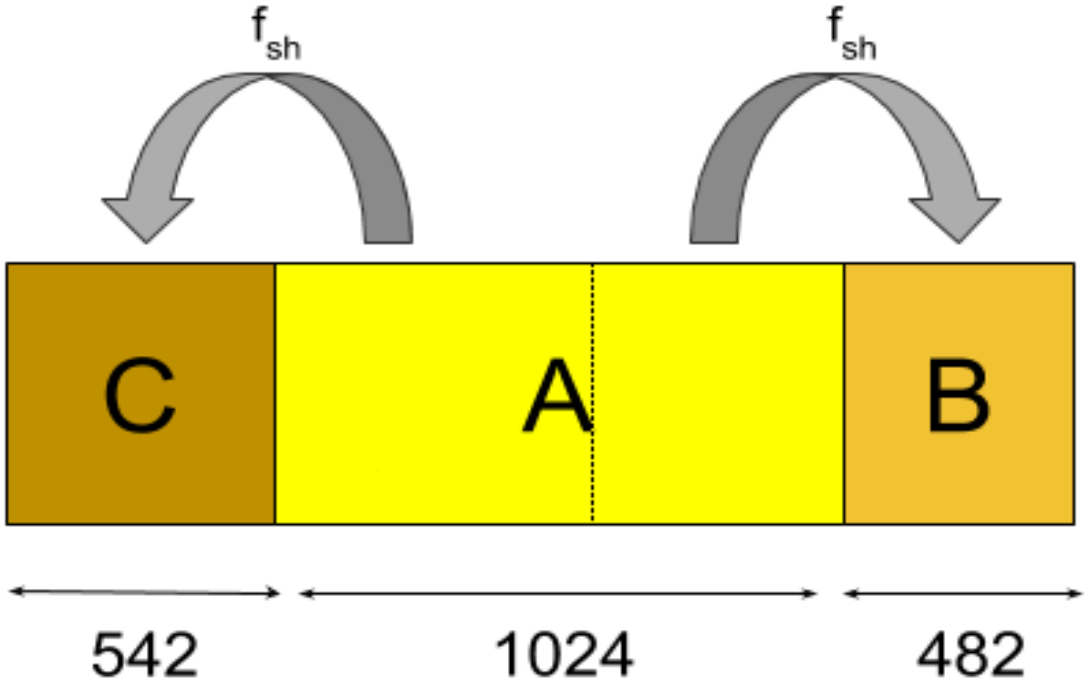

Figure 4.3: P1 Symbol Structure[37]

The structure of the P1 symbol was described in Figure 4.3

The P1 symbol structure can be broken up into 3 parts; A,B and C. Part A of the P1 symbol is the main part of the OFDM symbol and is generated using a 1K FFT consisting of 1024 samples. These samples correspond to an equal number in sub-carriers of which 384 are active carriers. Part A of the P1 symbol is then split in two, with the first 542 samples frequency shifted to the front of the P1 symbol and the remaining 482 samples frequency shifted to the back. These make up parts C and B respectively. This increases the length of the P1 symbol to 2048 samples. The length of the P1 symbol is always fixed regardless of other signal parameters thus making the detection process easier. The P1 is designed such that the detection can still occur regardless of the frequency offset of the received signal due to the receiver clock tolerance and/or deliberate offsets on the transmission.

The P1 is detected by correlating the parts C and B with the received signal. Only a single frame or 250 milliseconds of data is required for the P1 detection process. Due to the periodicity of a P1 symbol in a superframe, it is guaranteed that a single P1 symbol can be found within a single 250 millisecond frame. The P1 correlation block diagram can be seen in Figure 4.4. The correlation would be based on two branches correlating both parts in parallel.

f_{SH} is the frequency shift which applied to parts C and B of the 2k P1 symbol. The frequency shift is equivalent to one sub-carrier spacing. T_{A}, T_{B}, and T_{C} are the symbol

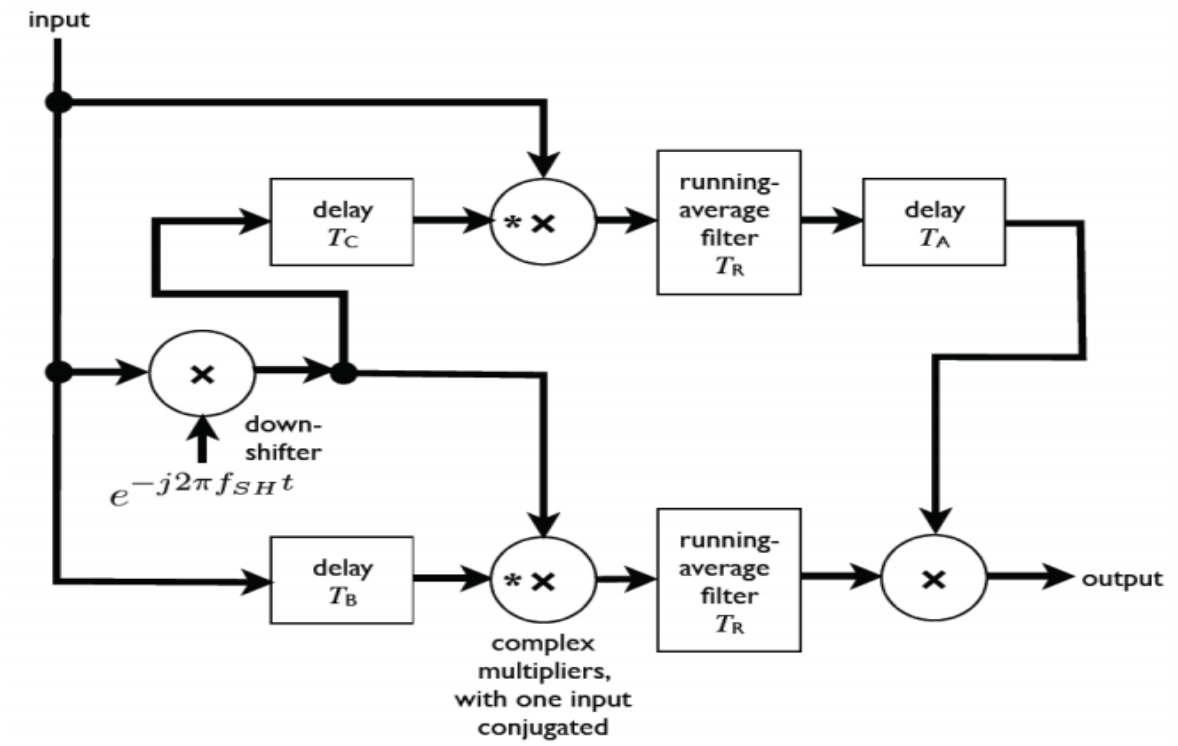

Figure 4.4: P1 Symbol Detection Block Diagram[37]

lengths of the three parts of the 2K; the 1K part A length, the 482 part B length and the 542 part C length of the P1 symbol. Part B and Cs delay elements, T_{C} and T_{B}, in association with the multiplier and running average filter form part of the correlator process to detect the frequency-shifted repetition in the signal. T_{A} lines up the output of the correlation branches. Lastly, T_{R} is chosen as $\frac{1}{f_{\mathrm{SH}}}$ thus equating T_{R} and T_{A} to eliminate the unwanted effects of the two correlators such as complex-constant terms. The argument of the block diagram can be used to to apply the coarse frequency offset compensation in the received signal.

From the P1 detection, the P1 is then validated to determine whether the signal received is indeed a DVB-T2 signal. The validation would output integer frequency offset estimate. This offset estimate is an integer frequency offset used to correct the received reference and surveillance channels. The main part of part A of the P1 symbol was demodulated by applying an FFT of the 1k OFDM symbol in order to validate the P1 symbol. This results in a set of complex amplitudes for each 1k carrier position. Only a subset of the 1k carriers carry information. This subset is 384 carriers in length. The validation is achieved by correlating the distribution across the carriers of the power of the received P1 symbol with the expected carrier sequence [37]. The surveillance and reference channels are then frame synchronised based on the location of the P1 symbol of the first frame.

The next preceding sections would be broken into the surveillance processing chain, the reference chain that continues the rest of the DVB-T2 demodulation and finally the

Range/Doppler Processing.

4.1.1 Surveillance Branch

DPI and Clutter Suppression

The direct path signal embedded in the surveillance channel is an unwanted signal component that is larger than the weaker target echo skin return. This leads to masking of the target return within the surveillance channel. The direct path signal typically consists of the line of sight transmitter signal leaking into the surveillance channel as well as the clutter return from the surrounding environment in the form of multipath signals reflected of objects. The surveillance channel can thus be modelled as

$$S_s(n) = S_{echo}(n) + S_{interference}(n) \tag{4.1}$$

Where S_s is the digitised surveillance signal, S_{echo} is the skin return from a target, and $S_{interference}$ direct path signal interference. Adaptive filtering signal processing techniques have been proposed as methods to remove the unwanted signal components embedded within the surveillance channel. Palmer [2] evaluated a number of adaptive filter algorithms for clutter cancellation such as,

- Wiener Filter
- Steepest Descent
- Conjugate Gradient
- Least Mean Square adaptive filter
- Recursive Least Square adaptive filter
- Euclidean Direction Search filter

An adaptive filter removes the unwanted signal components by estimating the direct path components using adaptive filter coefficients and subtracting the estimate from the surveillance channel such that

$$\hat{S}_s(n) = S_{echo}(n) + S_{interference}(n) - \hat{S}_{inteference}(n) \tag{4.2}$$

Where $\hat{S}_{interference}$ is the estimated clutter and direct path signal component and $\hat{S}_s$ is the output surveillance channel of from the DPI process. Assuming that the estimated inter-

ference signal is equivalent to the actual interference signal then the result of Equation 4.2 would be

$$\hat{S}_s(n) \approx S_{echo}(n) \tag{4.3}$$

In the PCL signal processing sense this and Equation 4.2 can be rewritten as

$$S_{echo}(n) = S_s(n) - \hat{S}_{inteference}(n) \tag{4.4}$$

Simplifying this further leads to

$$S_{echo}(n) = S_s(n) - A\hat{x} \tag{4.5}$$

Where $\hat{x}$ is the calculated filter coefficients, A is the matrix of vectors representing the DPI and clutter at specified range and Doppler bins. The size of the A matrix can be represented as a column of CPI samples and a rows of the size of the range and Doppler bins to be cancelled or N x M where N is the number of CPI samples and M is the ARD cancellation Matrix size. Generally speaking the number of samples N far exceed the matrix size M such that N >> M. Thus the Matrix A is generally almost never a square matrix. This means that A is not invertible. Thus to solve Equation 4.5 $S_s(n)$ is set to b and the Equation 4.6

$$A\hat{x} = b \tag{4.6}$$

can be solved to determine the optimal estimate of filter coefficients $\hat{x}$. As A is not invertible, Equation 4.6 can not be solved directly and thus the residual would need to be reduced in the least squares by [4]

$$min(||A\hat{x} = b||^2) \tag{4.7}$$

Each column in the matrix A would consist of delayed and Doppler shifted versions of the CPI samples corresponding to a cancellation range and Doppler. In practice for stationary receivers the only Doppler components to be modelled are minor sways of the antennas due to environmental effects, sway of clutter objects such as trees etc. Thus not much Doppler cancellation is required. However depending on the surveillance channel the extent of the range cancellation would be dependent on the stationary clutter environment such as buildings, mountains etc. As the system would be based at UCT in

the City of Cape Town, the urban and mountain environment could lead to severe clutter and multipath effects and thus cancellation over the full ARD range could be necessary.

For the Adaptive filters evaluated by Palmer, he found that in most instances the Conjugate Gradient and Steepest Descent based on experiments done on DVB-T data performed best using the optimal Wiener filter as the baseline. Both algorithms performed similar to the optimal solution based after a set number of iterations. [2] Proposed the Conjugate gradient method for real-time processing of FM PCL radar using commercial-of-the-shelf general purpose GPUs. Based on this, the Conjugate gradient method was initially chosen as the adaptive filter algorithm for this project, specifically the CGLS algorithm.

The conjugate gradient algorithm is a sub-optimal numerical solution to solve the optimal computationally intensive Wiener-hopf equations[2]. The suboptimal methods produce estimates of the filtered signal. Typically the optimal algorithm would iteratively update the filter coefficients for a given set of data until the filter converges. Once the filter has converged the final coefficients calculated would be used to filter out the clutter and DPI components. The suboptimal solutions don't solve the Wiener-Hopf equations directly but rather use an initial estimate of the filter coefficients and iteratively update the coefficients until the error signal falls below a predetermined threshold. This is done on a set of samples typically the length of the CPI which are used to setup the Wiener-hopf equations. The CGLS algorithm tries to solve the Wiener-hopf equations by minimising Equation 4.7.

To illustrate the effects that DPI has on the received surveillance channel, a simulated target was added to a surveillance channel recording 50 dBs below the direct signal peak amplitude. The target added was a swerling case 0 target. The target was added by scaling the reference signal by it's root mean square noise(RMS) level at a desired SNR. This done due to the fact that the target is typically several dBs weaker than the transmitted signal. The signal is then delayed equivalent to the desired range and frequency shifted by the required Doppler shift. Though it should be noted in this instance that the target radial velocity is unknown as the angle δ is unknown as in Equation 2.2. It is assumed the PCL system has some arbitrary geometry and this geometry leads to a target detection with a Doppler of 400 Hz and a range of 100 km. The target was clearly placed at 100 km bistatic range and 400 Hz bistatic Doppler. The CAF is then generated from the surveillance channel with the simulated target and the corresponding reference channel. The output of the CAF can be seen in Figure 4.5. The Peak DPI component can be seen at 0 bistatic Doppler and range. The DPI clutter is also notably visible as the ridge that spreads along the bistatic range at 0 Doppler. The target here remains masked amongst both the DPI component as well as the ambiguities due to the nature

of the DVB-T2 signal.

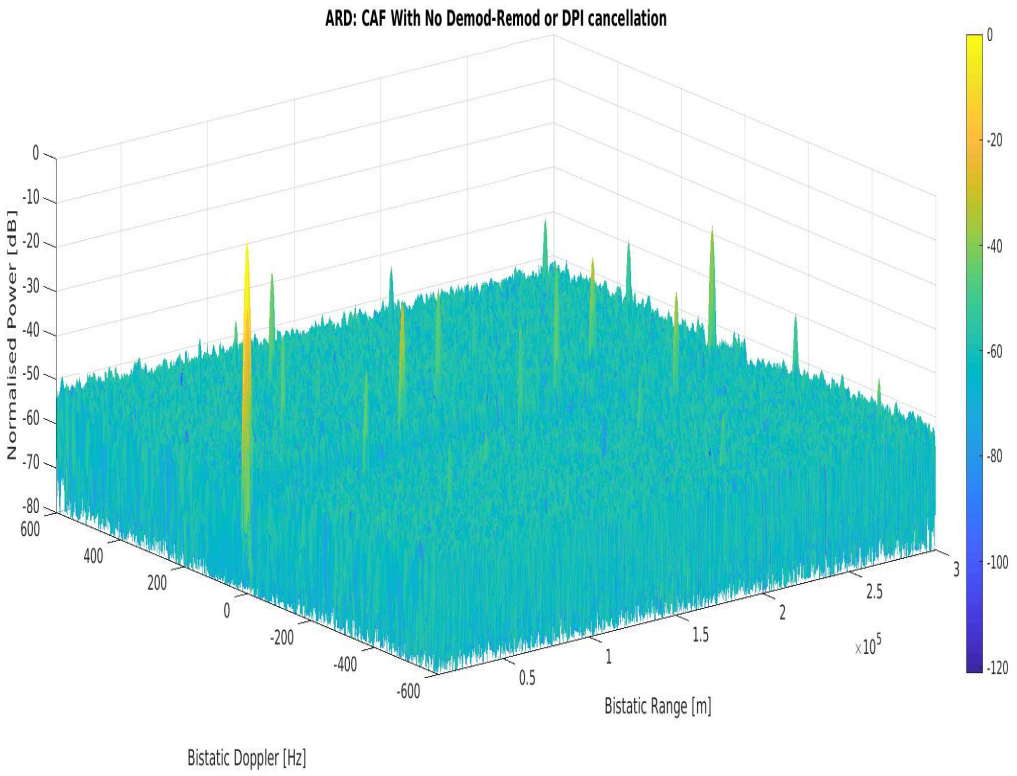

Figure 4.5: CAF map of DVB-T2 system with a simulated target at 400 Hz bistatic Doppler and 100 km bistatic range with no direct signal cancellation or demod-remod processing

DPI was applied to the surveillance channel with the simulated target using the CGLS algorithm developed by [4]. This implementation proceeds to do cancellation on a sub-block of a CPI worth of data. Thus the filter coefficients are generated and updated for each sub-block. This reduces the memory requirements of the system used. The result of the cancellation can be seen in Figure 4.6. It is shown that the DPI component and ridge at 0 Hz Doppler has been significantly suppressed. The Target is clearly more visible, although some ambiguities still remain. Thus for mismatch filtering to be successful, DPI cancellation is crucial. It is also important to note that the cancellation needs to be done with an unaltered version of the reference signal. This is due to the fact that the demod-remod process outputs an almost ideal version of the received signal, free from channel effects and clutter as well as the pilots and guard interval that causes the ambiguities. Even if the guards and pilots remain unchanged, the process would de-noise or remove the clutter and channel effects from the received signal. However, the DPI signal that is embedded in the surveillance channel still contains all these artefacts. Thus, for DPI cancellation to be successful the reference signal should be the original received signal with all clutter and multipath effects, such that the DPI signal that needs to be estimated and subtracted from the surveillance channel matches.

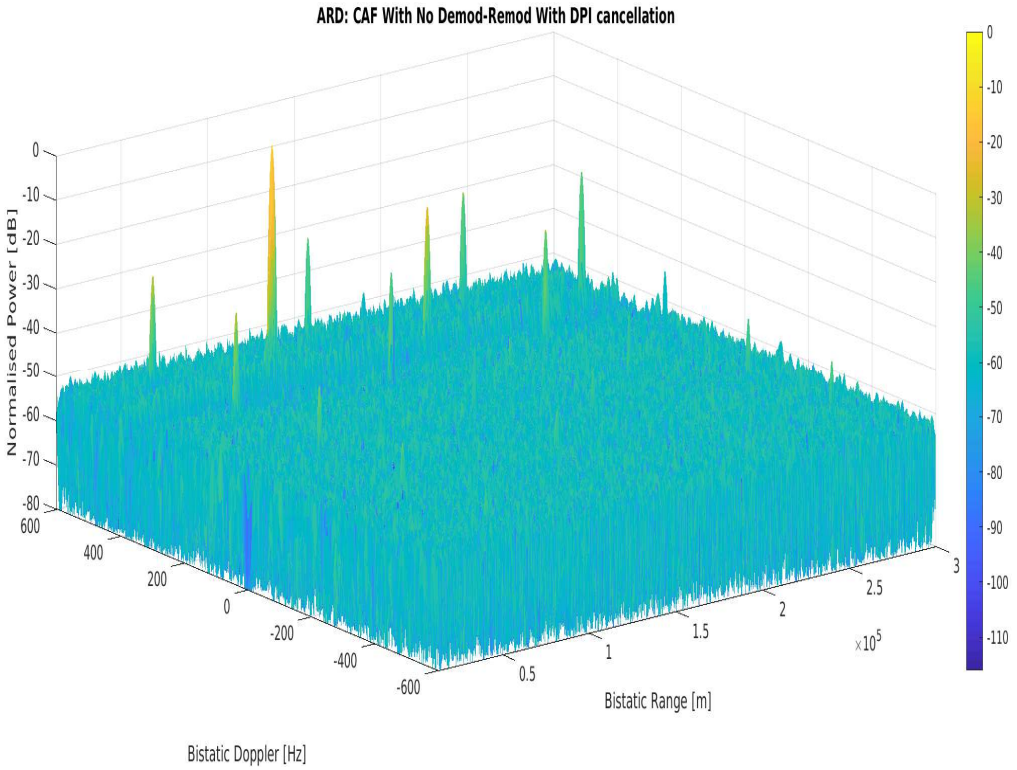

Figure 4.6: CAF map of DVB-T2 system with a simulated target at 400 Hz bistatic Doppler and 100 km bistatic range with direct signal cancellation or demod-remod processing.

It was found that the CGLS DPI cancellation process is not optimised for DVB-T2 signals. The A matrix of Equation 4.5 becomes to large due to the size of range bins needed to be cancelled over and the length of samples of the CPI. As previously mentioned, the A matrix has a size of MxN where M is the number number of ARD bins which must be cancelled over and N is typically the length of a CPIs worth of Samples. For example in [4] the CGLS was used for a FM based PCL radar system. The CPI length was 4s. The sampling rate of the system was 204.8 kSps. This corresponds to 819200 samples per CPI. The number of range cancellation bins is set to 150 bins. The DPI was calculated over 8 sub-blocks of CPI data, which corresponds to 102400 samples per block. This corresponds to an A matrix of 150x102400. To compare the DVB-T2 system used in section 3 samples data at 10 MSps. If similar parameters were used to the FM system that would increase the amount of data to be processed thus increasing the execution time of the cancellation process. However, if we were to use the typical DVB-T/T2 processing parameters this would equate to a CPI of 0.25 s. This corresponds to 2.5M Samples per CPI. Reducing this to 8 sub-blocks of data sets the number of samples to 312500 which is more than 3 times the amount of samples compared to the FM system. The range bins for the FM system correspond to a distance of approximately 220km. The number of range bins for a similar distance for a DVB-T2 based system would equate to 7333.33 range bins. This isn't feasible for DVB-T/T2 systems however as the distance is

typically in the 10s of km thus limiting the DVB-T2 range to a max 90km for example the range bins are 3000 bins, which is 20 times the number of range bins compared to the FM system. This corresponds to an A matrix of 3000x312500. This still increases the number of data to be processed leading to an increasing of the matrix operations as the size of the matrix drastically increased and an increase in the memory required due to the A matrix having to be stored during processing. This is still also assuming a single Doppler bin for both systems. In most cases however, additional Doppler indices either side of the zero Doppler range would have to be cancelled thus increasing the size of the M.

Thus, an investigation into optimisation of the cancellation process for DVB-T/T2 systems needs to be considered for future work.

4.1.2 Reference Branch

The reference branch continues the Demod-Remod process from the P1 detection to determine the location of the pilot tones in the DVB-T2 signal as well as the guard interval information of the signal. For successful demodulation of the DVB-T2 signal the P2 symbol and data symbols would need to be decoded following the successful decoding of the P1. The process would begin by decoding the P2 symbols and extracting information that pertains to the data symbols. The number of P2 symbols in a frame are dependent on the FFT size specified after the decoding of the P1. The data that was decoded from section 4.1 to generate AF and CAF Figures 2.6 and 2.7 respectively was

- Transmission Mode: Single Input Single Output (SISO)
- FFT size: 32k
- Type of Frame: Pure T2 Frame

These set of parameters would be used to decode the P2 and data symbols. For FFT sizes less than or equal to 8k there are more than one P2 symbols, however for FFT sizes greater than 8k there is only a single number of P2 symbols per frame. The P2 symbol can be broken up in to two parts. The L1-pre and the L1-post signalling. The L1-pre signalling contains basic transmission parameters as well as information to decode the L1-post such as the specific guard interval used, type of Peak-to-Average-Power ratio reduction used, L1-post size, Pilot tone pattern used by the data symbols and other transmission information. The L1-post signalling data contains parameters which provide information to decode the data symbols. The L1-pre is uses Binary Phase Shift Key, BPSK, with $\frac{1}{4}$ code rate and the L1-post can use either BPSK, Quadrature Phase Shift Key (QPSK),

16-QAM (Quadrature Amplitude Modulation) and 64-QAM modulation scheme with a code rate of $\frac{1}{2}$. Unlike the P1 symbol, the P2 symbol also contains dense number of pilot tones. The pilot tone pattern for the P2 is fixed depending on the size of the FFT and the transmission mode. For 32k FFT SISO transmission the P2 pilot symbol is a pilot tone every 6^{th} carrier frequency and the for other FFT sizes and transmission modes are a pilot tone every 3^{rd} carrier.

Lastly, the data symbols contain the Physical Layer Pipes (PLP) and pilots. The pilots in this case come in two forms, scattered and continual. The scattered pilots are spread across the symbol and frequency bins in any one of the 8 patterns available to DVB-T2. The type of scattered pilot that a DVB-T2 signal would use is dependent on the FFT size and the Guard Interval Fraction (GIF) used. A summary of the 8 pilot patterns possible for each data symbol as a function of FFT size and GIF using a SISO transmission is given as Table 4.1

Table 4.1: Scattered pilot pattern to be used for each allowed combination of FFT size and guard interval in SISO mode[36, 37]

FFT Size	Guard Interval						
	$\frac{1}{128}$	$\frac{1}{32}$	$\frac{1}{16}$	$\frac{19}{256}$	$\frac{1}{8}$	$\frac{19}{128}$	$\frac{1}{4}$
32k	PP7	PP4 PP6	PP2 PP8 PP4	PP2 PP8 PP4	PP2 PP8	PP2 PP8	N/A
16k	PP7	PP7 PP4 PP6	PP2 PP8 PP4 PP5	PP2 PP8 PP4 PP5	PP2 PP3 PP8	PP2 PP3 PP8	PP1 PP8
16k	PP7	PP7 PP4	PP8 PP4 PP5	PP8 PP4 PP5	PP2 PP3 PP8	PP2 PP3 PP8	PP1 PP8
4k,2k	N/A	PP7 PP4	PP4 PP5	N/A	PP2 PP3	N/A	PP1
1k	N/A	N/A	PP4 PP5	N/A	PP2 PP3	N/A	PP1

Where PP1-8 is the Pilot Pattern one to eight. Depending on the pilot pattern used, the boosted level of the pilot varies. The boosted level can be either $\frac{4}{3}$, $\frac{7}{4}$, and $\frac{7}{3}$. This is crucial to know depending on the pilot amplitude manipulation scheme that would be used during remodulation stage of the Demod-Remod process.

The continual pilots in the data symbols are placed at the same sub-carrier index for all data symbols in a particular frame. The number and location index of the continual pilot is dependent on the FFT size as well as the scattered pilot pattern in use of the frame. The continual pilots are boosted by a factor dependent on the FFT size and these are summarised Table 4.2. In the case that a carrier index is the same for both the scattered and continual pilots then the boost factor of the corresponding scattered pilot shall be used.

Table 4.2: Boosting for the continual pilots

FFT Size	1k	2k	4k	8k	16k	32k
Boost Factor	$\frac{4}{3}$	$\frac{4}{3}$	$\frac{4\sqrt{2}}{3}$	$\frac{8}{3}$	$\frac{8}{3}$	$\frac{8}{3}$

The continual and scattered pilot location across frames is the same. An example of both scattered and continual pilots across subcarrier index (frequency) and data symbol (time) can be seen in Figure 4.7. The PLP of the data symbol contains it's own different digital modulation scheme. This can either be QPSK or 16, 64, 256 QAM. The remaining cells in the data symbols are generally filled with either empty cells (dummy cells) or filled with auxillary streams which are transmitter specific and are not required for demodulation.

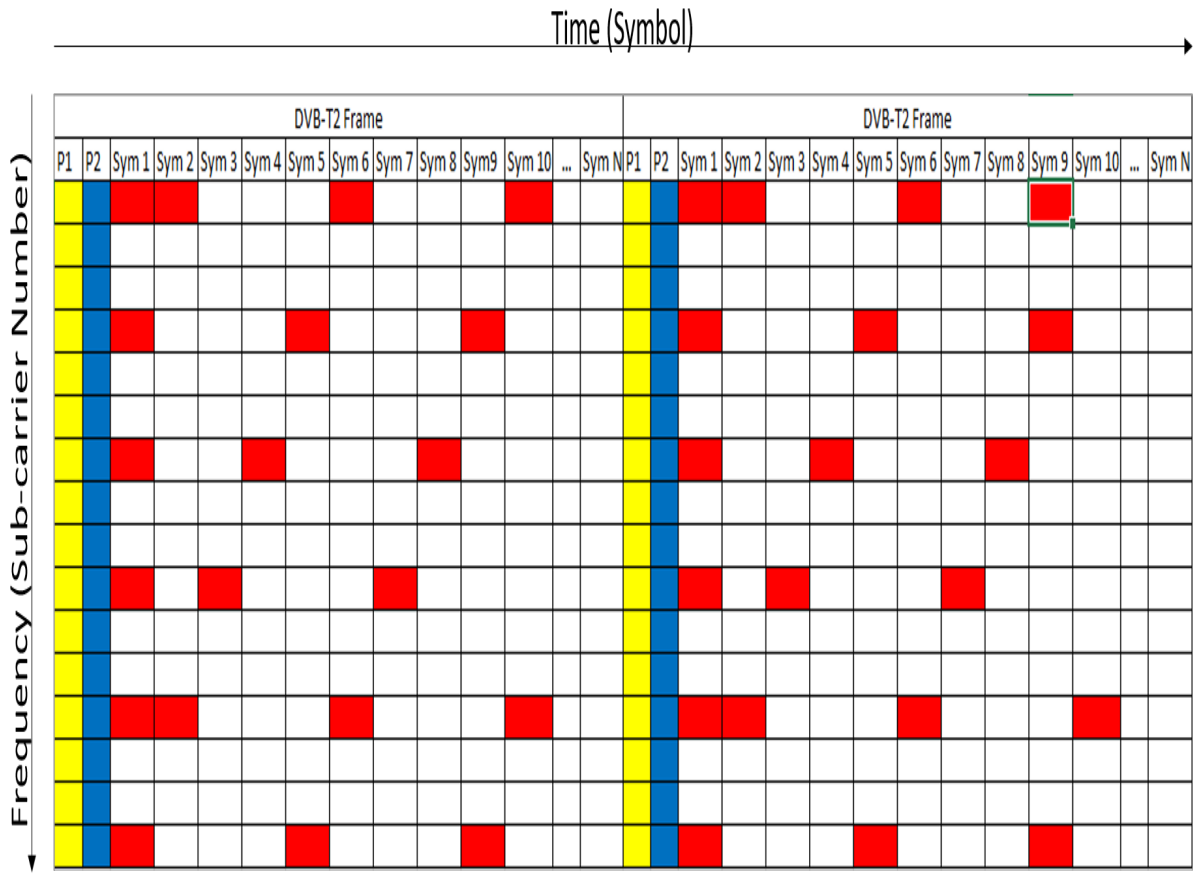

Figure 4.7: DVB-T2 Frame Structure with Scattered and Continual Pilots

To complete the demodulation of the reference signal, the noise in the data cell is then

removed using a simple hard decision as to their reference constellation point according to their PLP configuration. From the demodulation of the received DVB-T2 signal used by the Constantiaberg transmitter, the set of parameters defined for the DVB-T2 system based in Cape Town are described in Table 4.3

Table 4.3: Parameters Used In The Cape Town Region, South Africa

Parameters	Value
Frame Length	0.236 seconds
FFT Size	32768 (32k)
Active Carriers	27841
Bandwidth	7.77 MHz
Subcarrier Spacing	279 Hz
Scattered Pilot Pattern	PP4
Scattered Pilot Carrier Separation	12
Symbols per Scattered Pilot	2
Scattered Pilot Boosted Level	7/4 * Amplitude Data Symbols
Continual Pilots Boosted Level	8/3 * Amplitude Data Symbols
OFDM Symbol Length (T_u)	3584 μS
Guard Interval Fraction (GIF)	$\frac{1}{16}$
Guard Interval Length (T_g)	224 μS
Data Symbol Encoding	64 QAM

The effect of these parameters on the CAF shown in Figures 2.7 and 4.5 with respects to the ambiguous peaks are described as delay ambiguities, Doppler ambiguities and auxiliary ambiguities . These can be further described as [42]:

1. *Ambiguities in delay:* The scattered pilots should be noted to be separated at constant intervals of 24 carriers within a given symbol. This places the peaks of the scattered pilot in the CAF at every $\frac{T_u}{24}$ seconds in delay. This equates the scattered pilots to sinusoids evenly spaced by $\frac{24}{T_u}$ Hz.

2. *Ambiguities in Doppler* The ambiguities in Doppler can be associated to the scattered pilots. The scattered pilots are spaced regularly across symbols as well. Every 2^{nd} symbol contains scattered pilots occupying the same carrier. For the signal used in Figure 4.5 the guard interval spacing is $\frac{1}{16}$ this corresponds to a pilot spacing of 7.2 ms or ambiguities peaks to appear every 139.2 Hz in Doppler.

3. *Auxiliary ambiguities* There are other ambiguities that form part of the DVB-T2 signal. These can be correlated to the guard interval of the DVB-T2 Frame and data symbols. These are:

- **Cyclic Prefix:** These are due to the guard intervals that appear at the end of each OFDM symbol and repeat every T_u seconds. These, however, aren't that much of a concern in the processing. This is due to the fact that DVB-T/T2 based systems have lower detection ranges, this is in the order of 10s of km to 100 km at best depending on the region of operation, based on the propagation effects of UHF frequencies, the downward tilt of the commercial transmitter beams and low transmission power of the signal. The length of T_u corresponds to ranges of 1000 km for the Cape Town system which is well over the expected ranges of DVB-T/T2 systems. Thus due to this the guard ambiguities shall be ignored in the remodulation stage and remain unchanged.
- **Inter-symbol ambiguities:** These are continuous pilots that appear at the same index across consecutive OFDM symbols. However these pilots cause ambiguities to appear at delays greater than T_u thus can be ignored for similar reasons as the cyclic prefix.

The next stage of the Demod-Remod process is the remodulation of the demodulated reference signal. In this process the signal would be recreated, however, without the ambiguities caused by the pilots to produce a noise free reference of the signal by applying a inverse FFT (IFFT) on the reference signal. There are two methods that can be used to mitigate the effects of the pilots. These methods are either Pilot Blanking or Pilot Normalisation. Pilot blanking involves the zeroing of the indices of both the scattered and continual pilots. This causes the ambiguities caused by the pilots to be suppressed to a level below the noise floor. The disadvantage of using this method to remove pilot ambiguities however is the reduction in the total bandwidth of the signal leading to a small loss in range resolution. Pilot Normalisation/Equalisation involves normalising the boosted power levels of the pilots. The pilots, are not normalised to the power of the signal level but the normalisation occurs during the cross-correlation process of the range-Doppler processing. Thus, if the scattered pilots are boosted by $\frac{7}{4}$ above the data symbols the pilots new power levels are set to $(\frac{4}{7})^2$ of the original boosted level. Similar is done with respects to the continual pilots. The method of pilot manipulation used in the proposed processing chain is pilot normalisation/equalisation. The boosted power levels of both the continuous and scattered pilots of the reference signal as given in Table 4.3 were reduced by a factor of each boosted levels inverse squared. The scattered pilots were reduced by $(\frac{4}{7})^2$ and the continuous pilots by $(\frac{3}{8})^2$ respectively. The reference signal is then remodulated, the output of the reference signal before and after Demod-Remod process can be seen in Figure 4.8 with Figure 4.8b illustrating that the boosted pilots seen in Figure 4.8a are no longer visible. The Demod-Remod process implemented in this dissertation is derived from the work done by [42] in conjunction with this disserta-

tion. Thus, the Demod-Remod process did not form part of the scope of work for this dissertation.

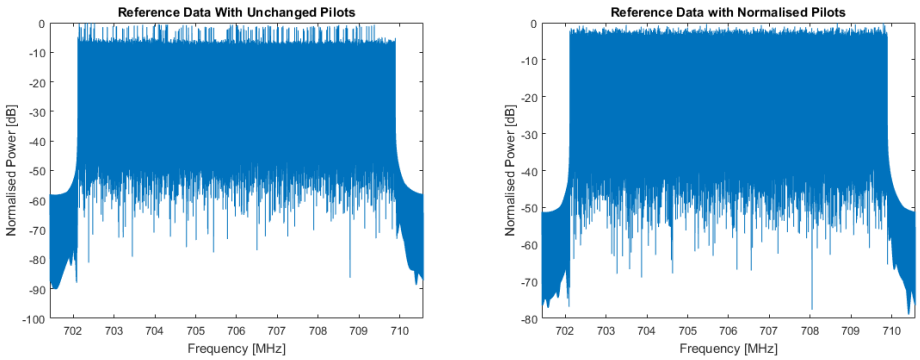

(a) Normalised Reference signal with unchanged pilot tones

(b) Normalised Reference signal with normalised pilot tones

Figure 4.8: Spectrum of reference DVB-T2 signal before and after Demod-Remod

The resultant CAF of the remodulated reference signal is shown in Figure 4.9. It can be seen that there are no longer any visible ambiguities.

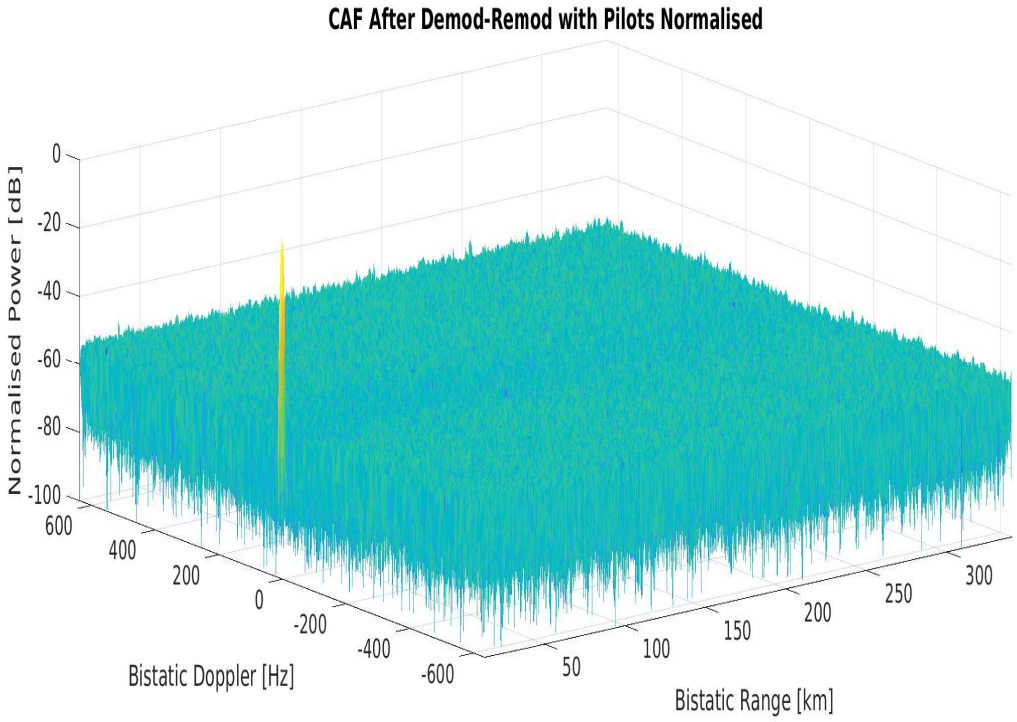

Figure 4.9: CAF of remodulated reference signal with normalised pilots

4.1.3 Range and Doppler Processing

The outputs of the reference branch and surveillance branch are used to do the Range/-Doppler processing in order to determine the location of the target. This can be done by determining the match filter which is the cross-correlation of the surveillance channel with the Doppler shifted versions of the reference channel as described by Equation 2.5.

The extent of the delay and Doppler shift of the reference channel is done to cover all possible target bistatic ranges and velocities respectively. The output of the Range/-Doppler processing is a 2-D map called the amplitude, range and Doppler map or ARD. To create the ARD map, it can be thought about as a bank of match filter outputs where the reference channel has a unique Doppler shift per match filter calculation to cover all the possible target velocities. This process is typically done with discrete-time sampled versions of the reference and surveillance signals and thus Equation 2.5 can be rewritten as

$$C[l,m] = \sum_{N-1}^{n=0} s_s[n]s^*[n+l]e^{j2\pi\frac{mn}{N}} \tag{4.8}$$

where l is the delay over an integer number of samples, m is the discrete Doppler shift, N is a CPI lengths worth of samples. The CPI, or coherent processing interval, is a chosen length samples to be combined coherently, that is in amplitude and phase, to improve the SNR of the matched filtered signal. The length of samples have to be carefully chosen such that it is long enough to provide a significant amount of SNR improvement through integration gain but short enough to avoid potential problems such as range and/or Doppler walk across the ARD map cells.

An ARD map is made up of multiple range and Doppler cells. A single cell is made up of a single range bin and a single Doppler bin. A range bin is defined as

$$\Delta R_{\text{bin}} = \frac{c}{f_s} \tag{4.9}$$

where c is the speed of light and f_s is the sampling frequency. A Doppler bin is defined as

$$\Delta f_{\text{d-bin}} = \frac{1}{T_{\text{CPI}}} \tag{4.10}$$

where T_{CPI} is the coherent processing interval in seconds. The total number of range and Doppler bins in an ARD map is dependent on the maximum bistatic range of the region of interest and the maximum velocity of the target of interest.

Correlation Equation 4.8 is highly computationally expensive due to the number of multiplications and summations needed. This can be however optimised to reduce the number of operations required. One such method is by utilising the FFT. For DVB-T based passive radar [4] recommended the FX, or FFT calculation first then point-wise cross correlation, method for calculating the ARD maps due to the dimension of the ARD Map

that is generated from the CAF. DVB signals typically have large bandwidths and thus have fine range resolutions which corresponds to a large number of range bins required. The FX method works by FFTing the reference and surveillance signal. The surveillance signal would be conjugated. The corresponding bins would be multiplied together and the result then inverse FFTed (IFFTed) resulting in the zero Doppler line across the full Range of interest. The other Doppler frequency range bins are determined by point-wise multiplying the conjugated FFTed surveillance signal with the FFTed Doppler shifted versions of the reference signal and then IFFTed. This generates ARD maps for the chosen number of Doppler bins up to the maximum Doppler range where the maximum range is dependent on the number of CPI samples. To exploit the fine range resolution of the DVB signals the FX method would be ideal as the Doppler bins to process can be chosen and have the range bins be covered by the range calculation up to N_{CPI} - 1 samples. An example of an ARD map is shown in

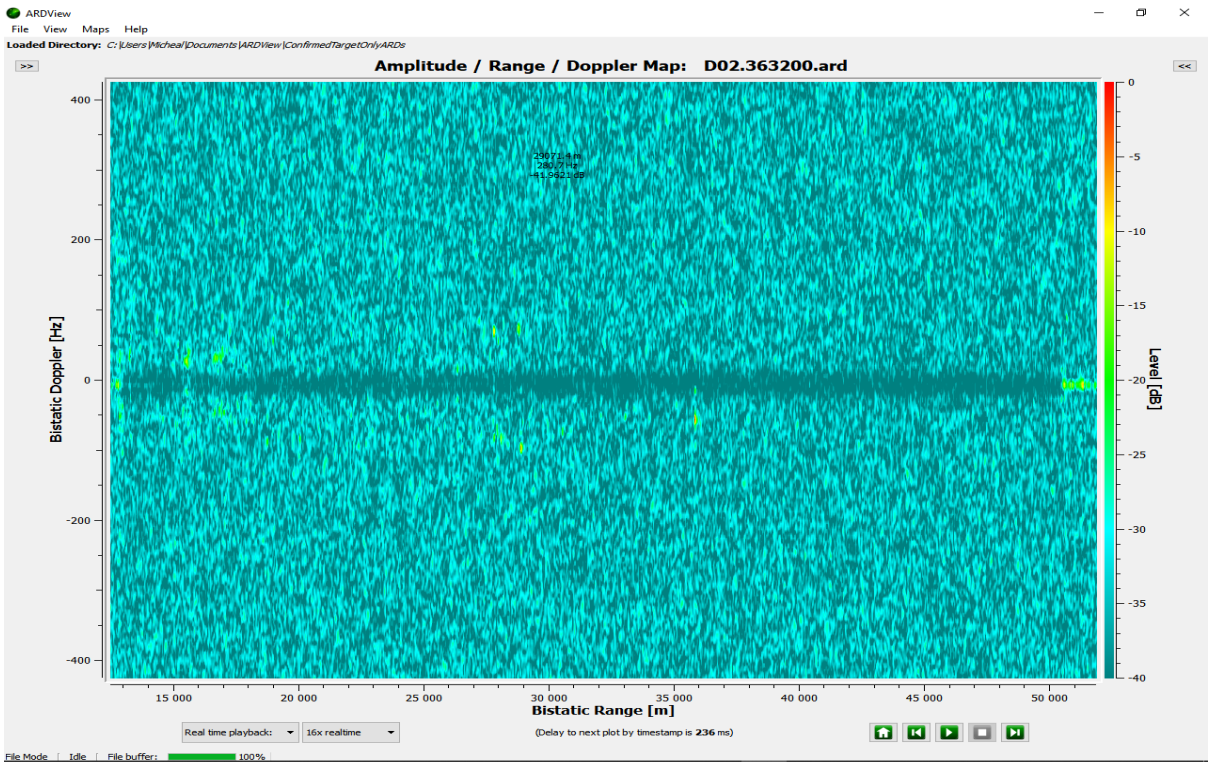

Figure 4.10: ARD Map of DVB-T2 signal for a CPI equal to the frame length. The maximum bistatic range is approximately 52 km with a range bin of 32.7898 metres. The maximum bistatic Doppler is approximately +/-425 Hz with a Doppler bin of 4.23155 Hz. This corresponds to an ARD map of 1201 range bins X 201 Doppler bins.

4.1.4 Target Detection

The output of the range and Doppler processing is typically fed into a target detector to extract the target from the range and Doppler space of the ARD. The amplitude of a range and Doppler cell is typically compared to a known amplitude threshold and dependent on whether the amplitude is greater or smaller than the threshold it can be

deduced that a target exists or not within a specific cell. One such detection method is the CFAR filter.

The CFAR filter evaluates a single cell, often known as the cell under test (CUT), to surrounding cells in range and/or Doppler[38]. The probability that a detection is determined in the cell under test is a target is called the probability of detection (P_d). However, the probability that a detection is not a detection but rather a large noise spike or clutter is the probability of false alarm (P_{fa}).

A radar system typically aims to have a high P_d and a low P_{fa}. Getting this tuning process correct however can be difficult, as the relationship between P_d and P_{fa} is not directly proportional and thus for most practical radar systems a certain degree of false alarms should be accepted. Typical radar systems aim to have a P_{fa} in the range of 10^{-4} to 10^{-8} and a P_d of 50 to 80 %. The detection method used for this project was the GOCA-CFAR, or the Greater of Cell Averaging CFAR. This was chosen as the clutter environment is non-homogeneous due to the multiple possible interferers surrounding the receiver site. The possibility of there being interfering targets, or a target within the reference cell of the CUT, were deemed to be minimal due to the nature of air traffic surrounding the Cape Town International Airport that a GOCA-CFAR was deemed to be sufficient.

4.2 Summary

A full processing chain for DVB-T2 PCL radar system was presented. This processing chain included the DPI cancellation, Demod-Remod process and the range and Doppler processing. The DPI algorithm implemented was the CGLS based on literature. It was found that the DPI cancellation process is not optimised for DVB-T2 signals and a further investigation into cancellation for DVB-T/T2 signals would be required. It was shown what effect the signal properties of an OFDM signal have in terms of radar signal processing. Methods on how to mitigate these effects was presented. It was shown how to integrate the demod-remod process into the typical radar signal processing chain. Finally, the mismatched filtering process was presented.

Chapter 5

Results

In this chapter the results of the proposed system would be demonstrated based on tests that were done at UCT. Firstly, the system configuration will be described. This would be followed by the results from field tests. The performance of the DVB-T2 PCL system would then be compared with an FM based PCL system and discuss the differences and the benefits of using multi-frequency, multi-static PCL system.

The airspace surrounding Cape Town International Airport was being monitored for these tests. The resultant radar results were then compared with Automatic Dependent Surveillance-Broadcast (ADS-B) data logs received from the aircrafts.

5.1 System Geometry and Configuration

5.1.1 System Geometry

The system was deployed at University of Cape Town with the goal to be the monitoring of the Cape Town International Airport. The system geometry illustrating the transmitter, receiver and the area of interest is depicted in Figure 5.1a. The receiver location is illustrated as Rx. The transmitter chosen is the Constantiaberg transmitter which is South-West of the receiver location. The transmitter has an ERP of 50 kW at 706MHz with a horizontal polarisation. The baseline between the transmitter and receiver is 12597 metres. The airport is to the East of the receiver location. There are two flight paths for take off and landing at the Cape Town international. Aircrafts can either take-off and/or land from the north side of the airport or can take-off and/or land from the south side of the airport. Thus the region of interest is the area to the east of the airport from immediate north to the south of the airport. The surveillance antenna beam pattern main lobe shown is in the direction of the blue triangle. The reference and surveillance

antenna were mounted on the roof of the Menzies building and the configuration can be seen in Figure 5.1b. With this configuration, the resultant analogue channel separation between the reference and surveillance antennas was approximately 20 dB.

(a) PCL Radar System Geometry illustrating the trans-

(b) Antenna Configuration on top of the Menzies building at the University of Cape Town. The reference antenna is facing South-West to the Constantia transmitter and the surveillance antenna is facing the airport to the east.

Figure 5.1: PCL Radar System Geometry with Antenna Configuration

5.1.2 System Configuration

Due to the limitations of the A matrix of the cancellation stage of the mismatch filtering process described in section 4.1.1 the maximum bistatic range of the system was limited to 50 km. This is based on the memory limitation of the GPU that was being used for the processing chain a 6 GB nVidia GTX 1060. This distance would be sufficient for the purpose of the trials as the airport is at a distance of 35 km bistatic.

The sampling rate of the receiver was 10 MSps. During the demod-remod process however the data was resampled to $\frac{64e6}{7}$. This was done to ensure that the FFT frequency resolution was equivalent to the subcarrier spacing of the OFDM signal. Both the reference and surveillance were resampled by a factor of $\frac{64}{70}$. The signal is upsampled by a factor of 64 and downsampled by a factor of 70. The output signal still adheres to Nyquist sampling theory thus avoiding any distortion due to anti-aliasing. This leads to a range bin resolution of 32.8 metres/bin from Equation 4.9. The CPI of the received system was equivalent to the length of a single DVB-T2 frame. The length of the frame for the Cape Town DVB-T2 signal was 0.23632 seconds. This is equivalent to 2160640 samples. The CPI length thus leads to a Doppler bin resolution of 4.23 Hz/bin from Equation 4.10. This corresponds to a velocity of 0.8987 m/s assuming system operating in the psuedo-monostatic region.

In the ARD map the 0 bistatic range is shifted by the length of the baseline during the ARD calculation as this is the delay length of the reference signal to the receiver location. Thus , this is the shortest distance measurable for the target from the transmitter to target to receiver. Thus, to measure a target that is 50 km away bistatic the number of range bins required was 1141 range bins. The number of Doppler bins was chosen was 101. This corresponds to 89.87 m/s or 323.54 km/h. Due to the area of surveillance and the maximum distance specified the targets around the airport would either be landing or taking off. The maximum takeoff velocity for a passenger aircraft is 285 km/h and the landing speed would be approximately 287 km/h thus which is well within the limits of the chosen dimensions.

The DPI cancellation was done across the full range bin due to the environment of the deployment. The CPI was broken up into 16 sub-blocks of data corresponding to 135040 samples per sub-block, or 0.01477 seconds worth of CPI data. The number of Doppler bins to apply DPI cancellation was chosen to be 3 including the zero Doppler line across the full range.

A summary of the full system parameters for the DVB-T2 PCL radar is provided in table 5.1.

Table 5.1: DVB-T2 System parameters

Transmitter (Tx)	
Antenna Beam Pattern	Isotropic
Antenna Altitude	850 metre
Carrier Frequency	706 MHz
ERP	50 kW
Bandwidth	7.77 MHz
Waveform	Commercial DVB-T2
Receiver (Rx)	
Antenna Beam Pattern	Sinc
Antenna Gain	13.3 dBi
Antenna Altitude	140 metre
LO Error	50 ppb
Noise Figure	5 dB
Digitisation	10 MSps Complex(Downsampled to $\frac{64}{7}$MSps) 14 bit quantisation
Tx To Rx Baseline	12 597 metres
Processing Parameters	
Processing Scheme	Mismatch Filtering
DPI Cancellation	1141 range, 3 Doppler bins
DPI Cancellation Block Length	135040 Samples(0.01477 seconds)
Range/Doppler Processing	1141 range, 201 Doppler bins
Range/Doppler CPI	2160640 Samples(0.23632 seconds)
CFAR Algorithm	GOCA-CFAR
CFAR Window	4 guard cells, 8 reference cells (either side of CUT)
CFAR Dimensions	Range
CFAR Threshold	$P_{fa} = 10^{-6}$

5.2 Target Detection

Recordings were done with the proposed front-end in chapter 3 and post processed using the parameters as described in table 5.1. On this day the aim of the recordings was to monitor the morning traffic coming in and out of the airport. Figure 5.2 illustrates two targets that were detected. The two targets were detected at bistatic ranges of 36.6 km and 36.1 km and at bistatic Doppler rates of -97 Hz and +94 Hz respectively. The white tails trailing the red centroids illustrate the detection history of the aircraft over a period of time in this instance the detection history corresponded to 20 seconds. The first target

was initially detected at 35.42 km bistatic taking off from the airport in the southern direction. The ADS-B data of the detected target can be seen in Figure 5.3.

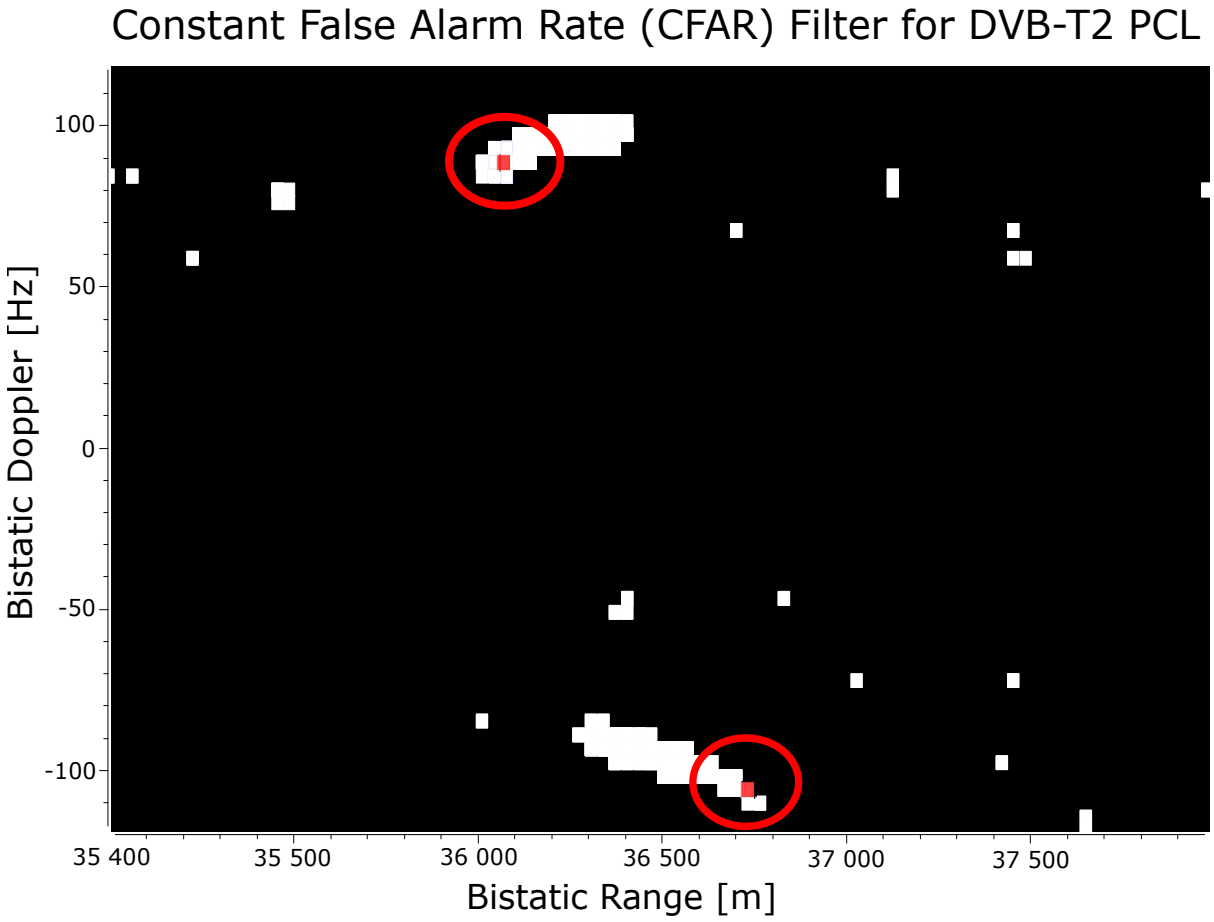

Figure 5.2: CFAR output with two targets detected around the Cape Town International Airport. First target at a bistatic Range of 36.6 km and a bistatic Doppler of -97 Hz. The second target was detected at 36.1km bistatic range and at +94 Hz bistatic Doppler. The results presented here are from real data collected in the field with UCTs prototype radar system and the Peralex ComRad receiver.

Through ADS-B data it was determined that the detected target corresponded to flight NMB703 taking off from the airport. The initial detected Doppler frequency of the specific target was low, at about -40 Hz due to the fact that the target was flying along the iso-contour and the angle δ from Equation 2.2 was slightly greater than 90 degrees relative to the bisector line. As the target was continuing to climb in the southern direction the angle relative to the bisector began to increase as did the velocity. The target was detected up to a bistatic range of 36.93km and a bistatic Doppler rate of -110 Hz where upon it had exited the receiver LOS.

While there was no received ADS-B data that corresponds to the second target at the time of recording, it was deduced that the target was located on the north of Cape Town International Airport. This was done by analysing the bistatic range ellipse of the PCL system based on the detected target. From the resultant analysis the target it was

deduced that the target was taking off from the north of the airport.

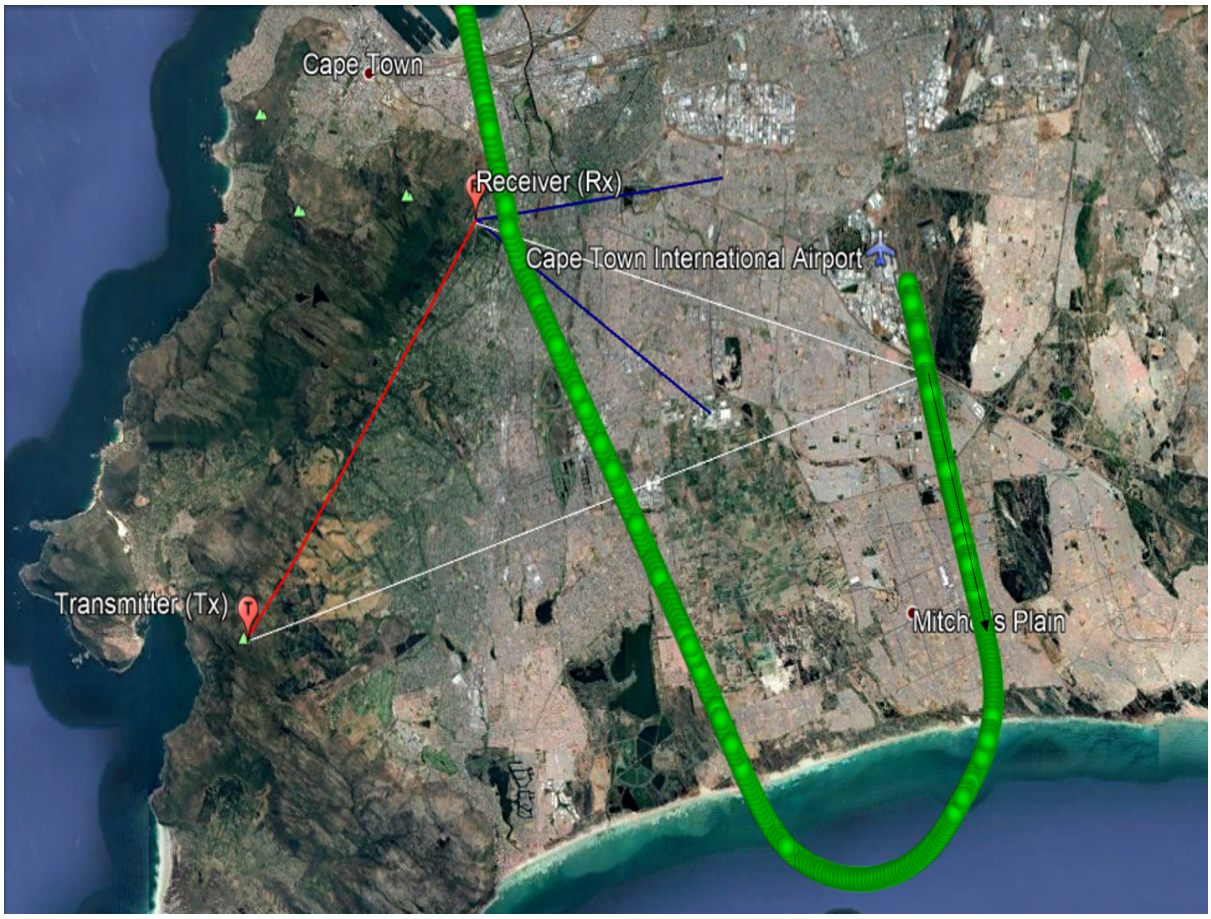

Figure 5.3: ASD-B Data of Air Namibia Flight NMB703 taking off from the airport from the south. The green dots correspond to the transmitted target GPS information at a certain instant in time. The white triangle illustrates the bistatic triangle with the black arrow the direction of the target.

5.2.1 Multi Band PCL Demonstrator

The trials above were extended to evaluate the benefits of using both FM and DVB-T/T2 systems in a multi-static configuration. The evaluation was done utilising industry partner, Peralex Electronics, commercial grade PCL system named the ComRad Passive Coherent system [12, 58]. The system has both an FM and a DVB-T/T2 variant. The ComRad system receiver, ComRad3R, is a coherent 3 16-bit channel wideband receiver. A single channel is used for the reference channel and the other two channels are used as surveillance channels. The extra surveillance channel allows for Angle of Arrival (AoA) calculations to determine the direction of the target echo return. The DVB-T2 system geometry for the ComRad receiver is similar to the geometry in Figure 5.1. Power splitters were used to split the signal from each antenna to the proposed UCT demonstrator in chapter 3 and the DVB-T/T2 ComRad receiver. The processing chain used for is the proposed processing chain in chapter 4 using the parameters in table 5.1 with exception

of the digitisation and noise figure. The ComRad DVB-T/T2 receiver has a 16 - bit ADC and samples at 12.8 MSps with a noise figure of 4 dB.

The system geometry of the FM system has a minor difference relative to the DVB-T/T2 system. Though the receiver location is the same the transmitter used in this instance is the Piketberg transmitter located 118,5 km north-east of the receiver site. The antennas used for the FM system are three VHF Yagi antennas where a single antenna is pointed directly at the transmitter and connected to the reference channel. The surveillance channel antennas are pointed in the direction of the airport spaced half a wavelength apart with a slight upward tilt. This is done to calculate the AoA using phase interferometry and to reduce the strong clutter return from the ground clutter. The system geometry and antenna setup of both the FM and DVB-T/T2 system can be seen in Figure 5.4

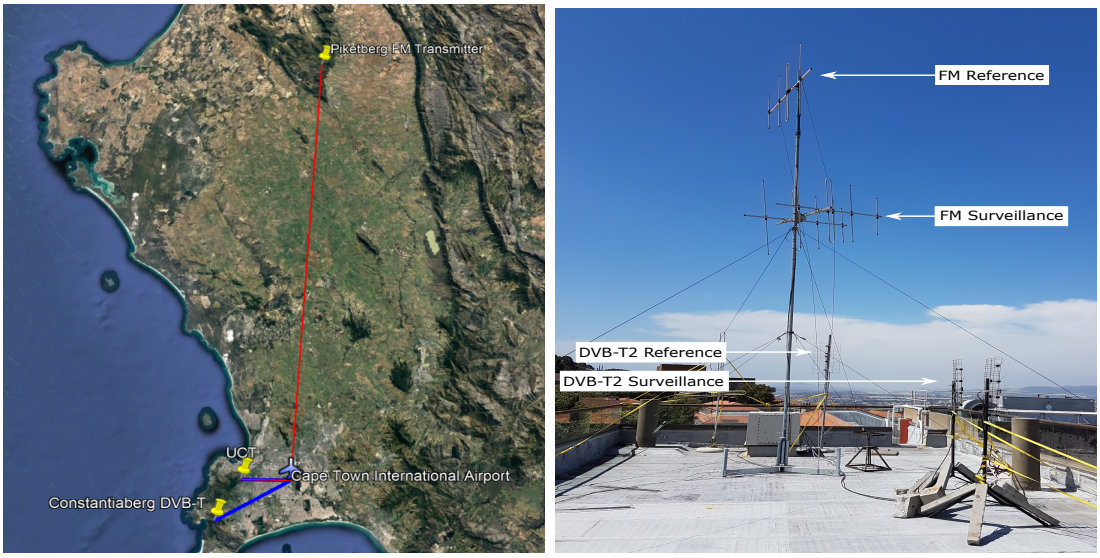

(a) PCL Radar System Geometry illustrating the transmitter, receiver and area of interest. The FM transmitter located in the North-East of the receiver site and the DVB-T/T2 transmitter is located to the South-West. Both the surveillance channels are facing Cape Town International Airport.

(b) FM and DVB-T Antenna Configuration on top of the Menzies building at the University of Cape Town.

Figure 5.4: Combined PCL Radar System Geometries with Antenna Configurations

The FM variant is a 3 channel direct conversion wideband receiver. The system has the capability of sampling the entire FM band from 88 - 108 MHz. The system is also capable of sampling one or more narrowband FM channels simultaneously. A single FM channel is 200 kHz wide where the FM signal has a bandwidth of 150 kHz and a guard interval of 25 kHz either side of the carrier signal. The processing chain for the FM system can be seen in Figure 5.5. The processing is done in real-time. The DPI cancellation algorithm is the CGLS algorithm as described in section 4.1.1 which provides up to 40 dB of DPI suppression. The output of the DSI cancellation on the surveillance channel is matched filtered with the reference signal for range and Doppler processing. Finally, the output

of the range and Doppler processing for each surveillance channel is combined to form a single ARD plot.

A summary of the system parameters for the FM based ComRad system are described in table 5.2.

Table 5.2: FM System parameters

Transmitter (Tx)	
Antenna Beam Pattern	Isotropic
Antenna Altitude	850 metre
Carrier Frequency	97.6 MHz
ERP	50 kW
Bandwidth	200 kHz
Waveform	Commercial FM
Receiver (Rx)	
Antenna Beam Pattern	Sinc
Antenna Gain	7.2 dBi
Antenna Altitude	140 metre
LO Error	50ppb
Noise Figure	4dB
Digitisation	204.8kSps Complex
	16 bit quantisation
Tx To Rx Baseline	118 500 metres
Processing Parameters	
DPI Cancellation	120 range, 5 Doppler bins
DPI Cancellation Block Length	102400 Samples(0.5 seconds)
Range/Doppler Processing	120 range, 1601 Doppler bins
Range/Doppler CPI	819200 Samples(4 seconds)
CFAR Algorithm	GOCA-CFAR
CFAR Window	4 guard cells, 8 reference cells
	(either side of CUT)
CFAR Dimensions	Doppler
CFAR Threshold	$P_{fa} = 10^{-5}$

The results from the FM system can be seen in Figure 5.6. Three targets can be seen at 124.3 km, 135.2 km, 155.6 km bistatic range on the positive Doppler axis moving towards the PCL system. Two targets can be seen moving away from the system on the negative Doppler axis at bistatic ranges of 136.5 km and 174.4 km. As FM radio operates at VHF frequencies as well as the typically high ERPs of FM transmissions

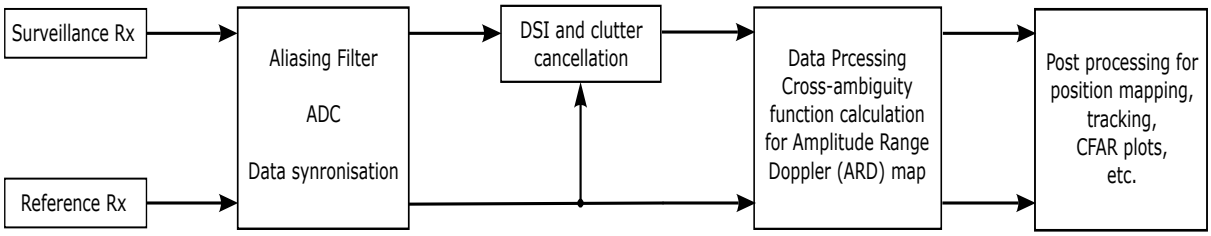

Figure 5.5: FM Processing Chain

leads to greater propagation distances thus detection ranges of an FM based passive radar can range in the order of 100 s of km as is seen in Figure 5.6. Another advantage for FM PCL is the significantly long integration times, typically 1 - 4 seconds, can lead to fine Doppler resolution from Equation 4.10 which can be exploited for Doppler only tracking as described in[5]. In this instance a CPI of 4 seconds was used which translates to a Doppler resolution of 0.25 Hz.

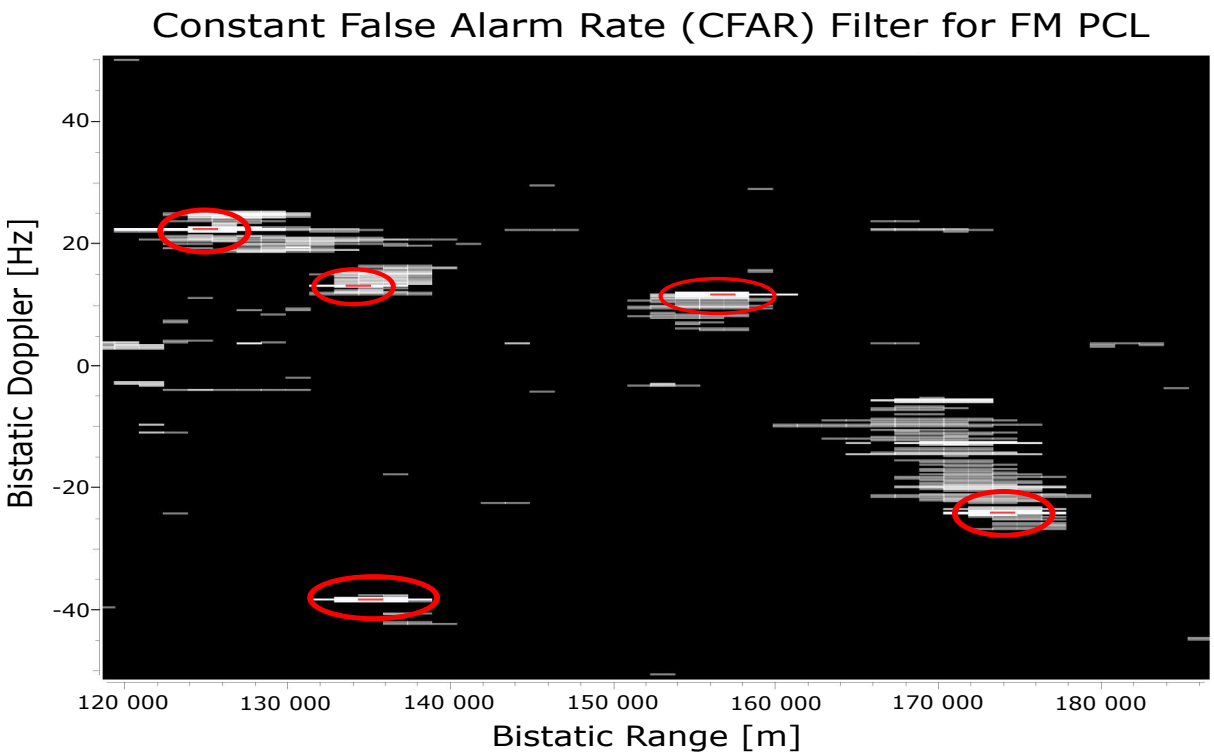

Figure 5.6: CFAR output with five targets detected around the Cape Town International Airport. Three targets can seen approaching the system from the positive Doppler. The other two targets are moving away from the system on the negative Doppler side. The results presented here are from real data collected in the field with the Peralex ComRad FM receiver

The two targets at 135.2 and 136.5 km bistatic at positive and negative Doppler coincide with the two targets detected from detected in the DVB-T2 systems as shown in Figure 5.7. The negative Doppler target coincides with the ADS-B data as in Figure 5.3 for flight NMB716. With the second target being the without ADS-B but was noted to be a flight taking off from the north side of the airport.

The one drawback of the FM based PCL system is the large range resolution which is 1 km assuming a bandwidth of 150 kHz and system operating in the pseudo-monostatic region. Due to the bandwidth of the FM signal being dependent on the content being transmitted an the analogue FM signal, the range resolution is likely to fluctuate. In these tests the FM range resolution was fluctuating between 2 - 3 km on average as seen in the CFAR plot. This is different for the DVB-T/T2 systems as the constant large bandwidths of the of the digital OFDM based signal allow for fine range resolutions in the order of 18 - 19 metres assuming pseudo-monostatic operation which is almost 50 times better than the FM system. However, DVB-T/T2 systems suffer from shorter CPI lengths, which can range from 150ms for DVB-T and 250 ms for DVB-T2. This leads to coarser Doppler resolutions which for the system used in these tests was 4.23 Hz.

From the results above it is clear that there are benefits to using the two PCL systems in a multiband multi-static configuration for detection of targets in the short-medium range. The system can benefit from the finer Doppler resolutions of FM based PCL radar and the fine range resolutions of DVB-T/T2 systems. Utilising two separate baselines in a multi-static configuration could allow for greater target localisation by analysing the bistatic ellipse intersection points. The fusion of the data from both systems would also allow for more reliable target tracking.

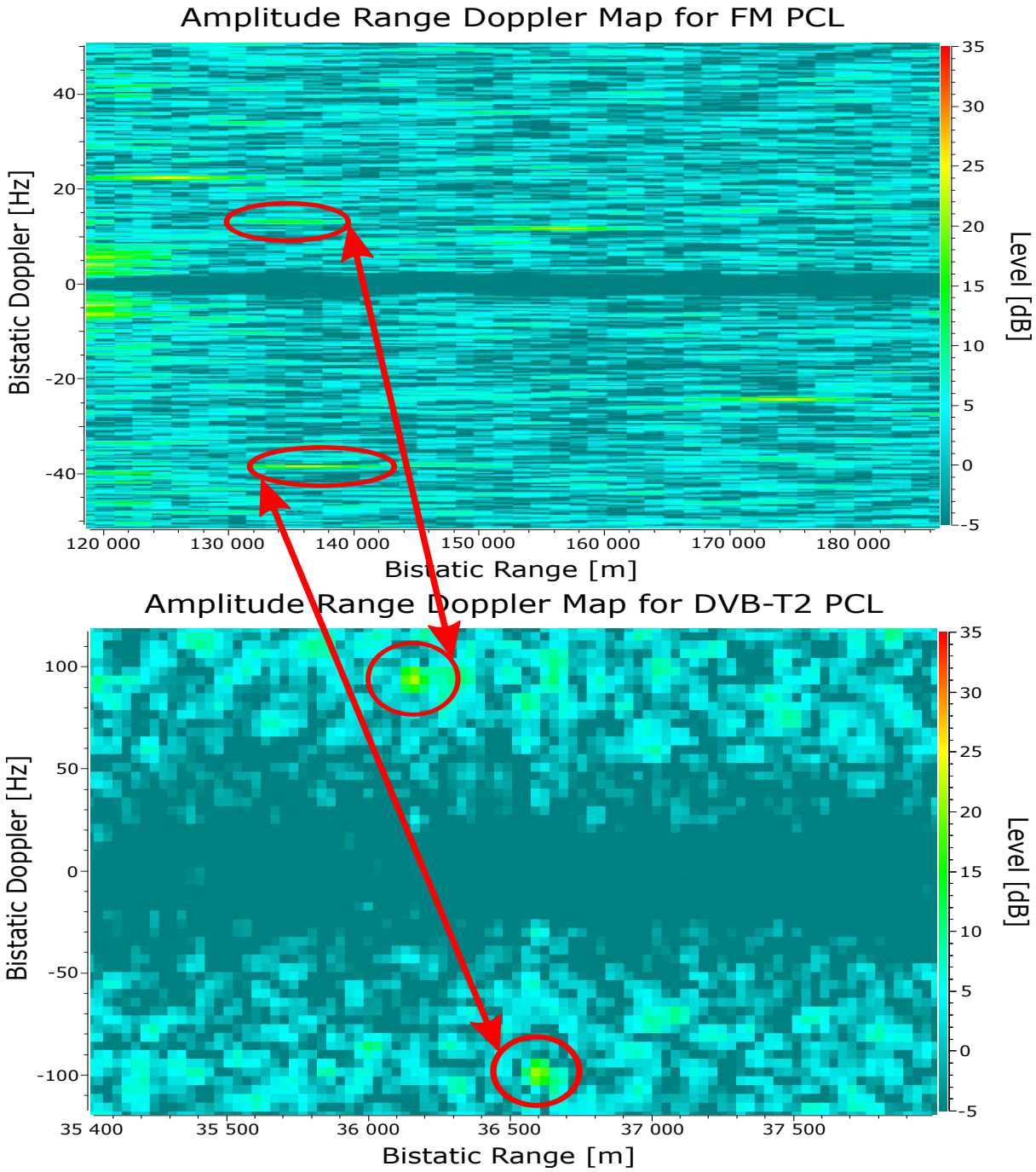

Figure 5.7: ARD comparison of the two detections from the FM and DVB-T2 based systems. The FM target at 135.2 km bistatic range and 15 Hz bistatic Doppler corresponds to the target at 36.1 km bistatic and 94 Hz bistatic Doppler. The second FM target at 136.5 km bistatic range and -40 Hz bistatic Doppler corresponds to the target at 36.6 km bistatic range and -97 Hz bistatic Doppler.

5.3 Summary

In this section detection of aircraft in the area of interest was successfully shown. The detected aircraft coincide with ADS-B data received from the transmitting target.

The evaluation of a multiband multi-static PCL radar system was also done utilising a FM and DVB-T2 based PCL radar systems. The benefits of utilising the strengths of each individual system in tandem was illustrated and discussed.

Chapter 6

Discussion and Conclusion

The objectives for this dissertation were to design and develop a DVB-T2 demonstrator. Part of this was investigation into a processing chain for the DVB-T2 system. This was achieved and successful demonstration of the system was illustrated with detection of targets in the vicinity of Cape Town International airport. While the system was fully operational certain limitations outlined in section 1.2.2 and chapter 3, improvements can be made to the system.

A detailed implementation of a processing chain for a DVB-T2 PCL system was also completed and tested. The system was able to be tested with both the proposed front-end system as well as a commercial receiver. The system however was not able to operate in real-time and be integrated with either the system and thus improvements can be made to the processing chain.

To cover the future work and conclusions, both the front-end design chapter (Chapter 3) and processing chain chapter (Chapter 4) will be presented on separately.

6.1 Front-end Design

System planning and propagation modelling was done to determine the ideal location to deploy the system as well as to aid the design of the receiver front-end for the aforementioned location. From the system planning and propagation modelling UCT was seen as an ideal site for initial deployment of the system. The transmitter of choice was chosen to be Constantiaberg due to the expected DPI based on the propagation modelling. Tygerberg would have been ideal due to the direct Line of Site to the transmitter with minimal mountainous ridges in-between the proposed receiver location and the transmitter. However, the Tygerberg transmitter has the limitation being on the northern flight path for Cape Town International Airport targets and thus targets could potentially be hidden

in what is called the cone of silence region for a radar, this is the region directly above the transmitter that a target is flying across. Secondly, the Tygerberg transmitter could potentially either mask targets in the surveillance channel due to the target flying past the baseline and thus being in the forward scatter region of a PCL radar system or more processing power would be required to remove the DPI from the surveillance channel dependent on the geometry of the surveillance channel. Alternatively, the surveillance channel could be rotated more south, however, this would make the system blind to targets from the north. Thus, the system geometry and greater surveillance area due to lower DPI made the Constantiaberg transmitter the ideal choice at the time.

A prototype DVB-T2 front-end was designed and implemented with the N210 and SBX daughterboard. The implemented prototype front-end worked well though the full dynamic range of the ADC couldn't be utilised due to the proposed front-end not being implementable due to specified limitations. Thus, parts of the future work would be the completion of the RF front-end as is designed to improve the system.

6.1.1 Future Work

Although the receiver location specified was ideal for research purposes and short range target detection, it is not the most ideal for ATM purposes. The surveillance of targets was limited to targets that had either just taken off and/or targets that were just about to land. This is due to two crucial factors. The LOS of the antenna main lobe in conjunction with the system geometry. This can be improved by either investigating different receiver locations based on the available transmitter information and known flight paths or investigate alternative antenna designs that give greater LOS coverage and/or integrating both solutions.

The prototype front-end needs to be completed and the full system design implemented. Part of completing the RF front-end would be the investigation and/or design of an RF filter to isolate a single DVB-T2 channel. This filter should have a sharp enough roll-off such that the out of band can be suppressed and the dynamic range be maximised.

Lastly, the integration of the system with the back-end for real-time processing was not implemented at the time. Future work should be done on the front-end either through optimising the Labview code or coding the board directly in C++ using the UHD API. Currently, the demonstrator has the ability to record the data and the data is then post-processed for target detection

6.2 Processing Chain

A complete design of a DVB-T2 processing chain was presented and implemented using demod-remod and mismatch filtering. The chain includes the process of DPI cancellation from the surveillance channel. The CGLS algorithm was used to suppress the direct path signal from the surveillance channel, However it was found that the CGLS algorithm was not optimised for high bandwidth signals such as DVB-T2.

The successful removal/suppression of pilot tones in the DVB-T2 OFDM signal to remove ambiguities in the amplitude range Doppler map through the demod-remod process. It was shown that the pilot equalisation method does well to suppress the pilots and normalise the pilots to the range Doppler map noise floor and remove potential ambiguities. It was also shown that the DVB-T2 signal poses significant complications to the radar processing process as the system parameters for DVB-T2 can vary dependent on the environment of operation. This is due to the DVB-T2 standard giving operators more freedom of to choose the most optimum set of parameters for their operating environment unlike DVB-T whereby the parameters options were limited. In this instance the system parameters for the city of Cape Town meant that the guard interval didn't need to be suppressed or blanked as the length of the guard interval was of sufficient length that the ambiguities would not be visible within the standard operating ranges of UHF DVB-T2 system. However, for FFT sizes less than 8k for example the guard ambiguities begin to become visible within the typical operating range of the DVB-T2 system and these guard interval ambiguities would need to be suppressed. This, complicates the demod-remod processing design as the signal processing chain would need to be able to be adaptable to the parameters of the environment of operation.

Lastly, the range and Doppler processing was implemented using the FFT and cross-correlation algorithm. The output of which was fed into a CFAR filter utilising the GOCA-CFAR.

6.2.1 Future Work

The processing chain needs to be improved to operate in real-time. This can either be done by optimising the current processes or by investigating different methods for each stage of the processing chain. One method of optimising the processing chain is by implementing a method known as inverse-filtering[39, 41, 59, 60] which removes the need to implement DPI cancellation. Inverse filtering can be described as taking the FFT of a symbol length worth of the surveillance and reference channel and dot dividing the surveillance channel by the reference channel. An FFT of the result is then calculated and this gives the range line. Packing sequential range lines into the form of a matrix

and calculating another FFT along the Doppler dimension results in an ARD map. It is shown that the target is clearly visible within the strong clutter environment and thus DPI cancellation wouldn't be necessary. Inverse filtering is a frequency domain approach that relies on the OFDM nature of the signal.

ECA-CD, or extensive cancellation algorithm - carrier and Doppler, is a cancellation process that can be implemented along side the inverse filtering approach to remove the multipath clutter. ECA-CD takes advantage of the of the fact that OFDM modulates on a discrete block of data on different sub-carriers which are IFFT'd to the time domain. This blocks are then transmitted in separate OFDM symbols. [61] demonstrates that the algorithm takes advantage of the fact that the spectrum of a single OFDM symbol is independent of its delay to the direct path signal. Thus, a high level of cancellation can be achieved at low computational cost.

AoA calculations through phase interferometry needs to be investigated incorporated to the processing chain. This is due to the availability of a 3 channel DVB-T/T2 receiver being developed by industry partner Peralex Electronics for investigation of DVB-T/T2 PCL radar.

Lastly, the current processing chain can be optimised by reducing the number of iterations performed by the CGLS algorithm. In the FM PCL radar it was successfully shown by [4] that once the CGLS filter has converged it is not necessary to perform more iterations. More so it was shown that running the CGLS algorithm for 2 iterations reduces the residual of DPI cancellation to within 3 dBs of the optimal least mean square estimator.

References

[1] H. D. Griffiths and C. J. Baker. "Passive coherent location radar systems. Part 1: performance prediction". In: *IEE Proceedings - Radar, Sonar and Navigation* 152.3 (June 2005), pp. 153–159. ISSN: 1350-2395. DOI: 10.1049/ip-rsn:20045082.

[2] J. E. Palmer and S. J. Searle. "Evaluation of adaptive filter algorithms for clutter cancellation in Passive Bistatic Radar". In: *2012 IEEE Radar Conference*. May 2012, pp. 0493–0498. DOI: 10.1109/RADAR.2012.6212191.

[3] H. D. Griffiths and C. J. Baker. "Measurement and analysis of ambiguity functions of passive radar transmissions". In: *IEEE International Radar Conference, 2005.* May 2005, pp. 321–325. DOI: 10.1109/RADAR.2005.1435844.

[4] C. Tong. "A Scalable Real-time Processing Chain for Radar Exploiting Illuminators of Opportunity". PhD thesis. University of Cape Town, 2014.

[5] F. Maasdorp. "Doppler-only target tracking for a multistatic radar exploiting FM band illuminators of opportunity". PhD thesis. University of Cape Town, 2015.

[6] J. Coetser. "Fixed Tuned, Narrowband Digital Commensal Radar Receiver". MA thesis. University of Cape Town, 2014.

[7] S. Heunis. "Passive Coherent Location Radar using Software-Defined Radio techniques". MA thesis. University of Cape Town, 2010.

[8] G. Lange. "Performance Prediction and Improvement of a Bistatic Passive Coherent Location Radar". MA thesis. University of Cape Town, 2009.

[9] C. Tong and J. Coetser. "A minimal architecture for real-time, medium range aircraft detection using FM-band illuminators of opportunity". In: *2015 IEEE Radar Conference (RadarCon)*. 10-15 May 2015.

[10] R. Collins and C. Armstrong. "Digital turmoil for South African TV". In: *International Journal of Digital Televison* 2 (Jan. 2011). DOI: 10.1386/jdtv.2.1.7_1.

[11] H. Griffiths et al. "Radar Spectrum Engineering and Management: Technical and Regulatory Issues". In: *Proceedings of the IEEE* 103.1 (Jan. 2015), pp. 85–102. ISSN: 0018-9219. DOI: 10.1109/JPROC.2014.2365517.

[12] S.T. Paine et al. “Multi Band FM and DVB-T2 Passive Radar Demonstrator”. In: *2018 19th International Radar Symposium (IRS)* (2018), pp. 1–10.

[13] N.J. Willis. *Bistatic Radar*. Electromagnetics and Radar. Institution of Engineering and Technology, 2005. ISBN: 9781891121456. URL: https://books.google.co.za/books?id=U0XG5WB-vY8C.

[14] C. Tong, M. Inggs, and F. Maasdorp. “Performance improvements using the separated reference configuration for a multi-static FM broadcast band radar system”. In: *2013 International Conference on Radar*. Sept. 2013, pp. 224–229. DOI: 10.1109/RADAR.2013.6651989.

[15] J. I. Glaser. “Fifty years of bistatic and multistatic radar”. In: *IEE Proceedings F - Communications, Radar and Signal Processing* 133.7 (Dec. 1986), pp. 596–603. ISSN: 0143-7070. DOI: 10.1049/ip-f-1.1986.0096.

[16] R. J. James. “A history of radar”. In: *IEE Review* 35.9 (Oct. 1989), pp. 343–349. ISSN: 0953-5683. DOI: 10.1049/ir:19890152.

[17] H. D. Griffiths and N. R. W. Long. “Television-based bistatic radar”. In: *IEE Proceedings F - Communications, Radar and Signal Processing* 133.7 (Dec. 1986), pp. 649–657. ISSN: 0143-7070. DOI: 10.1049/ip-f-1.1986.0104.

[18] H. D. Griffiths et al. “Bistatic radar using satellite-borne illuminators of opportunity”. In: *92 International Conference on Radar*. Oct. 1992, pp. 276–279.

[19] J. D. Sahr and F. D. Lind. “The Manastash Ridge radar: A passive bistatic radar for upper atmospheric radio science”. In: *Radio Science* 32.6 (Nov. 1997), pp. 2345–2358. ISSN: 1944-799X. DOI: 10.1029/97RS02454.

[20] V. Koch and R. Westphal. “New approach to a multistatic passive radar sensor for air/space defense”. In: *IEEE Aerospace and Electronic Systems Magazine* 10.11 (Nov. 1995), pp. 24–32. ISSN: 0885-8985. DOI: 10.1109/62.473409.

[21] J. Baniak et al. “Silent Sentry passive surveillance”. In: *Aviation week and space technology* 7 (1999), pp. 134–139.

[22] P. E. Howland, D. Maksimiuk, and G. Reitsma. “FM radio based bistatic radar”. In: *IEE Proceedings - Radar, Sonar and Navigation* 152.3 (June 2005), pp. 107–115. ISSN: 1350-2395. DOI: 10.1049/ip-rsn:20045077.

[23] C. Bongioanni, F. Colone, and P. Lombardo. “Performance analysis of a multi-frequency FM based Passive Bistatic Radar”. In: *2008 IEEE Radar Conference*. May 2008, pp. 1–6. DOI: 10.1109/RADAR.2008.4720805.

[24] F. Colone et al. “A Multistage Processing Algorithm for Disturbance Removal and Target Detection in Passive Bistatic Radar”. In: *IEEE Transactions on Aerospace and Electronic Systems* 45.2 (Apr. 2009), pp. 698–722. ISSN: 0018-9251. DOI: 10.1109/TAES.2009.5089551.

[25] F. Colone, C. Bongioanni, and P. Lombardo. “Multifrequency integration in FM radio-based passive bistatic radar. Part I: Target detection”. In: *IEEE Aerospace and Electronic Systems Magazine* 28.4 (Apr. 2013), pp. 28–39. ISSN: 0885-8985. DOI: 10.1109/MAES.2013.6506827.

[26] C. J. Baker, H. D. Griffiths, and I. Papoutsis. “Passive coherent location radar systems. Part 2: waveform properties”. In: *IEE Proceedings - Radar, Sonar and Navigation* 152.3 (June 2005), pp. 160–168. ISSN: 1350-2395. DOI: 10.1049/ip-rsn:20045083.

[27] J. M. Christiansen and K. E. Olsen. “Range and Doppler walk in DVB-T based Passive Bistatic Radar”. In: *2010 IEEE Radar Conference*. May 2010, pp. 620–626. DOI: 10.1109/RADAR.2010.5494548.

[28] P. Falcone et al. “Experimental results for OFDM WiFi-based passive bistatic radar”. In: *2010 IEEE Radar Conference*. May 2010, pp. 516–521. DOI: 10.1109/RADAR.2010.5494565.

[29] F. Berizzi et al. “USRP technology for multiband passive radar”. In: *2010 IEEE Radar Conference*. May 2010, pp. 225–229. DOI: 10.1109/RADAR.2010.5494622.

[30] D. Petri et al. “High range resolution multichannel DVB-T passive radar: Aerial target detection”. In: *2011 Tyrrhenian International Workshop on Digital Communications - Enhanced Surveillance of Aircraft and Vehicles*. Sept. 2011, pp. 129–132.

[31] H. Kuschel et al. “A hybrid multi-frequency Passive Radar concept for medium range air surveillance”. In: *2011 MICROWAVES, RADAR AND REMOTE SENSING SYMPOSIUM*. Aug. 2011, pp. 275–279. DOI: 10.1109/MRRS.2011.6053653.

[32] A. Schroeder and M. Edrich. “CASSIDIAN multiband mobile passive radar system”. In: *2011 12th International Radar Symposium (IRS)*. Sept. 2011, pp. 286–291.

[33] A. Di Lallo et al. “AULOS: Finmeccanica family of passive sensors”. In: *IEEE Aerospace and Electronic Systems Magazine* 31.11 (Nov. 2016), pp. 24–29. ISSN: 0885-8985. DOI: 0.1109/MAES.2017.160037.

[34] N. Millet et al. “Lesson learnt from decades of passive radar experiments”. In: *2014 International Radar Conference*. Oct. 2014, pp. 1–6. DOI: 10.1109/RADAR.2014.7060360.

[35] R. Prasad. *OFDM for Wireless Communications Systems*. Artech House, 2004. ISBN: 9781580537964. URL: https://www.amazon.com/Wireless-Communications-Systems-Ramjee-Prasad/dp/1580537960?SubscriptionId=AKIAIOBINVZYXZQZ2U3A&tag=chimbori05-20&linkCode=xm2&camp=2025&creative=165953&creativeASIN=1580537960.

[36] ETSI. *ETSI EN 302 755: Digital Video Broadcasting (DVB); Frame structure channel coding and modulation for a second generation digital terrestrial television broadcasting system (DVB-T2)*. Tech. rep. 1.1.1. France: ETSI, 2009.

[37] ETSI. *TS 102 831: Digital Video Broadcasting (DVB); Implementation guidelines for a second generation digital terrestrial television broadcasting system (DVB-T2)*. Tech. rep. 1.2.1. France: ETSI, 2012.

[38] J. Scheer, W. Holm, and M. Richards. *Principles Of Modern Radar: Basic Principles (Hb-2014)*. Scitech, 2014. ISBN: 978-1-891121-52-4. URL: https://www.amazon.com/Principles-Modern-Radar-Basic-Hb-2014/dp/B01CMY7QZS?SubscriptionId=AKIAIOBINVZYXZQZ2U3A&tag=chimbori05-20&linkCode=xm2&camp=2025&creative=165953&creativeASIN=B01CMY7QZS.

[39] Z. Gao et al. "DVB-T Signal Cross-Ambiguity Functions Improvement for Passive Radar". In: *2006 CIE International Conference on Radar*. Oct. 2006, pp. 1–4. DOI: 10.1109/ICR.2006.343131.

[40] C. Bongioanni et al. "A new approach for DVB-T Cross-Ambiguity Function evaluation". In: *2009 European Radar Conference (EuRAD)*. Sept. 2009, pp. 37–40.

[41] J. E. Palmer et al. "DVB-T Passive Radar Signal Processing". In: *IEEE Transactions on Signal Processing* 61.8 (Apr. 2013), pp. 2116–2126. ISSN: 1053-587X. DOI: 10.1109/TSP.2012.2236324.

[42] D. W. O'Hagan, M. Setsubi, and S. Paine. "Signal reconstruction of DVB-T2 signals in passive radar". In: *2018 IEEE Radar Conference (RadarConf18)*. Apr. 2018, pp. 1111–1116. DOI: 10.1109/RADAR.2018.8378717.

[43] Independent Communications Authority Of South Africa. *National Radio Frequency Plan 2018*. Government Gazette 41650. Pretoria: Independent Communications Authority Of South Africa, May 2018.

[44] K. Chang. *RF Microwave Wireless Systems*. Wiley-Interscience, 2000. ISBN: 0471351997. URL: https://www.amazon.com/Microwave-Wireless-Systems-Kai-Chang/dp/0471351997?SubscriptionId=AKIAIOBINVZYXZQZ2U3A&tag=chimbori05-20&linkCode=xm2&camp=2025&creative=165953&creativeASIN=0471351997.

[45] Keysight Technologies. *Spectrum and Signal Analyzer Measurements and Noise*. Tech. rep. Keysight Technologies. URL: https://literature.cdn.keysight.com/litweb/pdf/5966-4008E.pdf.

[46] Space and Naval Warfare Systems Center. *User's Manual (UM) for Advanced Refractive Effects Prediction System*. Tech. rep. 3.6. San Diego: Space and Naval Warfare Systems Center, Dec. 2006.

[47] D. W. O'Hagan et al. "Elevation Pattern Analysis of Common Passive Bistatic Radar Illuminators of Opportunity". In: *IEEE Transactions on Aerospace and Electronic Systems* 53.6 (Dec. 2017), pp. 3008–3019. ISSN: 0018-9251. DOI: 10.1109/TAES.2017.2724378.

[48] D.M. Pozar. *Microwave Engineering*. Wiley, 2004. ISBN: 9780471448785. URL: https://www.amazon.com/Microwave-Engineering-David-M-Pozar/dp/0471448788?SubscriptionId=AKIAIOBINVZYXZQZ2U3A&tag=chimbori05-20&linkCode=xm2&camp=2025&creative=165953&creativeASIN=0471448788.

[49] Ellies. *Digital Terrestrial TV Antenna 4 Element Wide Band UHF Grid*. Ellies. Cape Town, 2018.

[50] *SBX*. https://kb.ettus.com/SBX. Accessed: 2019-02-09.

[51] *MIMO Cable*. https://kb.ettus.com/Synchronization_and_MIMO_Capability_with_USRP_Devices. Accessed: 2019-02-09.

[52] Mini-Circuits. *Coaxial Low Noise Amplifier ZX60-P103LN+*. Mini-Circuits. 2018.

[53] National Instruments. *White paper: What Is NI USRP Hardware?* Tech. rep. National Instruments, Aug. 2018.

[54] T. B. Welch and S. Shearman. "Teaching software defined radio using the USRP and LabVIEW". In: *2012 IEEE International Conference on Acoustics, Speech and Signal Processing (ICASSP)*. Mar. 2012, pp. 2789–2792. DOI: 10.1109/ICASSP.2012.6288496.

[55] National Intruments. *Application Design Patterns: Producer/Consume*. Tech. rep. National Intruments, Nov. 2018.

[56] R. Saini and M. Cherniakov. "DTV signal ambiguity function analysis for radar application". In: *IEE Proceedings - Radar, Sonar and Navigation* 152.3 (June 2005), pp. 133–142. ISSN: 1350-2395. DOI: 10.1049/ip-rsn:20045067.

[57] H. A. Harms, L. M. Davis, and J. Palmer. "Understanding the signal structure in DVB-T signals for passive radar detection". In: *2010 IEEE Radar Conference*. May 2010, pp. 532–537. DOI: 10.1109/RADAR.2010.5494564.

[58] *ComRad*. https://www.peralex.com/passive-coherent-location/. Accessed: 2019-02-09.

[59] C. R. Berger et al. "Signal Processing for Passive Radar Using OFDM Waveforms". In: *IEEE Journal of Selected Topics in Signal Processing* 4.1 (Feb. 2010), pp. 226–238. ISSN: 1932-4553. DOI: 10.1109/JSTSP.2009.2038977.

[60] L. Fang et al. “Passive detection using orthogonal frequency division multiplex signals of opportunity without multipath clutter cancellation”. In: *IET Radar, Sonar Navigation* 10.3 (2016), pp. 516–524. ISSN: 1751-8784. DOI: 10.1049/iet-rsn.2015.0238.

[61] C. Schwark and D. Cristallini. “Advanced multipath clutter cancellation in OFDM-based passive radar systems”. In: *2016 IEEE Radar Conference (RadarConf)*. May 2016, pp. 1–4. DOI: 10.1109/RADAR.2016.7485166.

Appendix A

Labview

In this section a detail on how to use Labview with the USRP board will be described. In this instance the example will be done with a N21O USRP board and an SBX daughterboard. The example will begin with a section of how to setup Labview with the USRP. This process is assuming that you have a basic version of LabView installed. UCT has a licence for LabView 2015 and thus this example will be based on that version.

A.1 Setting Up Labview

Firstly, the ettus board has to be configured with the correct Internet Protocol (IP) address and that the USRP board has all the correct drivers installed. To do this Labview has an Configuration Utility package called NI-USRP Configuration Utility. This utility package is not installed with Labview and thus will need to be downloaded. The configurator can be downloaded from the National Instruments website `http://www.ni.com/download/ni-usrp-17.0/6952/en/`. Ensure that you download the latest version.

Connect the N210 board with an ethernet cable to the host PC. You can connect either a single board at a time or both at the same time with a MIMO cable. Ensure that you are on the same subnet mask as the USRP N210 default gateway. To do this the host PC needs to be set to a static IP that matches the default gateway of the N210 boards. Each N210 board is set with a static IP of 192.168.10.2 by default. Go to your settings and change the IP address to the following configurations:

- IP Address: 192.168.10.1
- Subnet Mask: 255.255.255.0
- Gateway: 192.168.10.1

After the change, open *cmd* and try and ping the N210 board with the default IP address. If the unit doesn't respond that then use the configurator to edit the IP address.

Open the NI-USRP Configurator Utility. See Figure A.1 for example of configurator

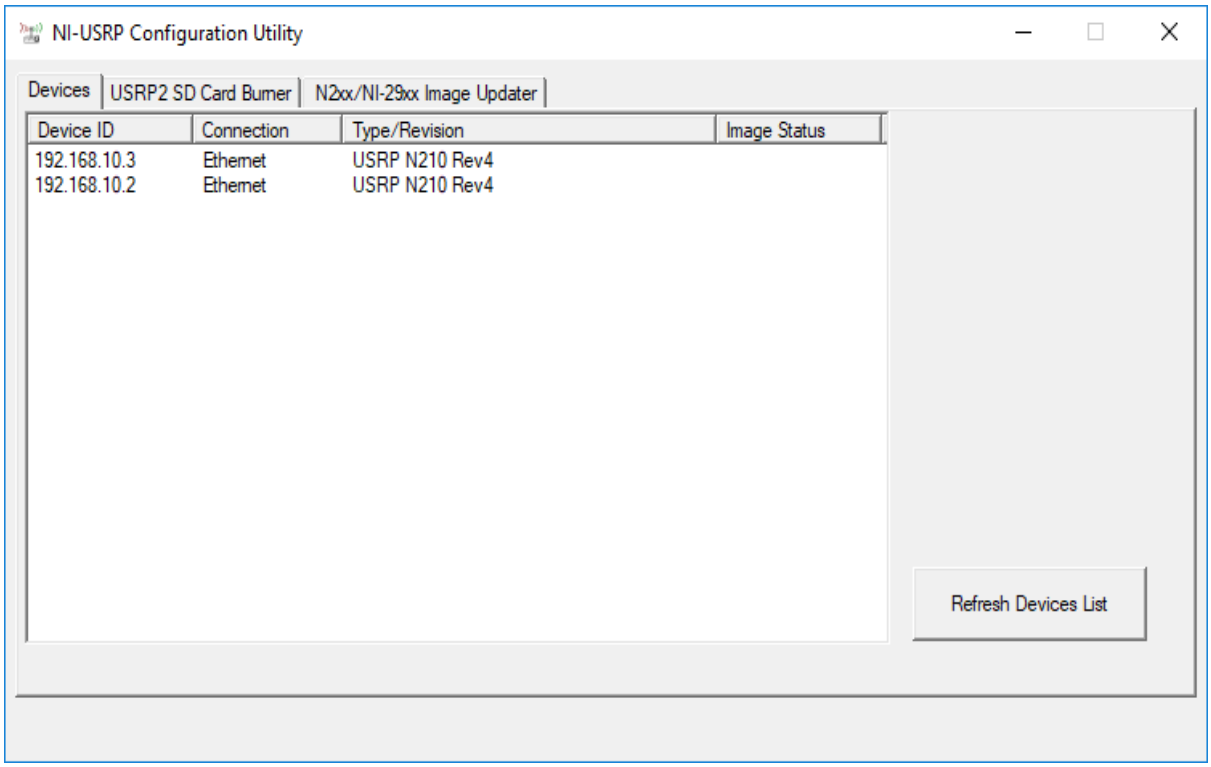

Figure A.1: Example of NI-USRP Configurator Utility

The devices tab will have the following headings:

- Device ID: Name of device
- Connection: Type of connection (ethernet)
- Type/Revision: Type of USRP connected.
- IP Address: The IP address of the connected device.

All the connected devices can be managed in this interface. If you have two boards connected with different IPs with the MIMO cable. Both boards will appear on the list.

To change the boards IP from default. Connect only a single board, and highlight it in the devices tab. On the right hand side of the UI there is two text boxes. These are "Selected IP Address" and "New IP Address" respectively. Selected IP address will be the connected devices current IP address. New IP address will be the IP address the user wants the board to have. Enter the new IP address and click "Change IP Address." The IP address will be updated. The second board can now be connected via MIMO and the steps can be repeated to change the IP address.

The devices should now both appear as in Figure A.2

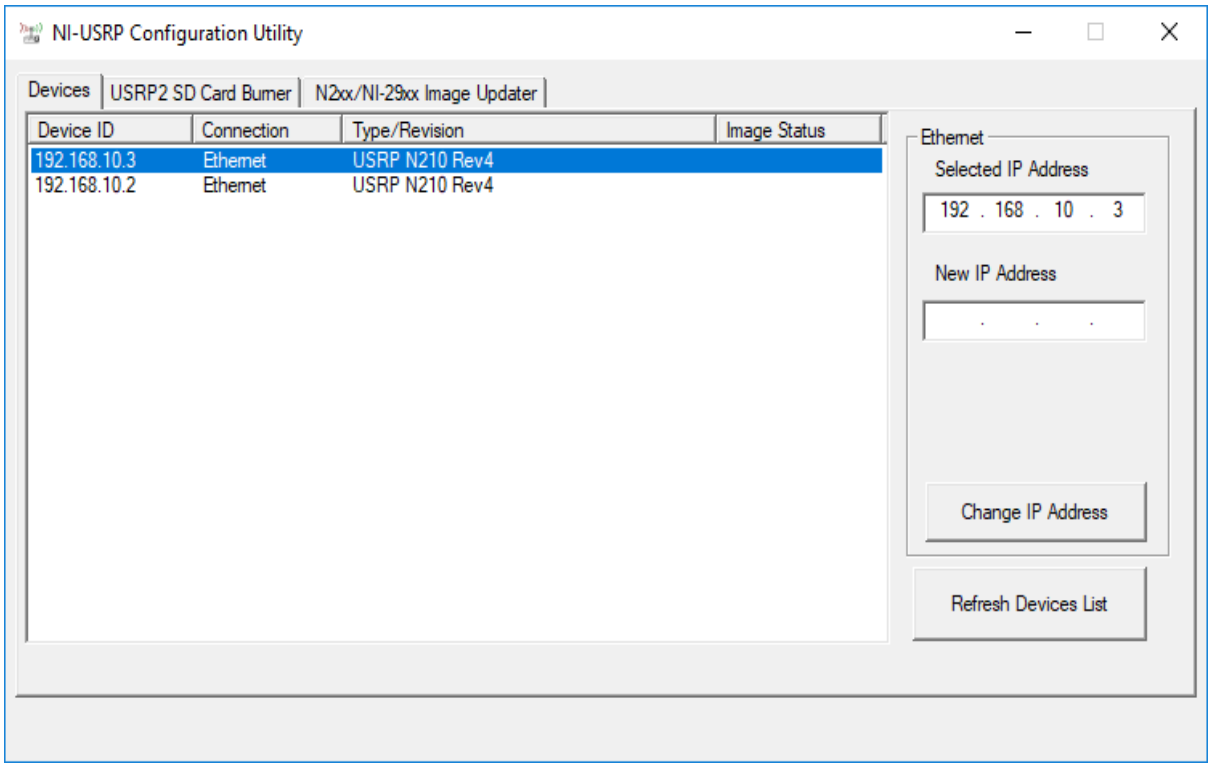

Figure A.2: Example of NI-USRP Configurator Utility with Connected Devices

Change tabs from Devices to "N2xx/NI-29xx Image Updater" to update the firmware of the devices. The devices will be updated with the basic firmware updates that come with the installation of Labview.To update a board press on the "Find Devices" button and select the board to be updated. See Figure A.3 for example.

Select the FPGA and Firmware updates to be used by using the browse buttons next each one. The updates can be found in the NI-USRP installation folder. Press "WRITE IMAGES" once you have selected the appropriate updates for both the FPGA and Firmware.

Both boards should be ready to be stream data at this point.

Test the functionality of the boards by running the niUSRP EX Spectral Monitoring example. This board can be tested on of two ways. Connect an antenna operating a known frequency to the receive channel of the device and or feed a signal from a signal generator into one of the receive channels and monitor the spectrum on the Labview interface. Locate the niUSRP EX Spectral Monitoring project named the niUSRP EX Spectral Monitoring.vi. The .vi is the extension of Labview projects. This vi will be in the examples folder of the stored directory under examples\instr\niUSRP. See Figure A.4 for example.

Configure the interface to run with the N210 board. Enter the IP Address of the device. Set the sample rate of the ADC. Configure the carrier frequency, ensure that the frequency

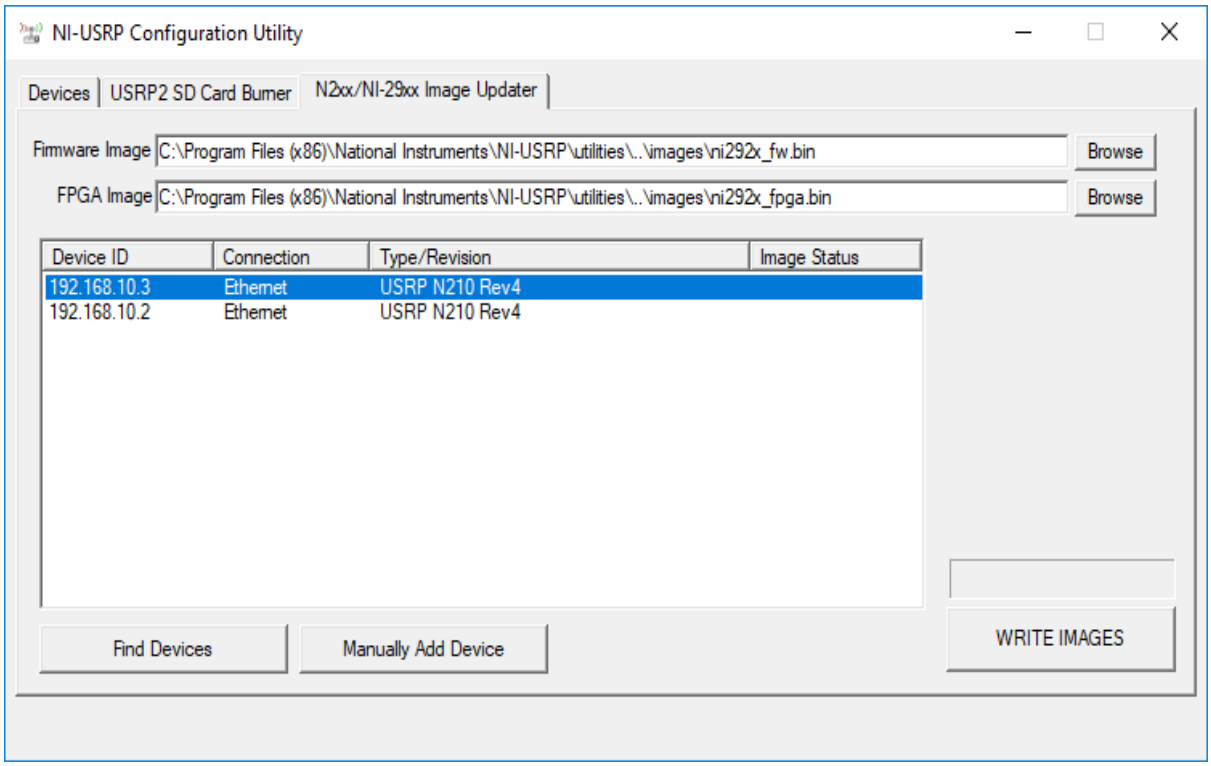

Figure A.3: Example of Updating Firmware and FPGA with NI-USRP Configurator

value is compatible with your daughterboard. Configure the gain. Choose the receiver channel you are measuring on RX1 is RF1 port on the board and RX2 is the RF2 port on the board. Run the example if the settings are incompatible, Labview will pull the best optimal parameters based on your other inputs from the device by pulling the information from the device. To run the code click on the white arrow underneath edit on the toolbar. The board should be running, see Figure A.5 below

From this point a user can continue on and program he's own project building this example and using other libraries that are available in the Labview toolset.

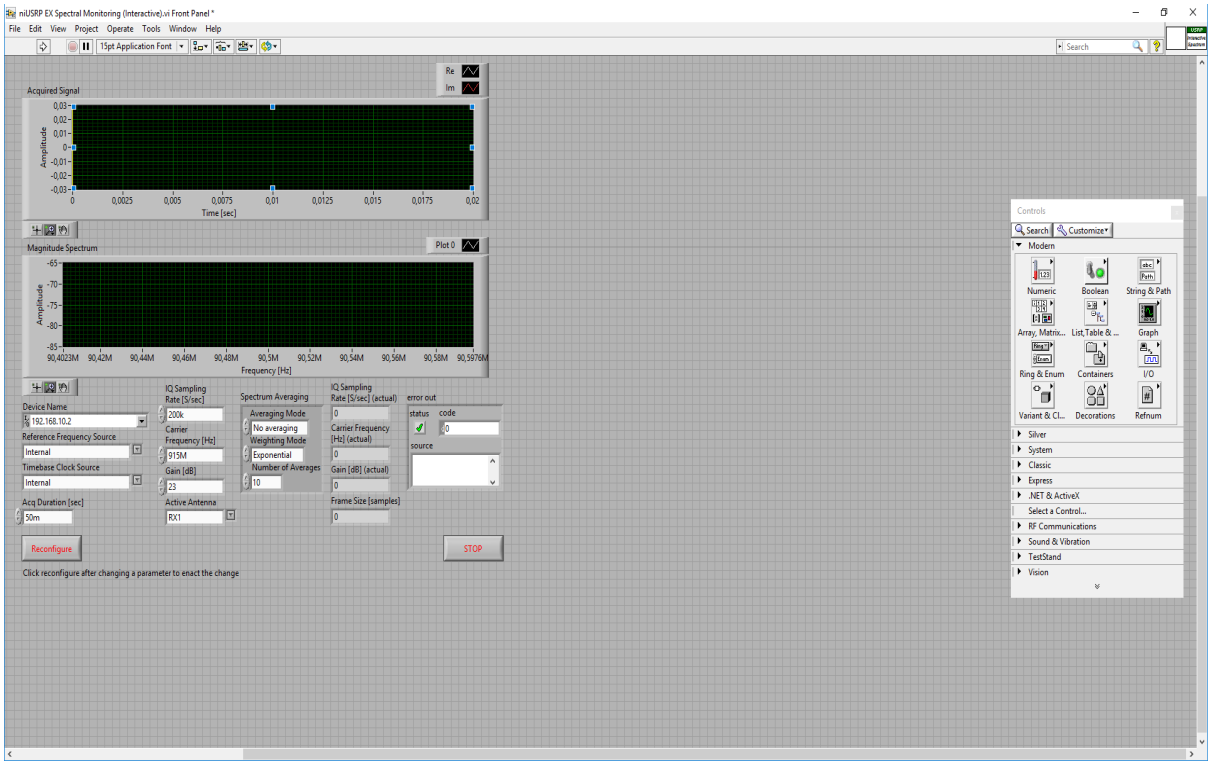

Figure A.4: Example of Labview USRP User Interface

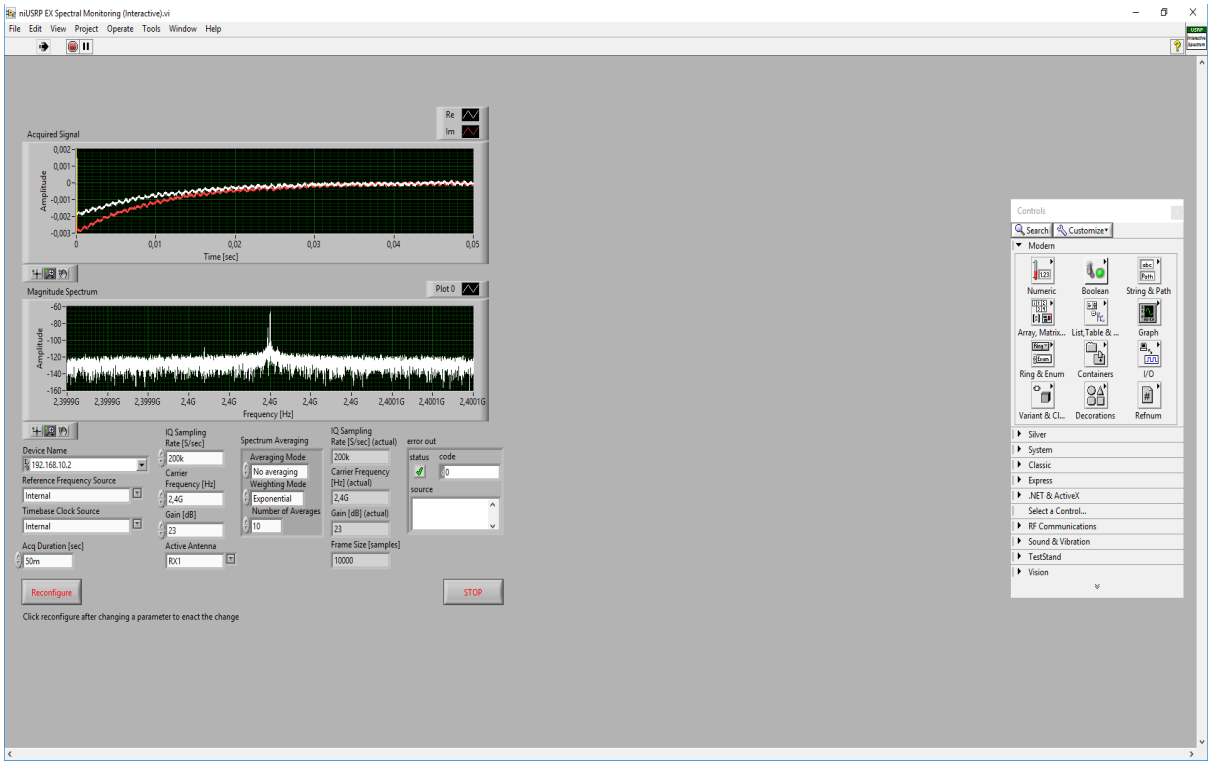

Figure A.5: Example of Labview USRP User Interface Sampling at 2.4GHz.